Analysis of Failure Mechanisms and Mechanical Properties of Hierarchical Bio-inspired Composites

A thesis submitted

in partial fulfillment for the award of the degree of

Doctor of Philosophy

by

Abhirami A J

Department of Aerospace Engineering

Indian Institute of Space Science and Technology

Thiruvananthapuram, India

December 2023

Certificate

This is to certify that the thesis titled ***Analysis of Failure Mechanisms and Mechanical Properties of Hierarchical Bio-inspired Composites*** submitted by **Abhirami A J**, to the Indian Institute of Space Science and Technology, Thiruvananthapuram, in partial fulfillment for the award of the degree of **Doctor of Philosophy** is a bona fide record of the original work carried out by him/her under my supervision. The contents of this thesis, in full or in parts, have not been submitted to any other Institute or University for the award of any degree or diploma.

Dr. Anup S
Supervisor
Professor
Department of Aerospace Engineering
IIST, Thiruvananthapuram

Dr. Deepu M
Professor and Head
Department of Aerospace Engineering
IIST, Thiruvananthapuram

Place: Thiruvananthapuram
Date: December 2023

Declaration

I declare that this thesis titled ***Analysis of Failure Mechanisms and Mechanical Properties of Hierarchical Bio-inspired Composites*** submitted in partial fulfillment for the award of the degree of **Doctor of Philosophy** is a record of the original work carried out by me under the supervision of **Dr. Anup S**, and has not formed the basis for the award of any degree, diploma, associateship, fellowship, or other titles in this or any other Institution or University of higher learning. In keeping with the ethical practice in reporting scientific information, due acknowledgments have been made wherever the findings of others have been cited.

Place: Thiruvananthapuram
Date: December 2023

Abhirami A J
(SC17D002)

This thesis is dedicated to my dear Dad, who encouraged me to take up this adventure; my sweet Mom and Sister for making me believe that anything is possible and to my loving Husband for making everything possible . . .

Acknowledgements

It was a great learning experience that I had at IIST, and I could feel the difference in me from the person I was at the joining time. I was able to learn and develop many academic and personal skills with the help of IIST community.

First and foremost, I would like to extend my most profound respect and gratitude to my research supervisor, Dr. Anup S, Professor, Aerospace Engineering, IIST, for his generous and continuous support and encouragement throughout my research work. His patience, immense knowledge, and keen guidance at every stage of the research work have been the impetus for this project's completion.

Additionally, I am immensely grateful to my doctoral committee (DC) members as well as Chairmen, DC: Dr. Deepu M, Head of the Department, Dr. Aravind V, Dr. Manoj T Nair, and Dr. Salih A, former Heads of the Department, Aerospace Engineering, IIST, for whom I owe a great debt of gratitude. I would also like to thank all of the Professors in the Aerospace Engineering department, especially, Dr. Bijudas C R, Dr. Devendra Prakash Ghate, Dr. Praveen Krishna I R, Dr. Kurian Issac, and former professor Dr. Arun C O, for generously dedicating their time and the valuable input comments to troubleshoot the issues faced during the research work. I also thank Dr. Prabhakaran K, Professor, Department of Chemistry, IIST, for critically reviewing my research outcomes and progress and for his help with this work's scope of experimental analyses. I would like to express my heartfelt gratitude to Dr. A. Arockiarajan from the Department of Applied Mechanics at IIT Madras, Chennai for generously sharing his expertise and offering invaluable contributions to enhance this research work.

Without the support of many people, this project would not have been possible. Thanks to my dear friends Dr. Aswathy M, Mrs. Anuja Vijayan, Mrs. Resmy J Devan, Mr. Sachin Chandran C, Dr. M Arrutselvi, Mr. Gaurab Kumar Khanra, Mrs. Lakshmi T N, Ms. Reshma M Raju and lab staffs, Mr. Satishkumar V, Mr. Mohammed Rijas A, Mr. Dinesh D, and Mr. Bipin D and all the people who knowingly or unknowingly helped me to get into the finishing point of my PhD and provided me a safe and comfortable research environment during my course duration.

I also thank all my dear students with whom I got a chance to work with, on this research area. Through those discussions we were able to learn deeper and solve the problems which we thought were unsolvable in this lifetime.

Ultimately, I would like to thank my supportive family, especially my husband Mr. Sheem Jayakumar, my parents: Mr. R Jayachandran Nair and Mrs. Anitha Nair, and my sister and brother in law: Mrs. Janaki A J and Mr. Karthik P Nair, and my in-laws, Mr. Jayakumar S, Mrs. Deepa P, and Mr. Keerthik Jayakumar for their unwavering love and support.

Thanks to that driving force, which motivated me whenever I was down, that shed light during my dark times, and for all happiness and good times I went through, and the ones yet to come!

To conclude, I deeply appreciate the collaborative effort and support of many individuals who have contributed to the completion of this thesis.

Abhirami A J

Abstract

Nacre, bone, spider silk, and antlers are some examples of biological composites which exhibit a great combination of mechanical properties such as high strength, stiffness, and toughness when compared to that of their constituents using which they made up of. This has inspired many researchers to investigate bio-inspired composites to explore the possibilities of making synthetic composites with superior mechanical properties using relatively weaker constituents. There are many reasons behind the achievement of a biological composite's superior mechanical properties, which range from the selection of constituents to its final arrangement. The basic structure of above mentioned biological composites is a kind of brick-and-mortar structure in which platelets with a defined configuration are dispersed in a pool of matrix. Here, the parameters that significantly influence the final mechanical properties are Young's moduli ratio of platelet to the matrix, the platelet aspect ratio, and the arrangement of platelets, especially the hierarchy.

In this thesis, we investigate the mechanical properties of hierarchical bio-inspired composites in which the two mostly observed staggering types found in nature: regular and stairwise staggerings are used. A preliminary failure study is conducted for one-hierarchical composites with regular and stairwise staggered configurations to get a clear idea of the failure sequence of different regions inside the composite such as the platelets and platelet-matrix interfaces. The influence of the failure sequence on the mechanical properties of the bio-inspired composite with a single hierarchy is also studied in detail. It is found that the inclusion of the first failure in the computation of the composite's toughness has a significant contribution, and we were able to quantify the same through our study. To obtain a more realistic approach, we conduct a case study using some material-set combinations used in the industries and recent research works. The results from the case study also reported the major contribution of the inclusion of the first failure towards the toughness of both regular and stairwise staggered composites.

Analytical models for predicting the properties of two hierarchical composites with different configurations at different levels of hierarchy (non-self-similar) are formulated and compared with the finite element analysis results. The results show a good agreement with the proposed model. We also generalize the two hierarchical analytical model to predict its mechanical properties. The optimized model of a generalized two hierarchical

composite enables the user to get the relevant design elements, like the platelet aspect ratio and number of platelets in a period, for a given input of material properties and strength, stiffness, and toughness requirements. This study could greatly help to simplify the design procedure in a hierarchical composite and to get an initial estimation of the mechanical properties of the final hierarchical composites before fabricating a full-scale model.

Contents

List of Figures

List of Tables

Abbreviations

2H	Two hierarchical
BC	Boundary condition
CPE4R	Four-node plane strain element
FE	Finite element
FEA	Finite element analysis
HIF	Horizontal interface failure
PBC	Periodic boundary condition
PF	Platelet failure
RS	Regularly staggered composite made with stairwise staggered composites as platelets
RSM	Regularly staggered model
RVE	Representative volume element
SBC	Symmetric boundary condition
SR	Stairwise staggered composite made with regular staggered composite as platelets
SS	Stairwise staggered composite made with stairwise staggered composite as platelets
SSM	Stairwise staggered model
TSC	Tension-Shear chain
VIF	Vertical Interface Failure

Nomenclature

α, β	Material parameters
α_R	Parameter in regularly staggered composite
α_{RS}	Parameter in 2H RS composite
α_S	Parameter in stairwise staggered composite
α_{SR}	Parameter in 2H SR composite
Δ_h	Horizontal displacement
Δ_v	Vertical displacement
δ_1	Magnitude of deflection along the $x_1$direction
δu_1	difference in u_1 between two adjacent nodes
ϵ	Strain
ϵ_1	Strain at first failure
ϵ_{11}	Strain along the $x_1$direction
ϵ_{22}	Strain along the $x_2$direction
ϵ_2	Strain at second failure
$\epsilon^P_{critical}$	Failure strain of platelet
$\epsilon^{RS}_{critical}$	Failure strain of 2H RS composite
$\epsilon^{SR}_{critical}$	Failure strain of 2H SR composite
ϕ	Platelet volume fraction
ϕ_R	Platelet volume fraction of regularly staggered composite
ϕ_S	Platelet volume fraction of stairwise staggered composite
ψ	Critical value of $\frac{\sigma^p_{critical}}{\tau^m_{critical}}$
ξ	Ratio of half non-overlap length to overlap length of platelet
ρ	Platelet aspect ratio
ρ_1	Platelet aspect ratio in first hierarchy
ρ_2	Platelet aspect ratio in second hierarchy
$\rho'_{critical}$	Critical aspect ratio of regularly staggered composite
$\rho''_{critical}$	Critical aspect ratio of stairwise staggered composite

$\rho'_{RS,critical}$	Critical aspect ratio of 2H RS composite
$\rho''_{SR,critical}$	Critical aspect ratio of 2H SR composite
ρ_R	Aspect ratio of platelet in regularly staggered composite
ρ_{RS}	Aspect ratio of platelet in 2H RS composite
ρ_S	Aspect ratio of platelet in stairwise staggered composite
ρ_{SR}	Aspect ratio of platelet in 2H SR composite
σ	Normal stress
σ'	Strength at first failure
σ''	Strength at second failure
σ_{11}	Normal stress along x-direction
$\sigma_{c,norm}$	Normalized strength of 2H SS composite
$\sigma^p_{critical}$	Strength of the platelet
$\sigma^p_{max,reg}$	Maximum value of normal stress in the platelet in a RSM
$\sigma^p_{max,sw}$	Maximum value of normal stress in the platelet in a SSM
$\sigma^m_{max,reg}$	Maximum value of normal stress in the matrix in a RSM
$\sigma^m_{max,sw}$	Maximum value of normal stress in the matrix in a SSM
$\sigma^R_{critical}$	Strength of regularly staggered composite
$\sigma^{RS}_{critical}$	Strength of 2H RS composite
$\sigma^S_{critical}$	Strength of stairwise staggered composite
$\sigma^{SR}_{critical}$	Strength of 2H SR composite
$\sigma^{SS}_{critical}$	Strength of 2H SS composite
τ, τ_{12}	Shear stress
$\tau^m_{critical}$	Shear strength of the matrix
A, B	Constants depending on material and geometric paramters
A_1, A_2	Areas of stress-strain diagram
b	Half the width of platelet
$E_{B=0}$	Young's modulus of Composite without vertical interface
$E_{B\neq 0}$	Young's modulus of Composite with vertical interface
$E_{c,norm}$	Normalized Young's modulus of 2H SS Composite
E_m, E_i	Young's modulus of matrix
E_p	Young's modulus of platelet
E_R	Young's modulus of a regularly staggered composite
E_{RS}	Young's modulus of 2H RS composite
E_S	Young's modulus of a stairwise staggered composite
E_{SR}	Young's modulus of 2H SR composite

G_{12}	Shear modulus of the composite
G_m, G_i	Shear modulus of matrix
h_m	Thickness of the matrix between two columns of platelets
k_1, k_2	Points of kinks
L_a	Overlapping length in a half platelet
L_b	Half the thickness of matrix along horizontal direction
m, n, k	Non-dimensional indices such that $m + n + k = 1$
n	Number of platelets in each period
n_1	Number of platelets in each period, in first hierarchy
n_2	Number of platelets in each period, in second hierarchy
P	Point load
[Q]	Stiffness matrix
Q_{11}	Stiffness matrix coefficient (1,1)
Q_{12}	Stiffness matrix coefficient (1,2)
Q_{22}	Stiffness matrix coefficient (2,2)
[S]	Compliance matrix
u_1	Displacement along x_1
u_2	Displacement along x_2
v_m	Thickness of the matrix between two rows of platelets
w	Toughness
$w_{c,norm}$	Normalized toughness of 2H SS composite
$w_{critical}^{RS}$	Toughness of 2H RS composite
$w_{critical}^{RS,max}$	Maximum toughness of 2H RS composite
$w_{critical}^{SR}$	Toughness of 2H SR composite
$w_{critical}^{SR,max}$	Maximum toughness of 2H SR composite
$w_{critical}^{SS}$	Toughness of 2H SS composite
$w_{critical}^{P}$	Toughness of the platelet
W_{rve}	Width of the RVE

Chapter 1

Background

Nature has perfected the art of designing and synthesizing materials with exceptional mechanical properties, often surpassing those of traditional synthetic materials. Bio-inspired hierarchical composites, mimicking the structural arrangements found in biological systems, offer a promising avenue for the development of advanced materials. This Chapter aims to provide a comprehensive overview of the mechanical properties exhibited by biological as well as bio-inspired composites, exploring their unique structural features, mechanical behavior, and potential applications. By studying and understanding these remarkable materials, we can unlock new insights that can pave the way for innovative engineering solutions in various industries, ranging from aerospace and automotive to biomedical and beyond.

1.1 Introduction

The stunning and sublime self-defense mechanisms observed in nature greatly inspired the invention of new materials. For example, the horns of a sheep can withstand an impact force as high as 3400 N, in the time of collisions for competing territory and hunting for food (Kitchener, 1988). Not only animals but various plants and fruits also exhibit excellent strength and energy absorption characteristics. For example, the energy dissipation of the mesocarp spongy layer of a pomelo fruit is around 80 J, which is obtained from free-fall tests for no visible outer damage on the peel (Fischer et al., 2010).

Biological composites refer to a wide range of natural materials such as nacre, antler, bone, spider silk, bamboo, and fish skin which possess superior mechanical properties (Fratzl et al., 2004; San Ha and Lu, 2020; Wegst et al., 2015). They possess exceptionally high strength and stiffness compared to that of their basic building blocks (Currey, 1977; Fratzl et al., 2004; Meyers et al., 2008). This makes them more special as well as useful

for developing synthetic materials. Even though the fundamental function of a biological material is serving as an armor for the body, they may also act as ion reservoirs in bones, as a chemical barrier in a cell membrane, as an energy converter in muscles, etc (Fratzl and Weinkamer, 2007).

Figure 1.1 shows the inner nacreous layer of a red abalone shell and the typical shells arrangement observed in nacre at different scales (Barthelat et al., 2007). The nacre, made up of about 95 volume percent of aragonite (stiff phase), and the remaining volume percentage of protein (soft phase) is claimed to have a tensile strength of the order of 300 MPa, an order of magnitude higher than that of the aragonite in pure monolithic form (a $CaCO_3$ form closer to calcite). The stiffness of nacre varies from 60 to 80 GPa, keeping up a reasonably high toughness of the order of 1000 times compared to the toughness of aragonite (Barthelat et al., 2007; Ji and Gao, 2004a).

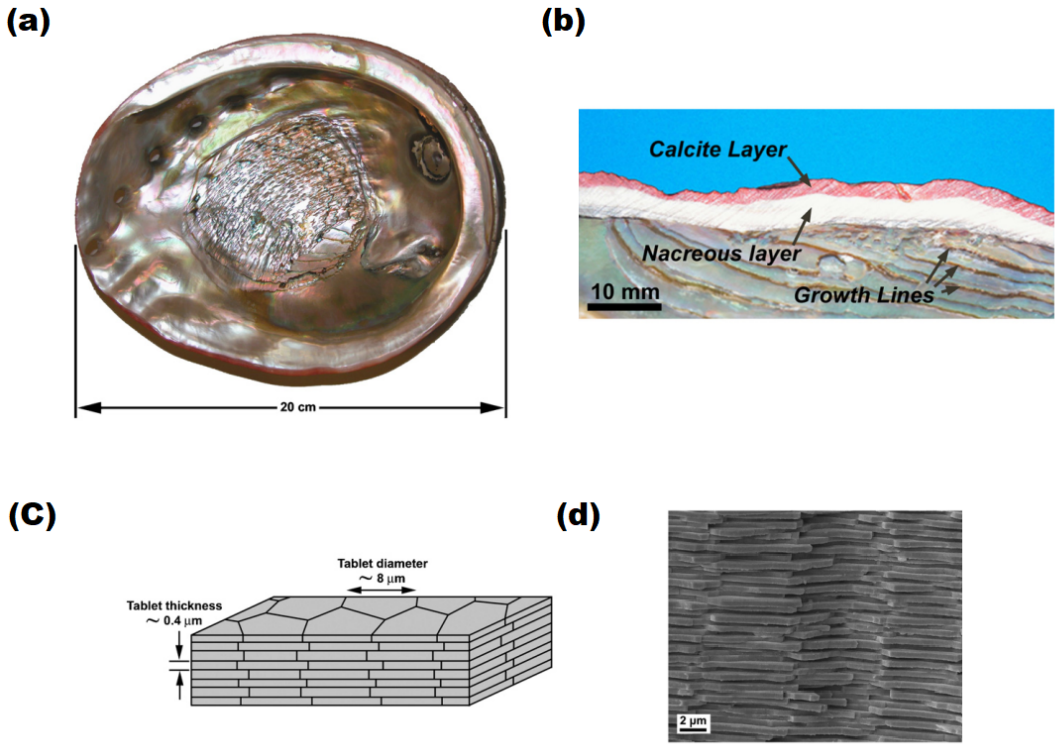

Figure 1.1: (a) The inner nacreous layer of a red abalone shell (b) Typical shells arrangement in nacre (c) transmission electron micrograph (TEM) of nacre from red abalone showing regular staggered arrangement of platelets (d) optical micrograph of nacre from fresh water mussel Lampsilis Cardium (Barthelat et al., 2007)

Biological materials have helped human society to learn from and improve in many ways. They played an indispensable role in shaping the world the one as we see today.

Most of the artificial materials/instruments were invented from inspirations by its natural counterpart. For example, the hook and pile fasteners developed by the company Velcro was inspired by the burdock plant (Luke and Vukusic, 2011).

Various pieces of research have reported the possible reasons behind the outstanding mechanical properties of biological composites. The pattern of arrangement of constituents at the elemental level of the composite is one of the major factors responsible for the excellent mechanical properties of biological composites (Ji, 2008; Mathiazhagan and Anup, 2016a; Melaibari et al., 2021; Wu et al., 2019). For example, the toughness of nacre in terms of energy is three orders of magnitude higher than that of the platelets of which it is composed of, which is chiefly attributed to its peculiar staggering structure (Espinosa et al., 2009). Fig. 1.1 (c) shows the brick and mortar arrangement observed in biological composites. In the brick and mortar structure of nacre or mother of pearl, the bricks are aragonite platelets and mortar is a protein matrix, with a platelet volume fraction of 95-99% (Barthelat and Espinosa, 2007; Ji and Gao, 2004a). For bones, the basic constituents are mineral platelets and collagen matrix, with a platelet volume fraction of around 40-45% (Ji and Gao, 2004a). The other factors which impart the superior mechanical properties to biological composites include the high Young's moduli ratio between platelet and matrix, optimum length to width ratio (aspect ratio) of platelet, the interface properties, and the nanoscale size and hierarchical arrangement of the constituents (Gao et al., 2003; Henry, 2018; Lei et al., 2013; Ma et al., 2018, 2016; Maghsoudi-Ganjeh et al., 2021; Mathiazhagan and Anup, 2016a,a, 2019; Wiener et al., 2020; Yao et al., 2011).

A good balance between high toughness and stiffness can be seen in nacre and bone-like biological composites rather than an inverse relationship between two properties as in other conventional materials (Barthelat and Espinosa, 2007; Ji and Gao, 2004a; Murali et al., 2011; Wilmers and Bargmann, 2020). Figure 1.2 shows the toughness and modulus comparison of various materials through an Ashby plot (Porter and McKittrick, 2014; Wegst and Ashby, 2004). It can be seen that the bone and nacre has high toughness as well as excellent stiffness.

Artificial composites derived from the inspiration of biological composites are collectively called bio-inspired composites. Bio-inspired composites are often considered as an ideal candidate in the field of light and innovative structures which the world is in need for. The matchless properties possessed by a biological composite such as nacre, bone or spider silk are mimicked to simulate a synthetic so-called bio-inspired composite (Barthelat et al., 2013; Guo and Gao, 2006; Valashani and Barthelat, 2014). In order to develop a bio-inspired composite with fine mechanical properties, it is required to study all the afore-

mentioned possible factors which are responsible for the superior mechanical properties of a biological composite (Singh et al., 2019; Yang et al., 2019).

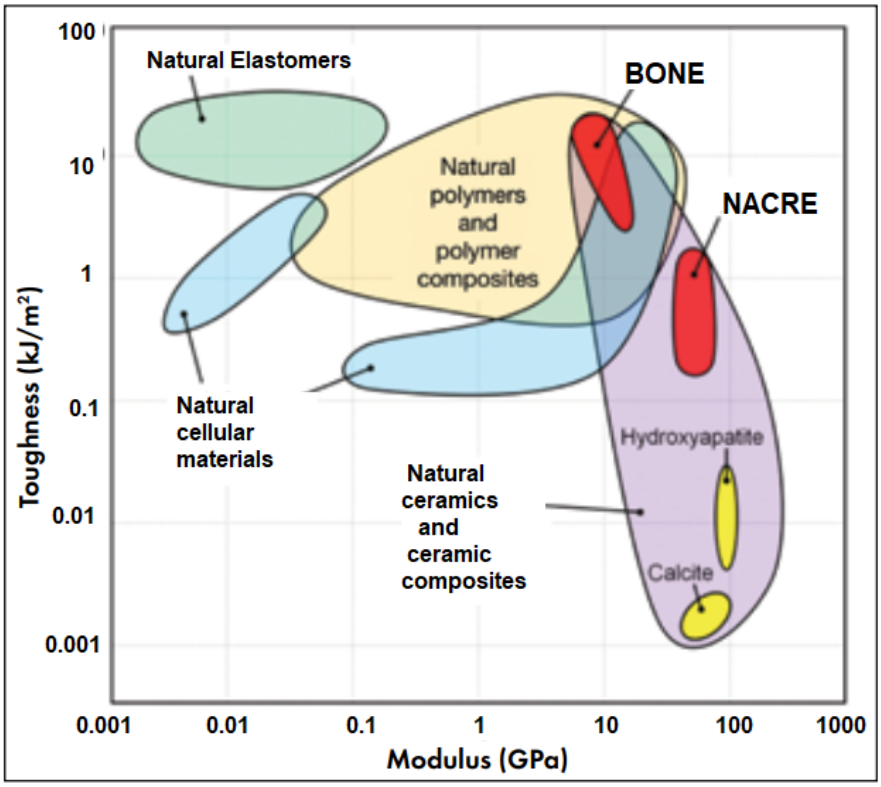

Figure 1.2: Comparison of toughness and modulus through Ashby plot. Despite of their low density, bone and nacre are having high toughness along with high stiffness. (Reproduced from Porter and McKittrick (2014))

In nature, there is always an endless competition for the survival of the fittest. This competition has played a significant role in the evolution of biological materials on their way to achieving superb mechanical properties such as strength, toughness, and impact resistance, also with light weights (Carreño et al., 2022). In contrast to the traditional materials, the ones from nature use very few constituents; yet possess amazing mechanical properties (Peng et al., 2022; Wegst et al., 2015). The utilization of the aforementioned strategies in the manufacturing of bio-inspired composites sets them apart from other existing composite materials, making them inherently distinctive. However, despite the recent advances reported in the manufacturing and materials, the existing biomimetic materials are found to be much to be improved to get the actual performance of the natural materials which they are inspired from (Libonati and Buehler, 2017).

Several pieces of research have reported that the alignment or staggering of platelets in the nano/microstructures plays an important role in biological materials attaining these superior mechanical properties (Anup et al., 2007; Bosia et al., 2012; Currey, 1984; Weiner and Wagner, 1998). There exist different kinds of staggering such as regular, stairwise, uniform, and random; of which the mostly observed in nature are the regular and stairwise, due to their most balanced mechanical properties (Zhang et al., 2010).

Figure 1.3 shows a regular staggered composite with an overlapping length of $L/2$ where L is the length of the platelet, in which the concept of a tension-shear chain (TSC) model is also illustrated (Ji and Gao, 2004a). The tension-shear chain model was developed by Ji and Gao (2004a) to demonstrate how the staggered alignment in the natural biological materials helps them to attain exceptional mechanical properties compared to that of their constituents. In a TSC model, it is assumed that the matrix at the vertical interfaces fails as the composite is stressed, and such portions are removed for simplifying the analysis.

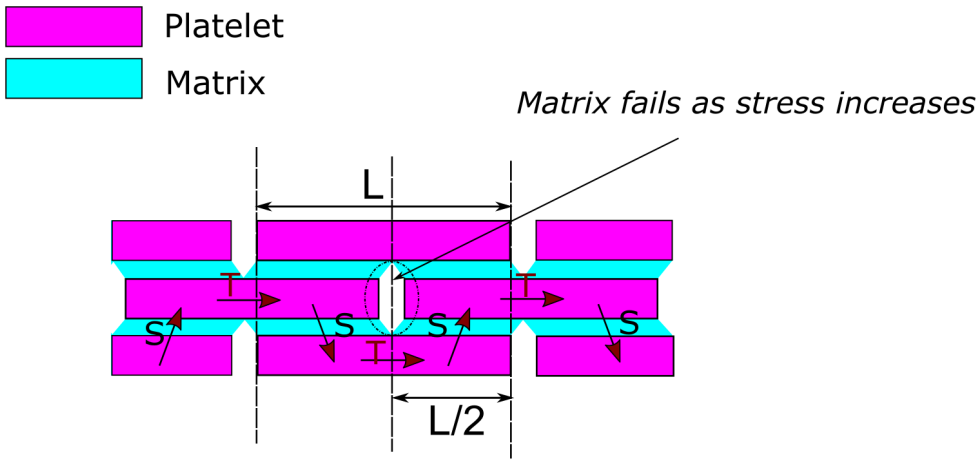

Figure 1.3: Schematic illustration of regular staggered composite with tension shear chain (TSC) model. T, S, and L represent tension inside the platelet, shear in the matrix, and the length of the platelet respectively.

Many underlying mechanisms in biological composites can be interpreted by a regular staggered model. However, there exist other patterns in biological composites such as stairwise staggering in which each platelet in the very next row is shifted up from the left platelet in the preceding row by a distance of L/n, as shown in Figure 1.4 where n is the number of platelets in each period.

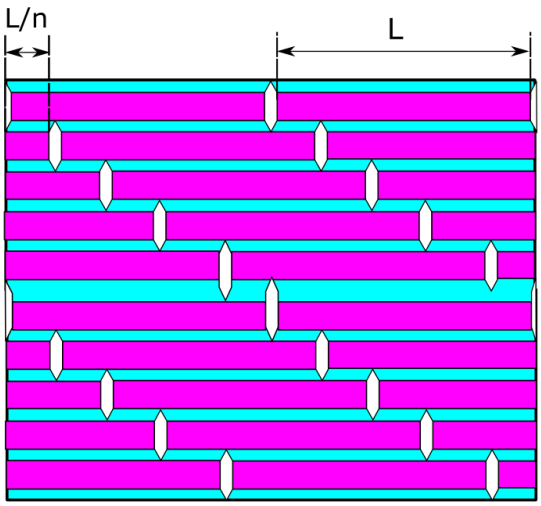

Figure 1.4: Schematic illustration of a stairwise staggered composite with tension shear chain (TSC) model. L and n represent the length of the platelet and number of platelets in a period, respectively. For the model shown in the figure, $n = 5$.

Mechanical properties of unidirectional biological and bio-inspired composites significantly depend on the type of staggered arrangement of platelets in the matrix (Zhang et al., 2010). The variation of mechanical properties of composite structures with the aspect ratio of platelet was compared for different types of staggering including regular and stairwise by Zhang et al. (2010) and it was found that the regular staggered composites possess very high toughness (at lower aspect ratios) whereas the stairwise staggered composites were seen to possess better strength properties.

A hierarchical composite refers to one which is composed of elements that themselves are composites. Several biological composites are hierarchical, including bamboo, bone, and nacre (Rho et al., 1998; Wegst et al., 2015). The hierarchical structure of bone and bamboo is shown in Figure 1.5, bone has a 7-layered hierarchy, where as bamboo has a 6-layered one (Wegst et al., 2015). Hierarchical structures have been shown to be useful to natural materials in obtaining desired mechanical properties. These can be broadly divided into self-similar and non-self-similar depending on whether the structure at each level of the hierarchy is exactly the same or not. If the staggering pattern of platelets is the same in all levels of hierarchy, it is referred to as a self-similar-hierarchical arrangement and vice-versa.

In studies based on quasi-self-similar hierarchical models, it is shown that there exist an optimal hierarchical structure (with an optimal number of hierarchical levels) and an optimal aspect ratio for achieving the maximum material toughness and damping capacity

respectively (Qwamizadeh et al., 2016; Zhang et al., 2011). For example, the modeling of dental enamel which is a hierarchical graded structure was done by Bargmann et al. (2013) and it was found that the fracture energy and fracture strength optimization can be controlled by the hard platelet aspect ratio. Both self-similar and non-self-similar hierarchical structures can be observed in nature, but there are some clear-cut advantages such as penetration resistance and fracture toughness in implementing non-self-similar designs (An et al., 2014).

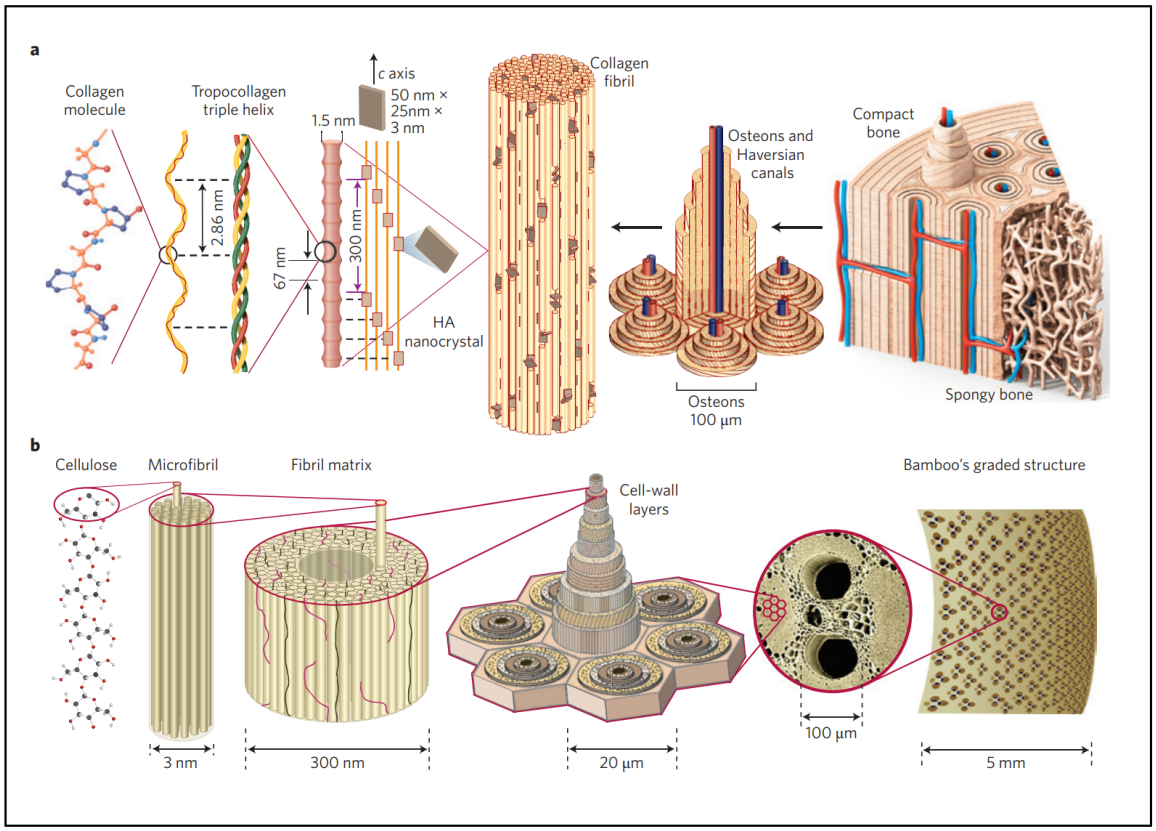

Figure 1.5: Hierarchical structure of bone and bamboo. (a) In bone, there is compact bone at the surface and spongy bone in the interior at macroscale. Compact bone is composed of Osteons and Harvesian Canals. Osteons possess a lamellar structure with fibres arranged in geometrical pattern. These fibres are comprised of several mineralized collagen fibrils which are composed of collagen protein molecules (b) Bamboo is made up of cellulose fibres embedded in a lignin-hemicellulose matrix shaped into hollow prismatic cells of varying thickness. (Reproduced from Wegst et al. (2015))

Bone, nacre, and antler are examples of biological composites that are formed from a bounded selection of components in such a manner that there is a hard and soft phase designed in a hierarchical network with suitable dimensions (Barthelat et al., 2006; Fratzl

and Weinkamer, 2007). The hierarchical arrangement present in the biological materials can be regarded as an attribute through which the properties at different length scales (from atomic scale) are bridged together to contribute to the overall properties at the macro-scale level (Huang et al., 2019). The biological composites so formed have comparatively improved mechanical properties than that of their constituents (Meyers et al., 2008; Raj and Murali, 2020).

Research reveal that the inclusion of hierarchy in structures results in an enormously increased defect-tolerance and toughness, which enables stable crack propagation for a broad domain of crack sizes (Dimas and Buehler, 2012; Sen and Buehler, 2011). It was shown in Dimas and Buehler (2012) that in a silica-based nanocomposite tensile specimen with a single-edged notch, the hierarchical arrangements of silica nanostructures notably changed the stress and strain transfer in the samples. In Mirzaeifar et al. (2015), computational modeling, as well as advanced multi-material 3D printing were used to examine the mechanics of defect-tolerant bio-inspired hierarchical composites. It was found out that the presence of a hierarchical design leads to superior defect-tolerant properties when compared to the brittle base constituents of the composites. Moreover, choosing hierarchical materials with weaker constituents over available synthetic materials can reduce pollution to a great extent thereby lending a helping hand to move a step closer towards a greener and sustainable environment (Meyers et al., 2013; Zhang et al., 2011).

In bio-inspired composites, the geometry plays an important role in achieving the strength required to fulfill their intended structural purposes. The experimental study conducted by Ghimire et al. (2021) on nacre-inspired one hierarchical bio-inspired composites shows that the variation of overlapping length through change in aspect ratio could enhance the hardening, and amplify the mechanical properties. Manno et al. (2019) investigated the effect of slight micro-structural modifications on materials inspired by biological materials, and found that the modification can enhance the properties of the materials by arresting crack propagation. Besides, the structurally inferior building blocks when arranged in a multilevel hierarchy can generate a composite with significantly improved strength compared to that of the constituents (Munch et al., 2008). Several composites and technologies mimicking biological structures have been conceived, designed, and realized (Bai et al., 2016; Carosio et al., 2016; Dutta and Tekalur, 2014; Ingrole et al., 2021; Lei et al., 2012a; Malik and Barthelat, 2016; Saroj et al., 2019; Wilkerson et al., 2018). Some of these were inspired by the hierarchical structural arrangements of biological composites.

A vital and decisive aspect in designing any material is its failure. It is essential to look upon the failure modes and its related influence over the mechanical properties during the

design process of a composite. The geometrical as well as the constituent material features, and the failure mechanisms in a bio-inspired composite governs its final properties. For example, the defect tolerant property observed in a bio-inspired composite is achieved through branching out the cracks through the hierarchical arrangements and letting them to absorb more energy by toughening mechanisms (Mirzaeifar et al., 2015; Shao et al., 2012).

The astounding fracture patterns and deformations in the nacre from pearl oyster were observed by Rabiei et al. (2010) using in situ optical as well as atomic force microscopy. They observed the deformation bands which looked "stair-like", forming an angle with the loading direction and resembling to a tree-like, dense network. The damage study on steel-polyurea nacre-inspired composite plates with nacre-like structure by Wu et al. (2022) analyses the failure toughening mechanisms in which an improved ballistic limit of the conceived composite material was reported. Also, the comprehensive review of various strategies practiced for obtaining composites with excellent mechanical properties by Peng et al. (2022) discusses the lack of theoretical grounds and guidance in the design and optimization in the field of composite materials. The outcomes from the aforementioned and many other studies confirm that the failure patterns and its transition indeed affect the mechanical properties, specially the toughness of the composites (Ghimire et al., 2021; Rabiei et al., 2010; Singh et al., 2019; Tran et al., 2017).

1.2 Objectives, Approach, and Scope of the work

A number of studies elucidating the superior mechanical properties of bio-inspired composites are available in literature (Cheng et al., 2023; Li et al., 2012; Lu et al., 2023; Shu et al., 2020; Wang et al., 2023). When it comes to the case of hierarchical composites, only a few number of studies are available, of which a very limited number of works are done on non-self-similar composites (An et al., 2014; Deng et al., 2023; Henry and Pimenta, 2021; Mazzotti et al., 2023; Song et al., 2023; Yulong et al., 2022; Zhang et al., 2016). The present work is aimed to study the mechanical properties of bio-inspired non-self-similar hierarchical composites, particularly involving the mostly observed staggering patterns in nature: regular and stairwise staggerings. We analyse the different types of failures that can occur in a one hierarchical staggered composite first, so as to get an idea about the failure mechanisms and its influence on the mechanical properties, and quantifying the improvement in the properties. The failure studies are done on one hierarchical models for ease in computation, since in the higher levels of hierarchy models, the analytical equations corresponding to failure mechanisms become more complex.

Optimization is a powerful tool that enables users to configure a composite, according to the requisites. When we looked over the active research, only a very few works probe into optimizing the properties of staggered composites (Barthelat, 2014; Zhang et al., 2011). In our thesis, we generalize and optimize the analytical model of the 2H composites.

The objectives of the present study can be summarized as follows:

- Analyse the failure mechanisms and the influence of failure sequence over the mechanical properties of staggered composites with a single hierarchy.

- Formulation of analytical model to predict the mechanical properties of two hierarchical (2H) non-self-similar bio-inspired staggered composites.

- Analysis of stress variations in 2H non-self-similar staggered composites using finite element analysis (FEA).

- Generalization and optimization of mechanical properties for two hierarchical bio-inspired non-self-similar staggered composites.

We start from analysing the failure mechanisms and their sequence in a one hierarchical staggered composite since only a narrow area of research has been done in the available literature, on the failure mechanisms and associated mechanical properties in a staggered composite (Kim et al., 2018, 2019). The influence of failure modes and their sequence of occurrence over the mechanical properties of the staggered composites is investigated in the present study.

The failure of a composite can occur at different regions such as the vertical or horizontal matrix interface, and the platelet. In Chapter 2, the various failure modes that can occur in a staggered composite and their sequence is analysed. To analyse the stairwise staggered model, we introduce a modified shear lag model (model in which the vertical matrix interface is included in the analysis, unlike the TSC model) capable of predicting the various properties such as the stiffness, strength, and the toughness. The proposed model can also be used to analyse the results from TSC model by altering certain variables in the equations.

Once the failure modes and sequences are studied in detail for a single hierarchical (1H) staggered composite, we develop the equations to compute the mechanical properties of two hierarchical (2H) composites with stairwise and regular patterns' non-self-similar combinations. These particular configurations are chosen, owing to their fine mechanical properties and their distinguishable presence in most of the biological composites (Zhang

et al., 2010). We formulate analytical equations to predict the mechanical properties and analyze them in detail for two hierarchical non-self-similar bio-inspired composites in Chapter 3. The model is then generalized later so that it can be used to find the mechanical properties for a wide range of inputs. The variation of stress inside a 2H non-self-similar model is examined using FEA in Chapter 4. The FEA is done for two different configurations of 2H non-self-similar staggered models.

The analytical model to evaluate the different mechanical properties for a 2H non-self-similar model is generalized for various parameters, in Chapter 5. The generalized model is then optimized with the help of ternary diagrams using MATLAB (The Mathworks, 2020). Finally, we conclude our study in Chapter 6, where the future scope of the work is also looked into. The results obtained seem to be promising and helpful in the design and analysis of two hierarchical bio-inspired composites.

Chapter 2

Effect of Failure Sequence on Mechanical Properties of Staggered Composites

In order to deal with the optimization of the mechanical properties of a bio-inspired composite, a study about the possible modes of failure in the composite is required. This Chapter is focused on the influence of failure modes over the mechanical properties such as stiffness, strength, and toughness after the failure of different interfaces in single hierarchical staggered bio-inspired structures such as regular and stairwise staggered arrangements where stiff platelets are embedded in a pliant matrix. In order to find these properties, a novel analytical model for stress transfer and effective Young's modulus of a stairwise staggered composite is developed based on composite micro-mechanics principles. The results indicate that the failure sequence influences mechanical properties such as stiffness, strength, and toughness. It is also found that the vertical interface joining the short end of platelets is more susceptible to fail first, rather than the more extensive matrix-platelet interface, and a major contribution of toughness is obtained from the vertical interface failure, which is ignored in previous studies for estimating the toughness. The influence of significant parameters like Young's moduli ratio of platelet and matrix (E_p/E_m) over the strength at different modes of failure showed that the strength at first and second failures increases as the E_p/E_m ratio increases. Also, the results from the case study show a good agreement with the parametric studies and reveal that the contribution of toughness from vertical interface failure is significant for the selected materials at higher platelet aspect ratios. The findings of this study hold significant potential for predicting the failure sequences with their quantified contributions towards the mechanical properties of a bio-inspired staggered composite.

2.1 Introduction

The development of exceptionally strong structural materials with lightweight, which can outperform the existing realized materials, is a trending area in the field of material science as well as engineering (Hao et al., 2020; Mirkhalaf et al., 2016; San Ha and Lu, 2020; Yang et al., 2018). As we discussed in the previous Chapter, naturally occurring materials such as nacre - the inner layer of a sea shell, bone, and bamboo are regarded as ideal candidates; they have markedly superior mechanical properties compared to that of their elemental constituents from which they are made up of (Abid et al., 2018; Anup et al., 2007; Ji and Gao, 2004a; Meyers et al., 2008, 2013; Wegst et al., 2015).

Failures are inevitable in all materials, which makes it essential to study the possible modes of failure in a material before using it for its intended purposes. The various failure modes that can occur in biological as well as bio-inspired structures shall be thoroughly analyzed in order to estimate their mechanical properties. Several researchers have come up with failures analysis of biological and bio-inspired structures (Barthelat et al., 2013; Häsä and Pinho, 2019; Khaderi et al., 2014; Slesarenko et al., 2017). The failure criterion developed by Barthelat et al. (2013) considers the initial defects and complex field of stresses inside the platelet; and two criteria, namely 'optimum criterion' and 'conservative criterion,' were developed. These analyses consider the shear traction occurring on the inclusions as uniform and point forces, respectively, and enabled a wide range of applicability of the criteria for different interface materials.

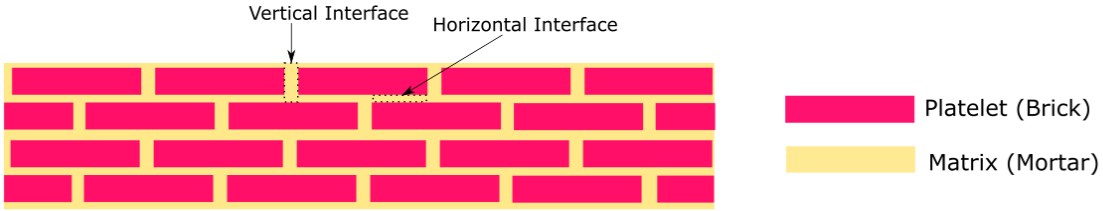

Figure 2.1: Schematic illustration of a regularly staggered composite in which vertical (between end sides of two platelets) and horizontal (between the longitudinal sides of two platelets) interfaces are shown. The stress transfer through the vertical and horizontal interface occurs through normal and shear stresses, respectively.

Kim et al. (2019) proposed a fracture map that could capture the transition of failure mechanisms spotted in the crack phase field simulations. In the study by Kim et al. (2019), three distinct failure mechanisms were identified according to the sequence of failure: the soft tip or the vertical interface, the soft shear zone or the horizontal interface, and the

platelet. Figure 2.1 shows the vertical and horizontal interfaces and platelets which are the regions in a brick-and-mortar structure where failure may occur.

The mechanical behavior of composite samples with different shapes of platelets was analyzed using damage mechanics by finite element simulations in the study conducted by Askarinejad et al. (2018). Here, the results indicated that the vertical interface failed first, after which the horizontal interface failed (Askarinejad et al., 2018). The numerical study using the Continuous Damage Random Threshold Fuse Network Model (CDRFM) by Nukala and Simunovic (2005) could effectively capture the B-and-M architecture as well as the damage unfolding in the matrix interface between the platelets in a nacre-like model. Moreover, the numerical response obtained by Nukala and Simunovic (2005) agrees well with the experimental responses of nacre, such as its stiffness, strength, and toughness. The aforementioned research works as well as several other studies, investigate either the failure mechanisms or the mechanical properties of bio-inspired composites (Askarinejad et al., 2018; Greco et al., 2020; Khaderi et al., 2014; Kim et al., 2018, 2019; Zhang et al., 2010; Zhou et al., 2021).

There exist only a few papers that have taken into account the failure modes as well as the mechanical properties of bio-inspired composites. In the work done by Askarinejad and Rahbar (2018), the closed-form solutions for layer displacements were formulated by developing a new imperfect interface shear-lag theory for regularly staggered models. They found that the interfacial properties hold a key role in controlling the mechanical properties of the lamellar structure. The importance of vertical interfaces over the stiffness and strength of the regularly staggered bio-inspired composites was investigated by Begley et al. (2012). Their work has also optimized peak strength, stiffness, and toughness by varying the brick geometry and mortar phase's strength. However, a detailed analysis of the effect of the failures on the mechanical properties of the bio-inspired composite is an area that is yet to be explored. The present study delves into the influence of different stages of failures occurring in bio-inspired composite and the formulation of mechanical properties considering these stages of failures.

In order to examine the failure process and, consequently, the mechanical properties, we need to use models depicting stress transfer in biological structures. There exist many such models for analyzing the stress transfer mechanism in biological composites, of which the tension shear chain (TSC) model by Ji and Gao (2004a) and the shear lag model by Kotha et al. (2000) are popular. The major difference between these models is that in the TSC model, the normal stresses at the ends of platelets are ignored (Ji and Gao, 2004a). In the TSC model, there is no stress transfer from one platelet to another through the vertical

interfaces at the ends of platelets. The stress transfer through the matrix at the vertical interfaces is also considered to predict the elastic properties of staggered composites in the improved analytical model proposed by Kim et al. (2018). In the present study, for regularly staggered arrangement, a modified version of the shear lag model put forward by Kim et al. (2018) is used for the failure criterion and estimation of mechanical properties. Even though a few pieces of research on which bio-inspired stairwise staggered models conceived using the Tension Shear Chain (TSC) model are available (Mathiazhagan and Anup, 2016a; Zhang et al., 2010), the formulation for mechanical properties for a stairwise staggered composite using the shear lag model is not available in the open literature. Here, we develop a novel analytical model to compute the stress transfer and composite modulus in stairwise staggered composites based on composite mechanics principles. The mechanical properties of regular and stairwise staggered composites are analyzed with varying significant parameters such as Young's moduli ratio of platelet and matrix (E_p/E_m) and normal strength of platelet ($\sigma^p_{critical}$), for a range of platelet aspect ratios. A case study is also done with the material-sets chosen from recent research papers (Askarinejad et al., 2018; Nukala and Simunovic, 2005; Yang et al., 2019), so that realistic and reliable data of mechanical properties could be generated.

Section 5.2 describes the methodology adopted for determining the possibility for different sequences of failure of vertical and horizontal interfaces and platelets. The study is done for two different staggerings, namely regularly and stairwise in Sections 2.2.1 and 2.2.2, respectively. The effect of the relevant sequence of failures on the mechanical properties such as stiffness, strength, and toughness is investigated in Sections 2.4.1, 2.4.2 and 2.4.3. A case study is included in Section 2.5 using different realistic material-sets from recent research works. We conclude the study in Section 2.6 where the significant outcomes and future scope of the study is summarized.

2.2 Methodology

Three possible modes of failure exist in a brick-and-mortar structure: failure of vertical and horizontal interfaces and the platelet (see Figure 2.1). These failure modes are examined for two different types of arrangement: regularly staggered and stairwise staggered composite. In order to undertake this analysis, we consider the modified shear lag model put forward by Kim et al. (2018) since it is the most recent model and it considers the horizontal as well as the vertical matrix thickness between two platelets.

The representative volume element (RVE) for a regularly staggered composite by Kim et al. (2018) is shown in Figure 2.2, with platelets of length (L_p), width ($2b$), the thickness of matrix along the horizontal and vertical direction, $2L_b$ and h respectively. In this figure, regions 1 and 2 represent platelets; the normal stress varies along the horizontal direction of the platelet. Moreover, the shear stress in region 3 is formulated as a function of the distance along the length of the platelet, which is discussed in detail in Section 2.2.1.

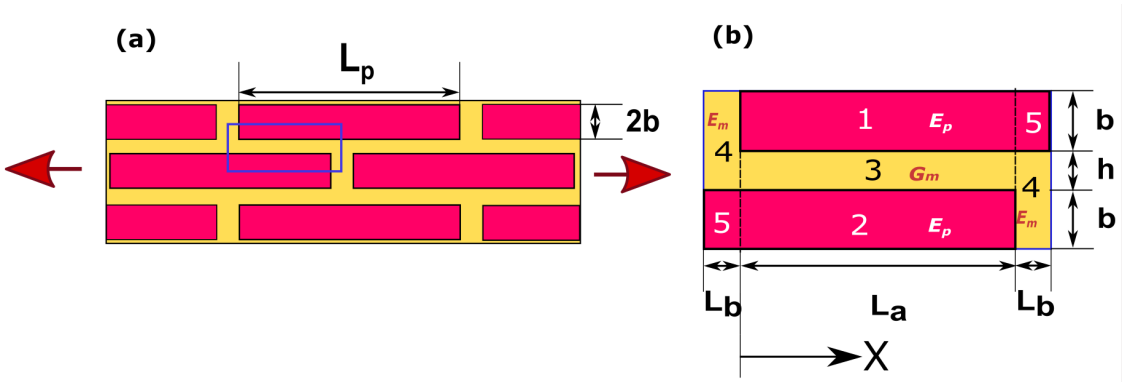

Figure 2.2: (a) Schematic diagram of a regularly staggered composite with length and width of platelet L_p and h respectively (b) Representative Volume Element (RVE) for a regularly staggered composite, proposed by Kim et al. (2018); E_p and E_m are Young's moduli of platelet and matrix respectively, and G_m is the Shear modulus of the matrix.

The normal stress at matrix region 4 is assumed to be equivalent to the normal stress at the end of the platelet owing to the compatibility requirements of the model. It is assumed that the stresses in regions 4 and 5 are under uniform tensile stress (Kim et al., 2018). For the analysis of the stairwise staggered model (SSM), we develop the analytical formulation using the existing representative volume element (RVE) proposed by Kim et al. (2018).

2.2.1 Regularly Staggered Composite

Figure 2.3 shows a full platelet in a regularly staggered composite, which is divided into 3 regions for defining the normal and shear stresses along the platelet and platelet matrix interface respectively, as a function of distance measured along the platelet (x). The expressions for the normal stress along a full platelet and the shear stress along the full platelet matrix interface with their maximum values and locations developed using the formulations by Kim et al. (2018) are given in Appendix A.

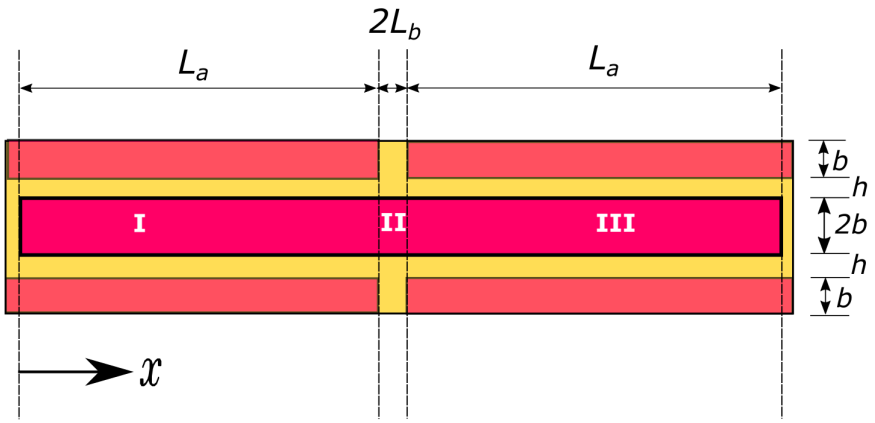

Figure 2.3: Regions defined for the formulation of variation of normal stress along a platelet in a regularly staggered composite. Region I ranges from $x = 0$ to $x = L_a$, Region II from $x = L_a$ to $x = L_a + 2L_b$ and Region III from $x = L_a + 2L_b$ to $x = L_p$, where $2L_b$ is the thickness of vertical matrix interface, L_a is the overlapping length in a half platelet and L_p is the length of a full platelet.

In the following section, the equations for the stress distributions in platelet and matrix for a stairwise staggered model are developed using the RVE shown in Figure 2.2 (b).

2.2.2 Stairwise Staggered Composite

Here, we develop the expressions for the normal and shear stresses along a platelet and matrix interface, respectively, in a stairwise staggered model. The maximum stress values (both normal and shear) would be used to determine the modes of failure. To develop these expressions, a model of stairwise staggered composite is considered as shown in Figure 2.4 (a), in which a single full platelet is chosen with the adjacent rows up to half the widths of the platelets in the adjacent rows. It can be noticed that any full platelet in the stairwise staggered composite shown in Figure 2.4 (a) can be represented using Figure 2.4 (b). This is done so as to identify the RVEs as shown in Figure 2.1(b), thereby making the computation easier. Four numbers of RVEs (ⓐ, ⓑ, ⓒ and ⓓ) as shown in Figure 2.4 (c) are obtained of which the RVEs represented by same colors have identical geometry.

The variation of stresses along a platelet in a stairwise staggered composite is found by taking the average stresses at the top (ⓒ&ⓓ) and bottom (ⓐ&ⓑ) sections according to the location of the point from the origin as shown in Figure 2.4 (c); using the available equations for the RVEs (See Figure 2.1 (b)). For defining the variation of stresses along a platelet, the coordinate axes of the different RVEs are shifted such that the left end of the chosen full platelet is set to the origin. This enables us to find out the stresses at any section

of a platelet in a stairwise staggered composite using a single function. It also offers a smoother computation procedure for finding the average stress at any section in a staggered composite when the strength is to be found out.

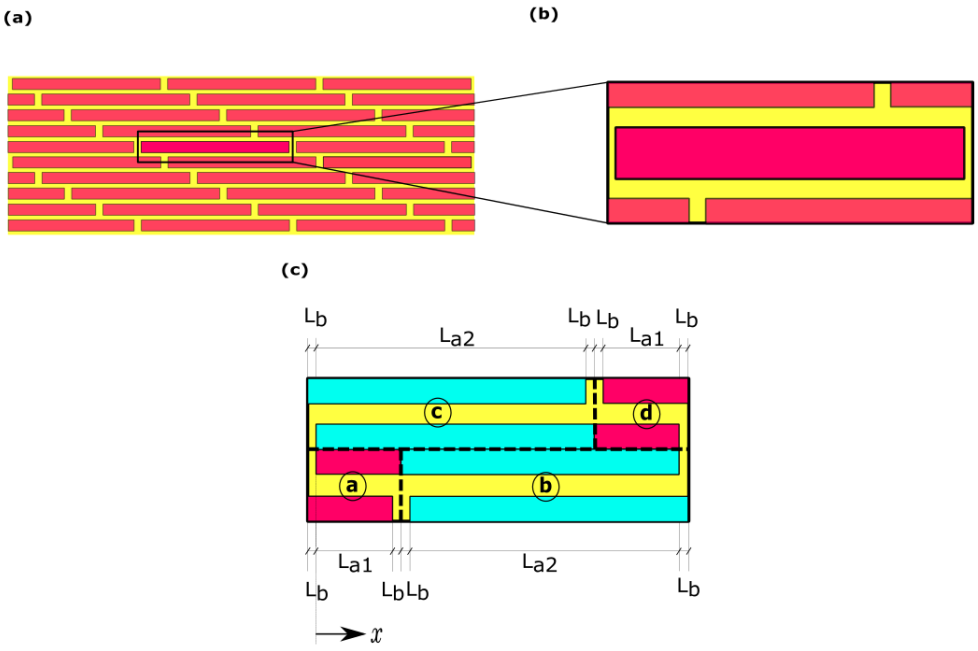

Figure 2.4: (a) Schematic diagram of a stairwise staggered composite in which a full platelet is chosen for formulating the variation of stress (b) The selected full platelet with the top and bottom rows (c) Identification of four RVEs ⓐ, ⓑ, ⓒ and ⓓ as shown in Figure 2.1 (b)

When the x-axis is set as shown in Figure 2.4 (c), the equations for RVE ⓐ and ⓒ can directly be obtained using the available equations for regular staggered composites by whereas for the RVE ⓑ, $X = x - (L_{a1} + 2L_b)$ and for the RVE ⓓ, $X = x - (L_{a2} + 2L_b)$ where X and x represent the x-coordinates of the regular staggered RVE (as shown in Figure 2.1 (b)) and in the present study, respectively.

On applying the above conditions and simplifying, the expressions for stresses in RVEs ⓐ, ⓑ, ⓒ and ⓓ along the center platelet shown in Figure 2.4 (c) as a function of the uniform stress in region 5 (refer Figure 2.1(b)) of the platelet (σ_u^p) are obtained as follows:

$$\sigma_a(x) = \sigma_u^p \left(\frac{\gamma A_1 \sinh(A_1) + B_1 \cosh(A_1) + \lambda A_1 \sinh\left(A_1 \left[\frac{2n(x+L_b)-L}{L-2nL_b}\right]\right)}{2A_1 \sinh(A_1) + B_1 \cosh(A_1)} \right) \tag{2.1}$$

$$\sigma_b(x) = \sigma_u^p \left(\frac{\gamma A_2 \sinh(A_2) + B_2 \cosh(A_2) + \lambda A_2 \sinh\left(A_2 \left[\frac{L(n+1)-2n(x+L_b)}{(n-1)L-2nL_b}\right]\right)}{2A_2 \sinh(A_2) + B_2 \cosh(A_2)} \right) \tag{2.2}$$

$$\sigma_c(x) = \sigma_u^p \left(\frac{\gamma A_2 \sinh(A_2) + B_2 \cosh(A_2) + \lambda A_2 \sinh\left(A_2 \left[\frac{2n(x+L_b)-L(n-1)}{(n-1)L-2nL_b}\right]\right)}{2A_2 \sinh(A_2) + B_2 \cosh(A_2)} \right) \tag{2.3}$$

$$\sigma_d(x) = \sigma_u^p \left(\frac{\gamma A_1 \sinh(A_1) + B_1 \cosh(A_1) + \lambda A_1 \sinh\left(A_1 \left[\frac{L(2n-1)-2n(x+L_b)}{L-2nL_b}\right]\right)}{2A_1 \sinh(A_1) + B_1 \cosh(A_1)} \right) \tag{2.4}$$

Thus, the normal stress along a platelet in a stairwise staggered composite, $\sigma_{sw}^p(x)$ can be written as,

$$\sigma_{sw}^p(x) = \frac{\sigma_{sw}^{p,top}(x) + \sigma_{sw}^{p,bot}(x)}{2} \tag{2.5}$$

where,

$$\sigma_{sw}^{p,top}(x) = \begin{cases} \sigma_c & \text{if } 0 \le x < L_{a2} \\ \sigma_u^p & \text{if } L_{a2} \le x < L_{a2} + 2L_b \\ \sigma_d & \text{if } L_{a2} + 2L_b \le x \le L_p \end{cases} \tag{2.6}$$

$$\sigma_{sw}^{p,bot}(x) = \begin{cases} \sigma_a & \text{if } 0 \le x < L_{a1} \\ \sigma_u^p & \text{if } L_{a1} \le x < L_{a1} + 2L_b \\ \sigma_b & \text{if } L_{a1} + 2L_b \le x \le L_p \end{cases} \tag{2.7}$$

where,

$$\sigma_u^p = \frac{2\sigma_{critical}^p \left(2A_2 \sinh(A_2) + B_2 \cosh(A_2)\right)}{2\left[\gamma A_2 \sinh(A_2) + B_2 \cosh(A_2)\right] + A_2 \lambda \left[\sinh\left(A_2\, C_1\right) + \sinh\left(A_2\, C_2\right)\right]} \tag{2.8}$$

The terms used in the above the expressions are provided in Appendix B.

It is seen that the maximum normal stress in the platelet (σ^p_{max}) in a stairwise staggered composite occurs at $x = L_{a1} + 2L_b$ and is equal to σ^p_u. Also, the shear stress at the top interface is maximum at $x = L_{a1}$, and at the bottom, it is maximum at $x = La_2$.

2.2.2.1 Formulation of equations for modulus of elasticity of stairwise staggered composites

There are a number of papers available in open literature for the evaluation of the mechanical properties of regularly staggered composites. However, for the case of stairwise staggered composites, only limited researches have taken place so far. The modified shear lag model by Kim et al. (2018) for regularly staggered composites which gives analytical results closer to Finite Element results is chosen to extend for obtaining the results for a stairwise staggered composite. Inorder to accomplish this, a Representative Volume Element (RVE) of a stairwise staggered composite with $n = 5$ as shown in Figure 2.5 is considered and is divided into several parts such that each part resembles to a regular staggered RVE. The modulus of elasticity for each part is then calculated, after which an integration for the whole volume is done to arrive at the corresponding equation for the stairwise staggered model. Here, we have considered $n = 5$ as an example, but the equations could be formulated for any other values of n along similar lines.

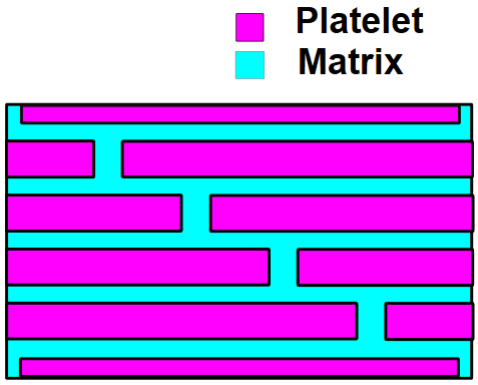

Figure 2.5: Representative Volume Element (RVE) of a Stairwise Staggered Composite with a period, n=5

Figure 2.6 shows the division of RVE of the stairwise staggered model. It can be seen that only for the first and last rows, complete unit cells are obtained. To obtain a complete unit cell for the remaining rows, the RVE is extended towards the right, and it can be seen that the left part matches with that of the extended right parts, and it forms a complete unit cell.

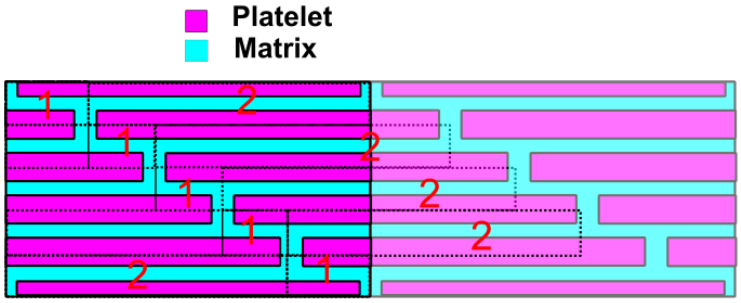

Figure 2.6: Division of Representative Volume Element of a Stairwise Staggered Composite with n=5

Figure 2.7 shows the zoomed view of parts 1 and 2. Young's modulus of part 1 and part 2 can be found using equation (23) or (24).

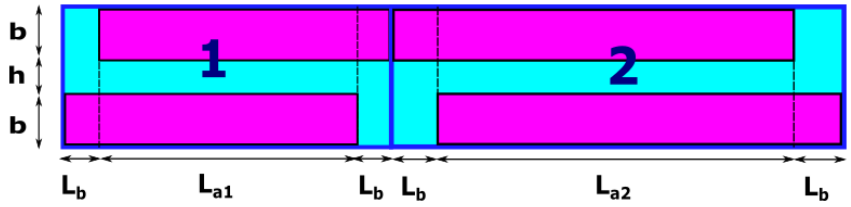

Figure 2.7: zoomed view of parts 1 and 2 forming Kim's model

The effective elastic modulus $\bar{E_R}$ for a regularly staggered composite as shown in Figure 2.2 (b), is given by Kim et al. (2018) in terms of non dimensionalized parameters as,

$$\bar{E}_R = E_p \frac{(B + (1 - \beta + \beta/2\phi)A\tanh(A))(\phi + (1-\phi)\beta + 2\xi\phi)}{(1 - \beta + \beta/2\phi + 4\xi)A\tanh(A) + 1 + \beta + B} \tag{2.9}$$

For limiting cases where $\alpha, \beta, \xi << 1$, the above equation becomes, (Kim et al., 2018)

$$\bar{E} = \frac{[A\sinh(A)] + [B\cosh(A)]\phi}{\cosh(A) + A\sinh(A) + B\cosh(A)} \tag{2.10}$$

Please refer to Appendix A for the abbreviations used.

For computing the Young's modulus of the stairwise staggered composite, we observe that parts 1 and 2 are in series. Therefore, the forces experienced by the parts are the same, while they share the total deformation.

This gives the effective Young's modulus as (Gibson, 2016),

$$\bar{E}_S = \left[\frac{A_{11}}{AE_1} + \frac{A_{22}}{AE_2}\right]^{-1} \tag{2.11}$$

which is similar to that of the inverse rule of mixture. In the above equation, A_{11} and A_{22} represent the respective areas of part 1 and 2 (see Figure 2.7), $A = A_{11} + A_{22}$. Also, E_1 and E_2 are the Young's moduli of part 1 and 2, respectively which are given by,

$$E_1 = E_p \frac{(B_1 + (1 - \beta + 2\beta/\phi)A_1 \tanh(A_1))(\phi + (1-\phi)\beta + 2\xi_1\phi)}{(1 - \beta + 2\beta/\phi + 4\xi_1)A_1 \tanh(A_1) + 1 + \beta + B_1} \tag{2.12}$$

$$E_2 = E_p \frac{(B_2 + (1 - \beta + 2\beta/\phi)A_2 \tanh(A_2))(\phi + (1-\phi)\beta + 2\xi_2\phi)}{(1 - \beta + 2\beta/\phi + 4\xi_2)A_1 \tanh(A_2) + 1 + \beta + B_2} \tag{2.13}$$

2.2.3 Comparison of Analytical results with Finite Element Results for the Stairwise Staggered Model

In this subsection, we compare the results of the developed expressions for normal stress along a stairwise staggered composite (Equation B.5) with that of the finite element analysis (FEA). For this, a stairwise staggered model (SSM) with a platelet volume fraction of 0.8 and platelet aspect ratio of 12 is modeled using the FEA software suite ABAQUS (SIMULIA, 2022). The material properties chosen for carrying out the FE analysis and subsequent comparison are Young's modulus of platelet, $E_p = 100$ GPa, Young's modulus of the matrix, $E_m = 4$ GPa, normal strength of the matrix, $\sigma^m_{critical} = 35$ MPa, normal strength of platelet, $\sigma^p_{critical} = 1400$ MPa, and shear strength of the matrix, $\tau^m_{critical} = 20.16$ MPa.

For the comparison of the developed analytical model of SSM, a displacement of 0.01 magnitude is applied on the right edge along with periodic boundary conditions (PBC) on the four edges of the FE model of SSM. PBCs are applied since the stairwise staggered configuration is a periodic structure in which the staggering repeats after n number of rows of platelets. We take $n = 5$ for the analyses in the present study. The periodic boundary condition is applied by using python script, which is given in the Appendix.

The model is meshed with plane stress (CPS4R) elements (a total of 25,002 elements). The normalized stress (stress/average stress) along a platelet from the FEA is compared with the values obtained using the developed Equation 2.5 as shown in Figure 2.8.

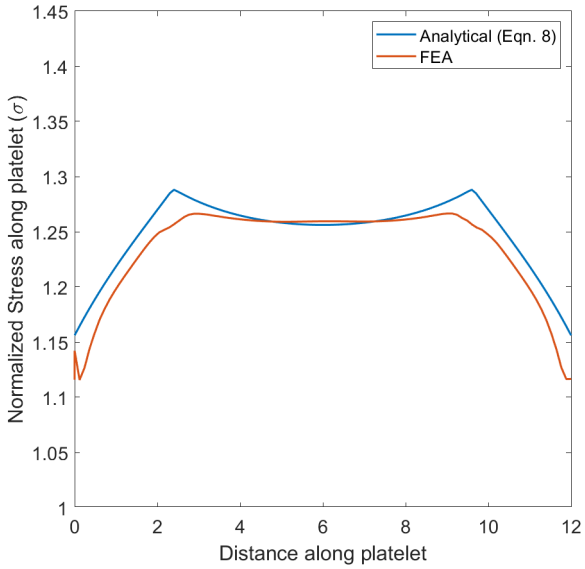

Figure 2.8: Comparison of normalized stress along a platelet in an SSM using analytical (Equation 2.5) and FE results (Note that the y-axis starts from 1; The link to the Python and Matlab scripts for reproducing this figure can be found here)

Figure 2.8 shows a very good match between analytical and FE results (maximum variation of 2.4%) except at the ends of the platelet, where there is a mismatch. This could be due to the fact that the equations of the modified shear lag model do not account for the stress concentration at the sharp ends of the rectangular platelets (Kim et al., 2018).

The strength of a staggered composite depends on the sequence and mode of failure. Here, mode represents the type of failure, i.e., whether it is a vertical interface failure (VIF) or horizontal interface failure (HIF), or platelet failure (PF) that occurs. Sequence refers to the order of the above-mentioned modes of failure. In order to examine the mode and sequence of failures, we compute the maximum values of stresses in the vertical interface, matrix, and platelet and then normalize with the corresponding strength of the materials at the respective regions to define three different non-dimensional numbers $\frac{\sigma^m_{critical}}{\sigma^m_{max}}$, $\frac{\tau^m_{critical}}{\tau^m_{max}}$, and $\frac{\sigma^p_{critical}}{\sigma^p_{max}}$; comparing these ratios, the mode of failure can be ascertained. These three non-dimensional numbers are analyzed by varying the platelet aspect ratios for the regular and stairwise staggering types of composites in the following sections.

The non-dimensional parameters $\frac{\sigma^m_{critical}}{\sigma^m_{max}}$, $\frac{\tau^m_{critical}}{\tau^m_{max}}$, and $\frac{\sigma^p_{critical}}{\sigma^p_{max}}$ indicate the state of stress at the different regions (vertical interface, horizontal interface, and platelet) with respect to the corresponding strengths. The region with the least value of the parameter will reach its strength with minimum increase in stress, leading to failure of that particular region. Once the vertical interface failure (VIF) has occurred, the parameter B in the equations

for calculating stresses is set to zero since the load transfer through the vertical interface is absent. Figure 2.9 shows the classification of failure modes in which the possibility of occurrence of different types of failures and the sequence in which they can occur in a regular or stairwise staggered composite are indicated as a flow chart.

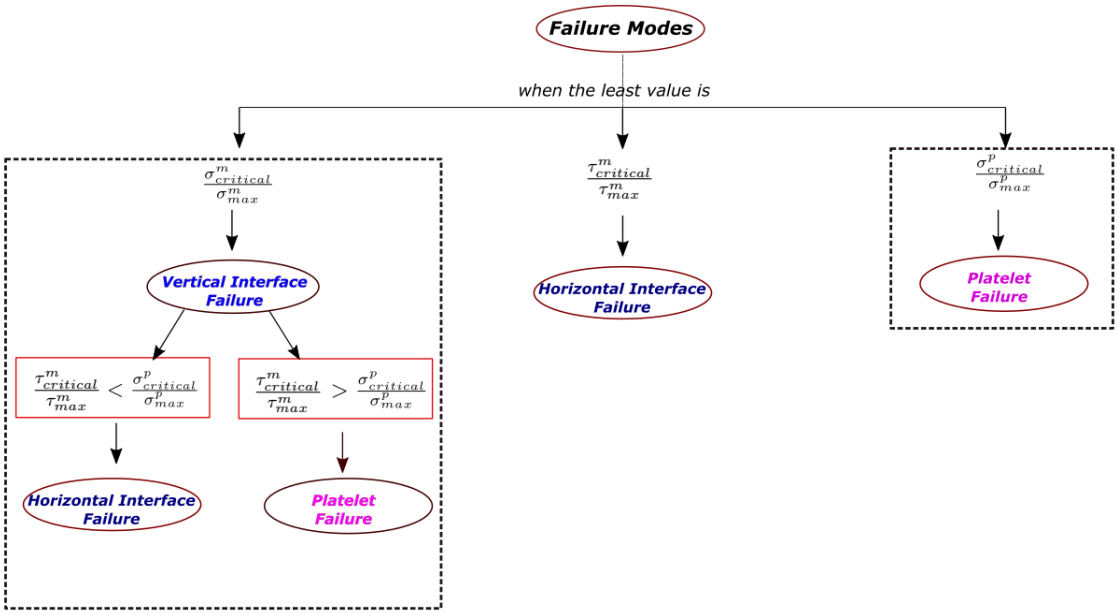

Figure 2.9: Flowchart showing Classification of Failure Modes, the sequences shown in dashed boxes represent the ones identified by Kim et al. (2019)

The first two sequences begin with the vertical interface failure, where the stress in the vertical interface reaches the normal strength of the matrix at the vertical interface. Once the VIF has occurred, either the matrix at the horizontal interface or the platelet may fail, which gives two sequences of failure starting with VIF. The third and fourth failure sequences are commenced by HIF in which the stress in the horizontal interface of the matrix reaches the shear strength of the matrix at that region. After HIF, it is assumed that the stress transfer in the composite takes place through only normal stresses. The last sequence of failure corresponds to a single-step failure where the stress in the platelet reaches the platelet strength. The composite will no longer be able to transfer the stresses if the platelet fails first since a significant amount of stress is transferred through the platelets before platelet failure. Of the five sequences of failures shown in Figure 2.9, the sequences identified by Kim et al. (2018) are represented in dashed boxes. The sequence in which the primary failure of the horizontal interface occurs is mainly influenced by the lesser thickness of the horizontal interface. i.e., in staggering structures with a horizontal interface

having considerably higher thickness than that of the vertical interface, the horizontal interface is more likely to fail first.

The strength of a bio-inspired composite increase with an increase in overlap length (L_a), but after a critical value, it decreases (Gao, 2006). One critical parameter which could influence the stress transfer in these composites is the half non-overlap length to overlap length ratio ($\xi = \frac{L_b}{L_a}$, see Figure 2.2) (Kim et al., 2018). In this study, the half non-overlap length to overlap length ratio (ξ) is kept constant (1/50) to ensure this parameter does not influence the results.

2.3 Results and Discussion

The three modes of failure, as described in Figure 2.9 could affect the mechanical properties of composites in different ways. For example, if the first mode of failure is platelet failure, the composite is considered to be failed; it will no longer be able to carry any further load. However, if the first model of failure is vertical interface failure, the composite would be able to carry the load through the horizontal interface and platelets. The analysis of the composite in which VIF has occurred first can be done by ignoring the vertical interface. The variation of mechanical properties such as stiffness, strength, and toughness are analyzed in the following sections by considering the failure modes as a major parameter. In order to accomplish this, we compute the mechanical properties for the following cases: (a) structure with no failure, (b) structure which has undergone failure, and corresponding stress transfer element removed from the equations.

2.4 Mechanical Properties

The mechanical properties obtained for bio-inspired structures depend on the modes and sequence of failures. To find the sequence and mode of failure, the ratios $\frac{\sigma^m_{critical}}{\sigma^m_{max}}$, $\frac{\tau^m_{critical}}{\tau^m_{max}}$, and $\frac{\sigma^p_{critical}}{\sigma^p_{max}}$ are drawn against the platelet aspect ratio (ρ) varying from 1 to 120. Here as an example, we show the failure ratios in Figure 2.10 drawn with representative mechanical properties values similar to that of nacre with aragonite platelets and organic matrix (Askarinejad et al., 2018). These values are further used for case studies in section 2.2.3 (See material set-5, Table 2.1).

It can be seen from Figure 2.10 (a) that the VIF occurs first for aspect ratios less than 65, beyond which PF occurs first. Similarly, for the stairwise staggered composites (see Figure 2.10 (b)), it is seen that the VIF occurs first for aspect ratios less than 31, beyond which HIF

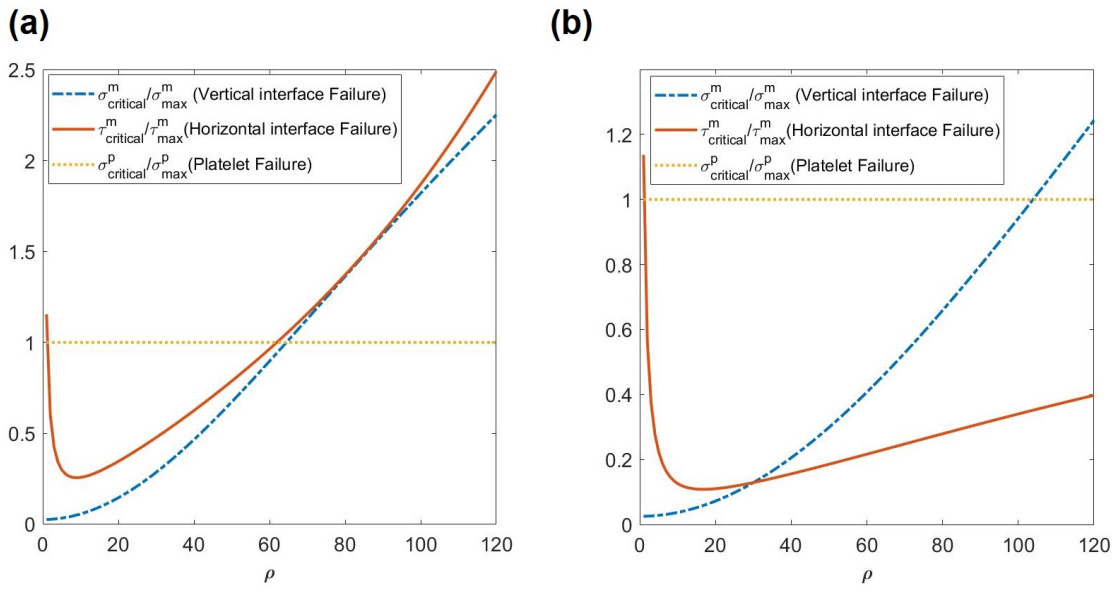

Figure 2.10: Variation of $\frac{\sigma^m_{max}}{\sigma^m_{critical}}$, $\frac{\tau^m_{critical}}{\tau^m_{max}}$ and $\frac{\sigma^p_{critical}}{\sigma^p_{max}}$ with aspect ratio ρ, for (a) regularly staggered composites and (b) stairwise staggered composites, with material properties Set-1 (The link to the Matlab scripts for reproducing this figure can be found here)

occurs first. (VIF was observed to occur first at lower aspect ratios for all the material-sets in Table 2.1). In order to analyze the sequence of failures and their influence on mechanical properties, we take up the stress-strain curve depicting such a sequence of failures. Here, the sequence of failures is VIF followed by either HIF or PF. Wherever these sequences differ, we explicitly state that and compute mechanical properties accordingly. Consider a representative stress-strain plot for a regular staggered model with stress transfer even through the vertical interface as shown in Figure 2.11. In Figure 2.11, σ' is the maximum stress at the first failure (VIF). The strain corresponding to this point is obtained by dividing the strength by the Young's modulus of the composite ($E_{B\neq 0}$). The strength at the first failure ($\sigma'_{B=0}$) can be obtained by multiplying the strain at the first failure with the Young's modulus of composite with vertical interface removed ($E_{B=0}$). The first failure is observed to be VIF for most of the cases. Once VIF has occurred, the parameter B in the equations for calculating stresses is set to zero since the load transfer through the vertical interface region is absent. Thus, the strength at the second mode of failure (σ'') is computed using equations with the parameter $B = 0$.

The toughness is found in terms of the work of fracture-area under the stress-strain curves and is plotted against the aspect ratio. The toughness so obtained is compared with that of the tension shear chain (TSC) model put forward by Zhang et al. (2010) and is found

to match except at a few points in the initial region. For plotting the toughness graphs, the parameters were set such that $E_p/G_m = 1000$, $\sigma^p_{critical}/\tau^m_{critical} = 10$ and $\xi = 1/50$ in the equations for stresses (Eq. A.8 & 2.5).

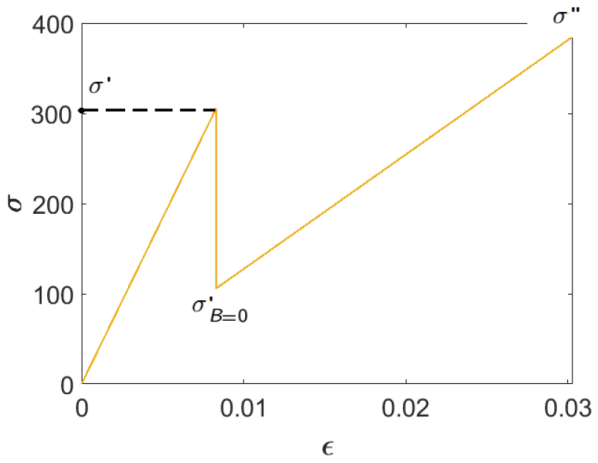

Figure 2.11: Stress (σ) vs strain (ϵ) for a regularly staggered model, σ' and σ'' denotes the strengths at the first and second failures, $\sigma'_{B=0}$ is the strength after VIF.

The area under the stress-strain curve is computed to obtain the toughness of a staggered composite as,

$$w = \frac{\sigma'^2}{2E_{B\neq 0}} + \frac{\sigma''^2}{2E_{B=0}} - \frac{\sigma'^2 E_{B=0}}{2E^2_{B\neq 0}} \tag{2.14}$$

where σ' is the strength at the first failure, $E_{B\neq 0}$ is the corresponding Young's modulus at the first failure, $\sigma'_{B=0}$ is the strength after the first failure, and σ'' is the strength at the second failure.

The most important material parameters that could be responsible for the overall mechanical properties of a composite are the Young's moduli ratio between the platelet and matrix (E_p/E_m) and the normal strength of the platelet. So, for analyzing the effect of failure modes on the mechanical properties of the composite, we consider the variation in the aforementioned parameters. First, we choose a model with Young's modulus of platelet (E_p) and matrix (E_m) as 220 GPa and 1.1 GPa, respectively. Keeping the normal ($\sigma^m_{critical} = 30$ MPa) and shear strength ($\tau^m_{critical} = 17.3$ MPa) of the matrix as a constant, the normal strength of the platelet ($\sigma^p_{critical}$) is varied from 10 to 200 times that of $\tau^m_{critical}$, to study the effect of change of platelet strength in the mechanical properties. In the second case, keeping $\sigma^p_{critical} = 2500$ MPa, $\sigma^m_{critical} = 43.4$ MPa, $\tau^m_{critical} = 25$ MPa, and $E_m = 4000$ MPa, E_p is varied from 10 to 1000 times that of E_m to study the effect of the

E_p/E_m ratio over the failure modes and the mechanical properties. The material properties are selected so as to represent a range of material combinations used in realistic studies. Here, we examine how the mechanical properties of the regularly and stairwise staggered models vary with aspect ratio for these variations in parameters. We also look at the effect of failure on these properties. For the case of stairwise staggered composites, we consider a period (n) of 5.

2.4.1 Stiffness of the staggered composites

Here, we discuss cases where the first failure is VIF. An essential aspect of the stiffness is the values before and after the first failure. Even after the failure of the vertical interface, the composite is still able to transfer load, albeit with lower stiffness. Of the two material parameters we considered, only the E_p/E_m ratio affects the stiffness of the composite, whereas the normal strength of the platelet does not affect this stiffness in any way. Therefore, we discuss only the effect of E_p/E_m on the stiffness ratio in this section. Figure 2.12 shows the effect of E_p/E_m on the stiffness ratio of regular and stairwise staggered models. Here, the x-axis is plotted in log-scale to comprehend the difference between the curves at lower aspect ratios.

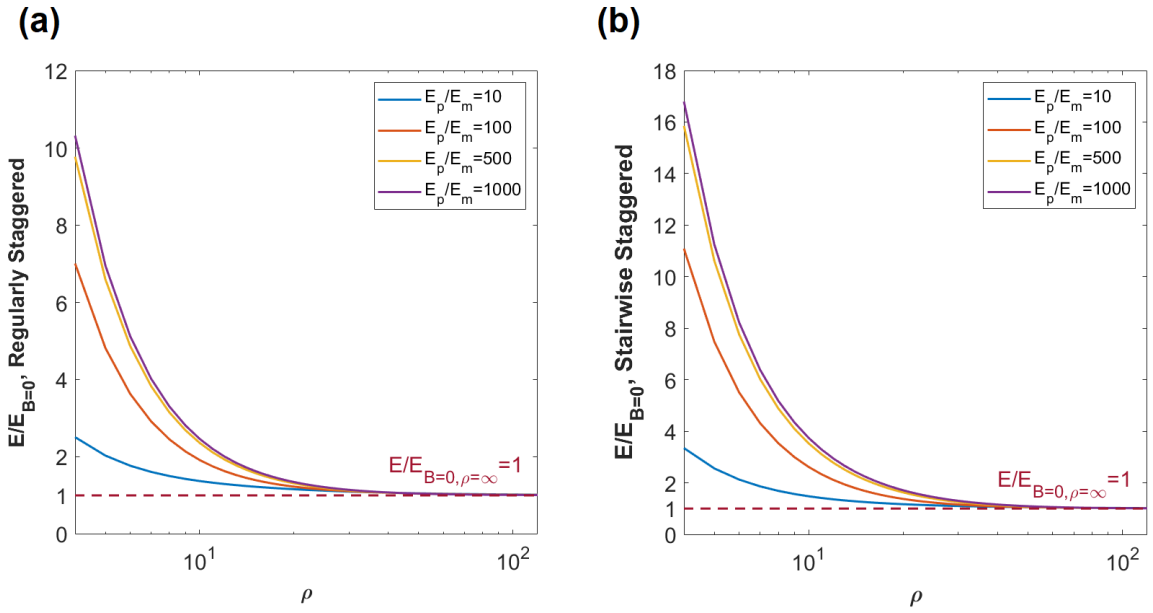

Figure 2.12: Variation of the ratio between stiffness before and after the first failure of (a) regularly and (b) stairwise staggered composite; w.r.t the platelet aspect ratio (ρ) for different values of E_p/E_m. Note that here, the first failure is found to be VIF in most cases. (The link to the Matlab scripts for reproducing this figure can be found here)

For both types of staggering, a decreasing trend of the stiffness ratio is observed with increasing aspect ratios from Figure 2.12. It is also observed that the stiffness ratio increases and the plots converge as E_p/E_m ratio is increased. Moreover, comparing Figure 2.12 (a) and (b), it can be seen that for the same material properties, the ratio of stiffness before to that after the first failure is greater for a stairwise staggered type composite than a regularly staggered composite, at lower aspect ratios. However, at higher aspect ratio, the effect of E_p/E_m is very small, and the stiffness ratio converges to 1, which is obtained for the limiting case as $\rho \to \infty$ for both stairwise staggered and regular staggered models.

Here, it is seen that as the aspect ratio decreases, stiffness ratio increases. The maximum values of stiffness ratio, $\left(\frac{E}{E_{B=0}}\right)_{max}$ for regular and stairwise staggered models can be obtained using Equation 2.15 given below (see Appendix C for more details) where $\left(\frac{E}{E_{B=0}}\right)_{max} = f(\rho, \nu_m, v_f, b, \xi, n)$.

$$\left(\frac{E}{E_{B=0}}\right)_{reg} = \frac{(A\sinh(A) + B\cosh(A))(\cosh(A) + A\sinh(A))}{(\cosh(A) + A\sinh(A) + B\cosh(A))A\sinh(A)} \tag{2.15}$$

For example, for a realistic small aspect ratio (say, $\rho = 4$), $E_p/E_m = 100$ in the present model with the given values of parameters in Section 2.4, the $\left(\frac{E}{E_{B=0}}\right)$ values are found out to be 7 and 11 respectively for regular and stairwise staggered models; which implies that the stiffness after vertical interface failure in the regular staggered model is around 36% higher than the stairwise staggered model.

2.4.2 Strength

The strength of a composite is referred to as the average stress in a composite section when the stresses in either of the components (i.e, platelet or matrix) reaches their respective material strengths (Zhang et al., 2010). Here, the matrix possesses two kinds of strength: tension and shear. The expressions for the stress variation along a platelet in a staggered structure is used to compute the average stress in a representative volume element (RVE). It is assumed that the stress at the vertical interface (which is composed of the matrix) is equal to the stress in the platelet at its ends.

The strength for regular and stairwise staggered composites is computed as the maximum of the stresses at the first and second failures. The model proposed by Kim et al. (2018) is used to estimate the stresses before the first failure. For the second failure, the model for stress computation shall comply with the first failure; if the first failure is a VIF, we set the parameter $B = 0$ both in the equation for the regular staggered model in the orig-

inal Kim's model as well as in the developed equations of the present study. This means that we ignore the stress transfer through the vertical interface for determining the second failure. If HIF occurs first, we consider the model as a combination of vertical interfaces and platelets (ignoring the horizontal interface) for computing the stress at the second failure. For all the studies, we consider regularly staggered models with an overlap ratio equal to $1/2$ since this would provide the most beneficial mechanical properties (Zhang et al., 2010). In the case of stairwise staggered composites, we consider a period (n) of 5.

The strength at the first failure of the regular and stairwises staggered composites are analyzed by varying aspect ratio (ρ) as shown in Figure 2.13. The strength is seen to increase with an increase in aspect ratio. For the regular staggered model (Figure 2.13 (a)) with $\frac{\sigma^p_{critical}}{\tau^m_{critical}} = 10$, the first failure is observed to be VIF at lower aspect ratios ($\rho < 23$), and for $\rho \geq 23$, PF is found to occur first. Here, $\rho = 23$ is a critical aspect ratio, after which the failure mode changes from VIF to PF. This critical aspect ratio can be observed as a kink in the graph (point k_1).

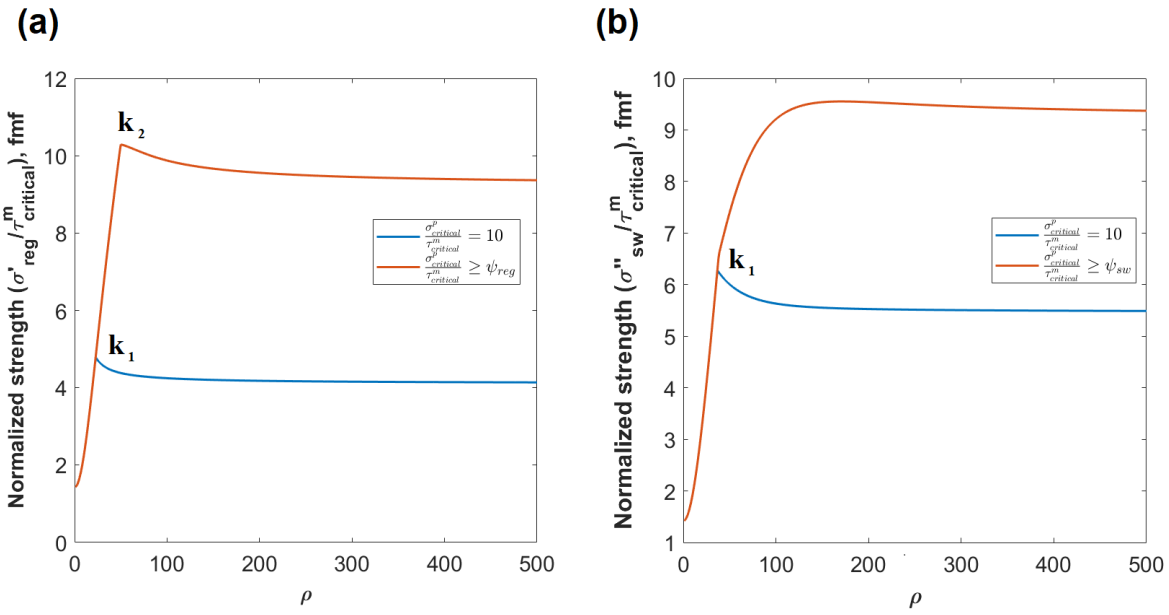

Figure 2.13: Variation of normalized strength of (a) Regularly and (b) Stairwise Staggered Composite, at first failure; with platelet aspect ratio (ρ), for different values of $\frac{\sigma^p_{critical}}{\tau^m_{critical}}$. Here, k_1, k_2 represent the points of kinks and ψ ($\psi_{reg} = 23.6, \psi_{sw} = 17.3$) represents the limiting value of $\frac{\sigma^p_{critical}}{\tau^m_{critical}}$ for the model, beyond which the plots converge. (The link to the Matlab scripts for reproducing this figure can be found here.)

It can be seen from Figure 2.13 that the strength at the first failure remains the same

for a critical value, $\psi \geq \frac{\sigma^p_{critical}}{\tau^m_{critical}}$. This value of $\psi = \psi(E_p, E_m, \nu_m, v_f, b, \xi, n)$ is obtained by comparison of strength ratios (as illustrated by Figure 2.9) and solving associated non-linear equations (See Eq. A.11 and Eq. A.12 in Appendix A) using a search algorithm in MATLAB (The Mathworks, 2020). For the geometrical and material parameters used, the value of ψ for regular and stairwise staggered models are obtained as 23.6, and 17.3, respectively.

From Figure 2.13 (b) also, it can be seen that the normalized strength values are the same for $\frac{\sigma^p_{critical}}{\tau^m_{critical}} \geq \psi_{sw}$, which is attributed to the limiting value of $\frac{\sigma^p_{critical}}{\tau^m_{critical}}$ as explained above. The critical aspect ratio for the stairwise staggered model with $\frac{\sigma^p_{critical}}{\tau^m_{critical}} = 10$, is found at the point of kink (k_1, Figure 2.13 (b)) at $\rho = 37$; from where the first failure changes from VIF to PF.

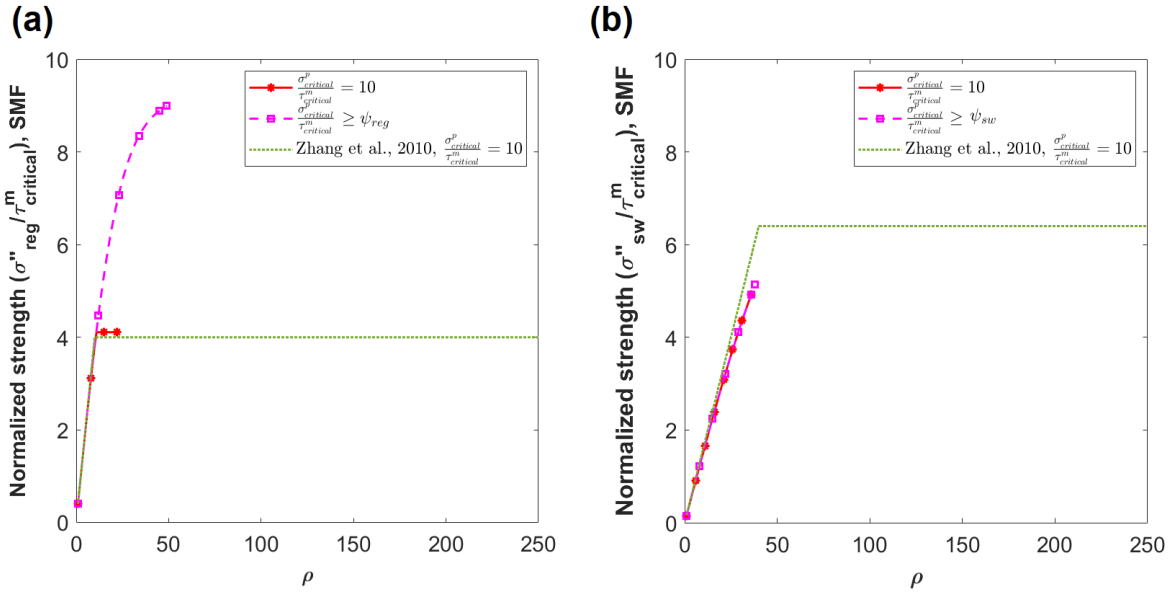

Figure 2.14: Variation of normalized strength of (a) Regularly and (b) Stairwise Staggered Composite, at second failure (VIF); with platelet aspect ratio (ρ), for different values of $\frac{\sigma^p_{critical}}{\tau^m_{critical}}$. The plots are drawn for aspect ratios up to which platelet or horizontal interface failure does not occur first. Here, ψ ($\psi_{reg} = 23.6, \psi_{sw} = 17.3$) represents the limiting value of $\frac{\sigma^p_{critical}}{\tau^m_{critical}}$ for the model, beyond which the plots converge. (The link to the Matlab scripts for reproducing this figure can be found here)

Figure 2.14 shows the variation of normalized strength at the second failure with platelet aspect ratio for different values of $\frac{\sigma^p_{critical}}{\tau^m_{critical}}$. The plots for strength at second failure are drawn up to aspect ratio beyond which the platelet or horizontal interface fails first; since a second failure is not possible for such cases. Also, the strength at second failure is observed to be

the same for stairwise staggered models in the selected range of $\frac{\sigma^p_{critical}}{\tau^m_{critical}}$ values, but the aspect ratio at which platelet failure occurs first, is seen to be different for some cases. For example, for models with $\frac{\sigma^p_{critical}}{\tau^m_{critical}} = 10$, platelet failure is seen to occur beyond $\rho = 36$. Similarly, for stairwise staggered models with $\frac{\sigma^p_{critical}}{\tau^m_{critical}}$ values of ψ_{sw} and greater, the platelet failure was seen to occur first, beyond an aspect ratio value of 38. The normalized strength at second failure is also compared with the analytical solution by Zhang et al. (2010) and a good agreement is observed.

Figure 2.15 shows the variation of strength at first failure with platelet aspect ratio (ρ), for different E_p/E_m ratios. It can be seen that the strength values at first failure increases with increase in E_p/E_m ratio.

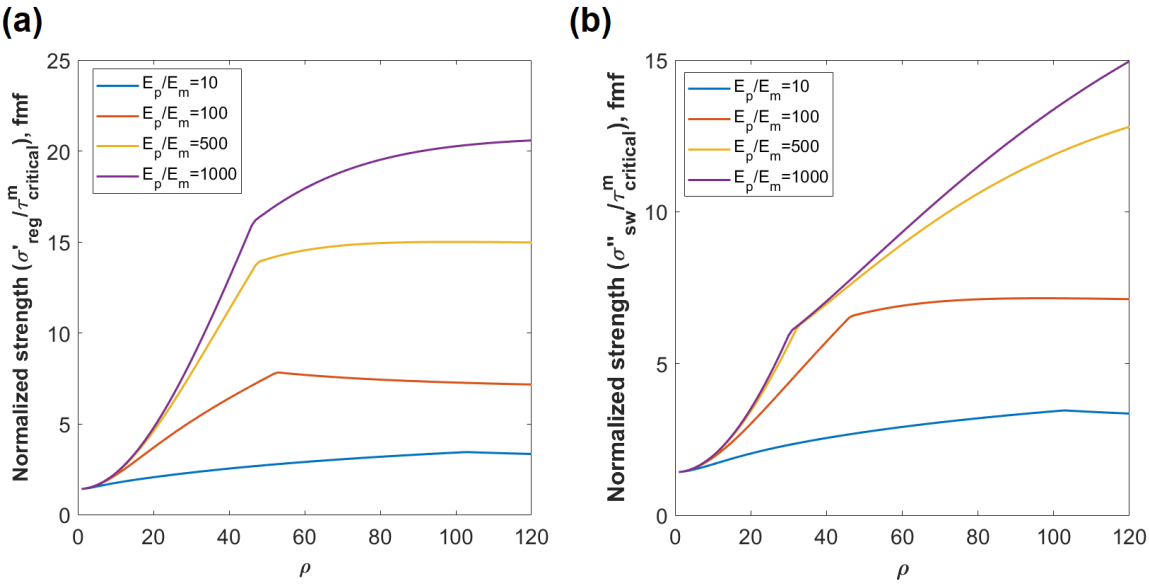

Figure 2.15: Variation of normalized strength of (a) Regularly and (b) Stairwise Staggered Composite, at first failure; with platelet aspect ratio (ρ), for different values of E_p/E_m. (The link to the Matlab scripts for reproducing this figure can be found here)

The variation of strength at the second failure with platelet aspect ratio (ρ), for different E_p/E_m ratios is shown in Figure 2.16. The strength values at second failure also increases with increase in E_p/E_m. Moreover, at higher aspect ratios, the rate of increase of strength decreases. Here also, the stairwise staggered models are seen to have a lower range of second failure strength values.

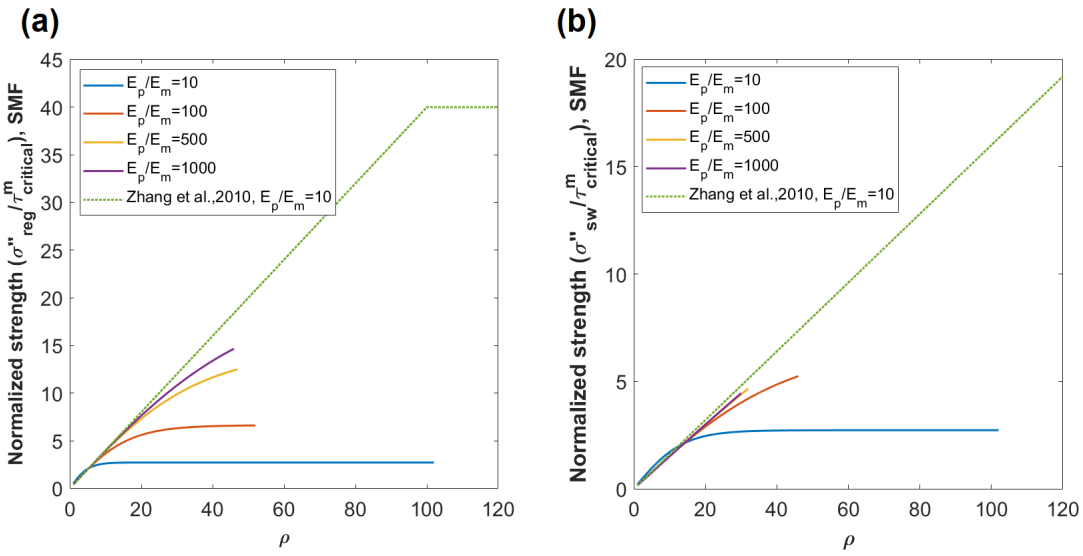

Figure 2.16: Variation of normalized strength of (a) Regularly and (b) Stairwise Staggered Composite, at second failure (VIF); with platelet aspect ratio (ρ), for different values of E_p/E_m. The plots are drawn for aspect ratios up to which platelet or horizontal interface failure does not occur first. (The link to the Matlab scripts for reproducing this figure can be found here)

Comparing the two graphs (Figure 2.15 and 2.16), we find that the strength at second failure is higher than that at first failure for the range of parameters considered. Therefore, for calculation of strengths, a model without the vertical interface could be sufficient.

2.4.3 Toughness

The normalized toughness for a regular and stairwise staggered composites with respect to the platelet aspect ratio is drawn using equation 2.14 and compared with the TSC model (Zhang et al., 2010) and is shown in Figure 2.17 (a) and (b) respectively. In order to compare the results of the present study with the TSC model (Zhang et al., 2010), we select properies same as that used in Zhang et al. (2010). Here $E_p = 700$ GPa, $E_m = 1.96$ GPa, $\sigma^m_{critical} = 243.05$ MPa, $\sigma^p_{critical} = 1400$ MPa, and $\tau^m_{critical} = 140$ MPa.

It can be seen from Figure 2.17 (a) that the analysis matches with the results of TSC model except for a few points in the initial region. Moreover, the toughness at the initial points seems to be higher for the TSC model in the case of the regular staggered structure where as the TSC model show comparatively lower values for stairwise staggered arrangement. Figure 2.17 (b) shows the comparison of normalized toughness in a stairwise staggered model in which it can be seen that there is a marginal difference between the

peak points of the toughness predicted using Zhang's model and the present study (Kim et al., 2018; Zhang et al., 2010). The models with 'VI ignored' refer to the model in which it is assumed that VIF has taken place and the parameter B is set to zero in Equation A.8 and B.5.

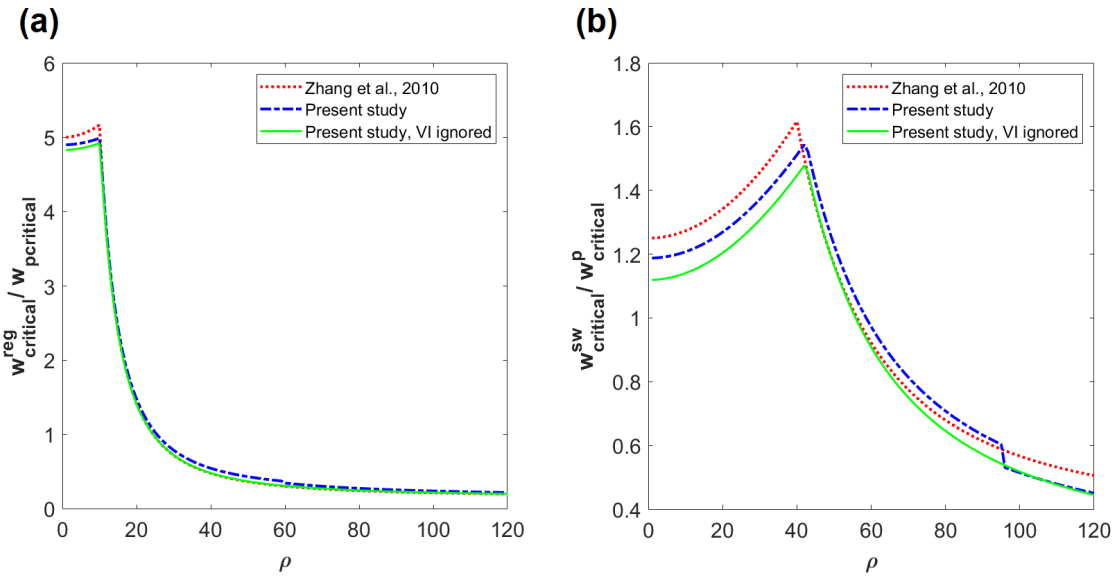

Figure 2.17: Comparison of normalized toughness in (a) regular staggered model (b) stairwise staggered model; the VI ignored models denote those in which VIF has already occurred so that there is no stress transfer across the vertical interfaces. (The link to the Matlab scripts for reproducing this figure can be found here)

There is a difference in the critical aspect ratio (aspect ratio which separates matrix failure and platelet failure) predicted by the three models. The critical aspect ratio depends on the stress distribution in platelet and matrix, which differs for the three models considered. The critical aspect ratio for the three models: Zhang, present study with and without VI are observed to be 40, 42 and 42 respectively. Also, there is a dip at an aspect ratio of 95 for the stairwise staggered model developed in the present study, which is due to the change in sequence of failure modes. For aspect ratios upto 42, the failure sequence is observed to be HIF followed by PF. For aspect ratios from 43 to 95, the sequence of failure is observed to be VIF followed by PF. However, for aspect ratio values beyond 95, PF occurs first. This creates a kink in the toughness plot (Figure 2.17 (b)) at an aspect ratio of 42 and 95 for the present study.

In Figure 2.18, the curves OABD and OBD show representative graphs illustrating a typical stress-strain curves for models with and without VI. Here, A_1 represents the area

enclosed by the triangle OAB and A_2 represents the area enclosed by the triangle ODE. A_1 can be physically interpreted as a measure of the toughness contribution from the first failure and A_2 is the toughness of the composite when the vertical interface (VI) is ignored in the computation. Note that in literature, the contribution from A_1 is usually ignored (Zhang et al., 2010).

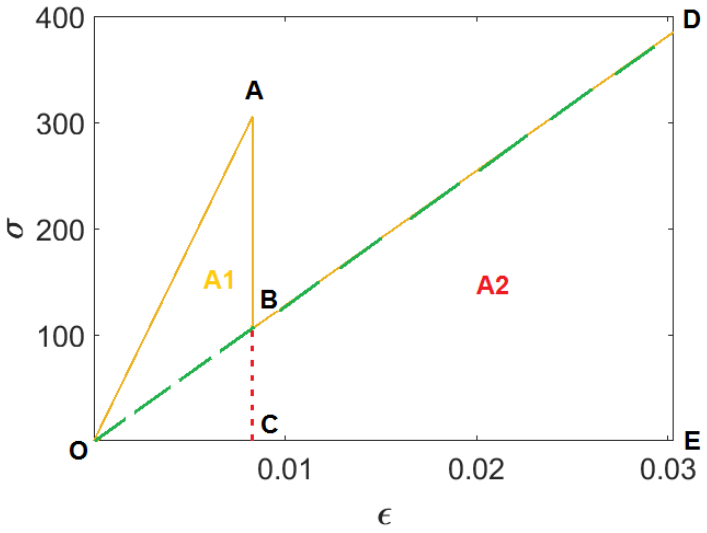

Figure 2.18: Schematic diagram of stress (σ) vs strain (ϵ) showing areas contributing to the toughness in the first and second modes of failure, A_1 and A_2 represents the areas of triangles OAB and ODE respectively.

Figure 2.18 is drawn for typical cases where the second mode strength (σ'') is higher than the first mode strength (σ') (refer Figure 2.11). There can be cases where the strength and/or strain at second failure is less than the corresponding values at first failure. In all cases, A_1 would be the additional toughness due to consideration of VI.

Figure 2.19a and 2.19b shows a representative graph of the stress strain variation for a regularly and stairwise staggered model respectively, composed of the material-set adopted in section 2.2.3 (material-set-1, refer Table 2.1) with a platelet aspect ratio of 10. From these figures, it can be seen that a major portion of the toughness is contributed by the area A_1 (see Figure 2.18) which is obtained as a result considering the first failure which is a VIF. The ratio of the areas depicted as A_1 and A_2 (see Figure 2.18) is found out to analyze the influence of VIF in the computation of toughness. Note that the equations for stress and Young's modulus by Kim et al. (2018) is used for computing the stress and strain values in a regular staggered model.

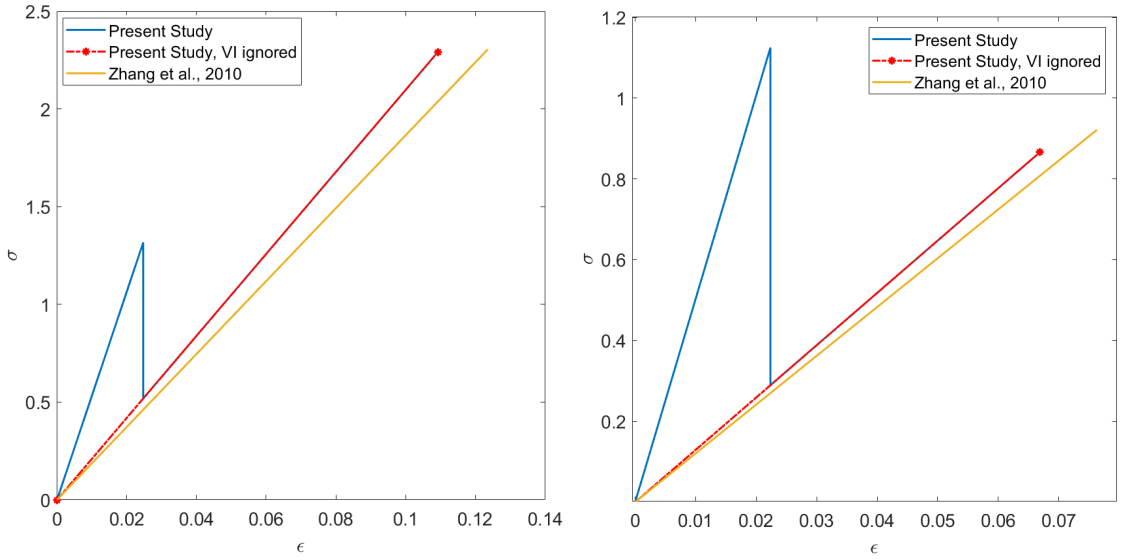

(a) Regularly staggered **(b)** Stairwise staggered

Figure 2.19: Comparison of stress (σ) - strain (ϵ) variation in TSC and modified shear lag models with a platelet aspect ratio $\rho = 10$, with material properties Set-1

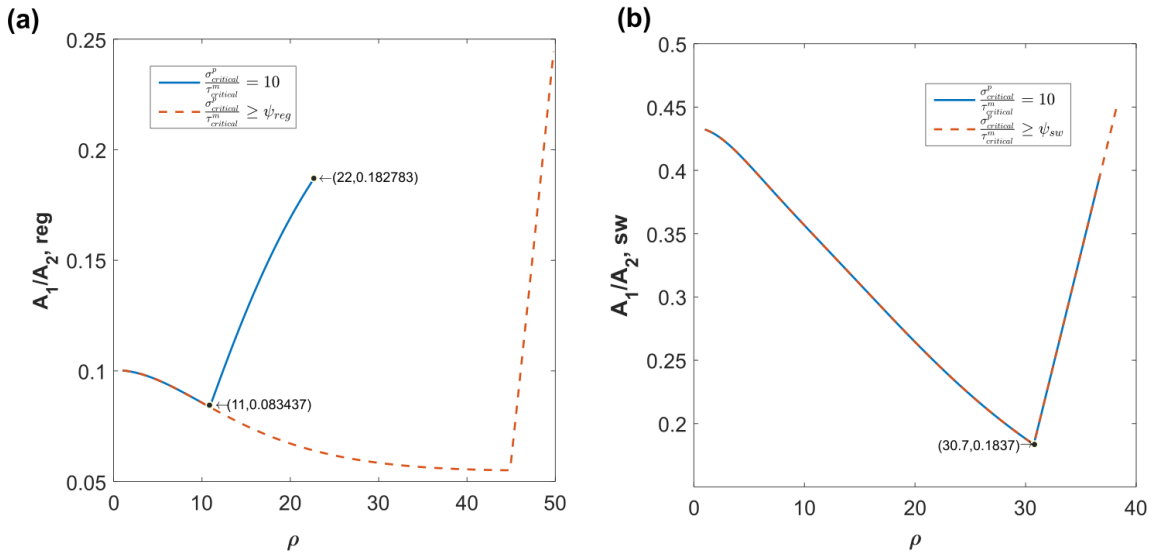

Figure 2.20: Variation of toughness contribution from the first failure expressed as A_1/A_2 (increase in toughness while considering the first failure and toughness due to the second failure ignoring vertical interface) for materials with different $\sigma^p_{critical}$ in (a) regular staggered model (b) a stairwise staggered model. Here, ψ ($\psi_{reg} = 23.6, \psi_{sw} = 17.3$) represents the limiting value of $\frac{\sigma^p_{critical}}{\tau^m_{critical}}$ for the model, beyond which the plots converge. (The link to the Matlab scripts for reproducing this figure can be found here)

Here, we examine the influence of various parameters on the ratio A_1/A_2. First, we

look at how the strength ratio of platelet to matrix ($\frac{\sigma^p_{critical}}{\tau^m_{critical}}$) influence this ratio. Here we vary $\frac{\sigma^p_{critical}}{\tau^m_{critical}}$ from 10 to 200 while keeping other parameters at values E_p= 220 GPa, E_m = 1.1 GPa, $\sigma^m_{critical} = 30$ MPa and shear strength $\tau^m_{critical} = 17.3$ MPa; as done in the previous analysis. Figure 2.20 shows the variation of the toughness contribution from the first failure expressed as the area ratio A_1/A_2 (see Figure 2.18 for the definition of A_1 and A_2) for regular and stairwise staggered models with different $\frac{\sigma^p_{critical}}{\tau^m_{critical}}$.

It is also seen that for $\frac{\sigma^p_{critical}}{\tau^m_{critical}} \geq \psi$, the variation of $\sigma^p_{critical}$, the toughness contribution from the first failure is observed to be the same and the plots overlap. This is so because the failure sequence is VIF followed by HIF in the aspect ratio range considered, which is independent of $\sigma^p_{critical}$. Moreover, the toughness contribution from the first failure compared to that without considering it is observed to be greater for a stairwise staggered model. For example, the A_1/A_2 ratio for a regular and stairwise staggered model with $\frac{\sigma^p_{critical}}{\tau^m_{critical}} = 200$ for an aspect ratio $\rho = 4$ is observed to be 9.7 % and 41.34 %, respectively.

2.4.4 Physical mechanisms affecting the toughness

Here, we discuss the physical mechanisms responsible for the variation in toughness with the geometrical and material parameters. For instance, in Figure 2.20, the plot of A_1/A_2 decreases initially, reaches a lowest point and thereafter increases. Why is such a behaviour observed? To explore the reason for this response, we look at the stress-strain curves corresponding to a set of chosen values of aspect ratios. Toughness being the area under the stress-strain curve, the information obtained can provide insights in to the physical mechanisms behind the variations in the toughness contribution with the aspect ratio. Here, we consider the regular staggered and stairwise staggered models separately, for which the observations obtained are discussed as follows:

2.4.4.1 Regular staggered models

Consider the A_1/A_2 plot for regular staggered composite with $\frac{\sigma^p_{critical}}{\tau^m_{critical}} = 10$, shown in Figure 2.20 (a). The toughness contribution from the first failure is observed to decrease up to an aspect ratio value of 10, after which it is seen to increase. The decreasing and increasing trends are checked one by one as follows. Consider Figure 2.21 in which the stress strain graphs for regular staggered composite with $\frac{\sigma^p_{critical}}{\tau^m_{critical}} = 10$, for aspect ratios of $\rho = 8, 10, 11, 12, 22, \& \ 23$ are shown; the corresponding sequence of failures are also illustrated.

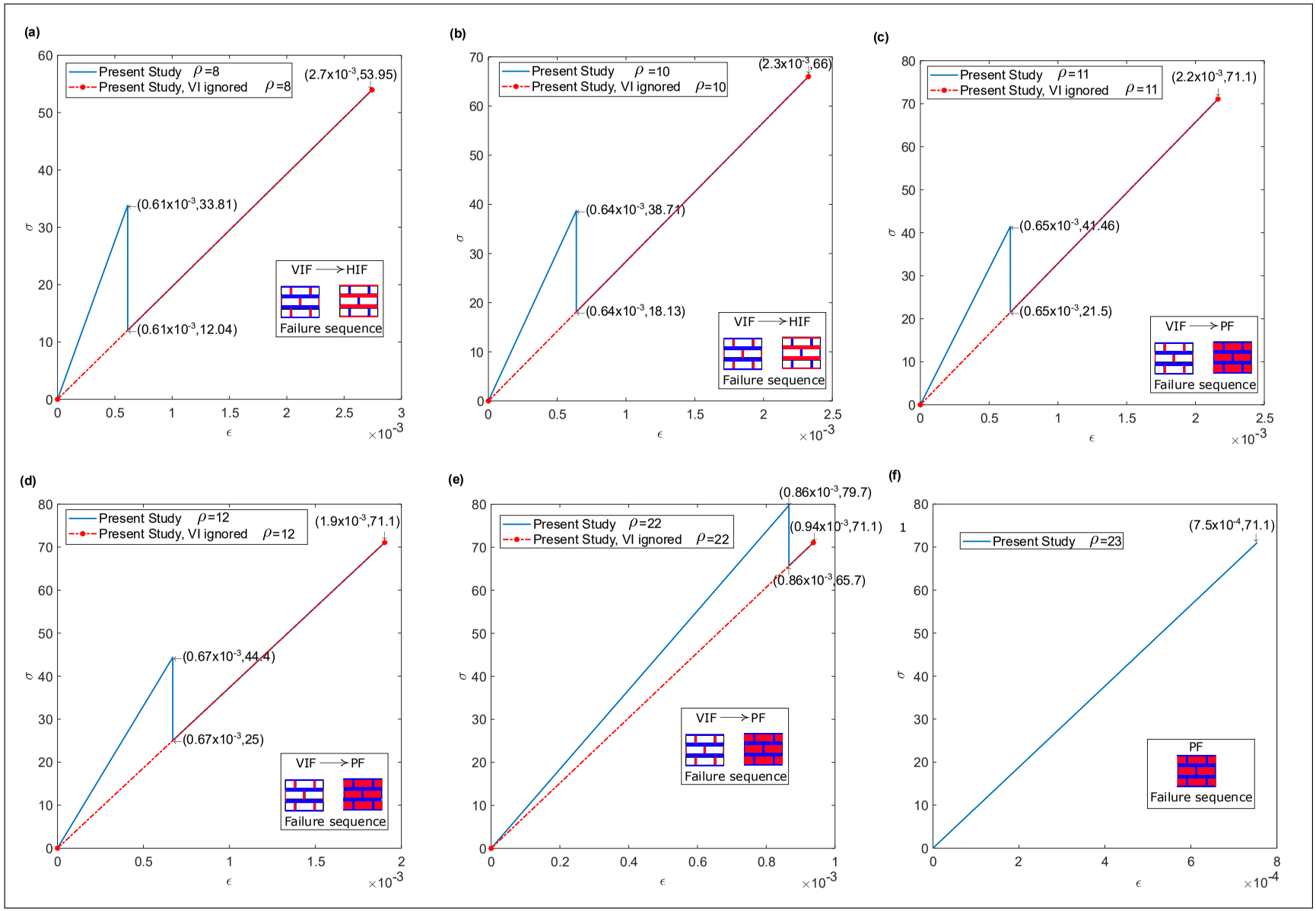

Figure 2.21: Variation of stress-strain plots for regular staggered model with $\frac{\sigma^p_{critical}}{\tau^m_{critical}} = 10$ for aspect ratios: (a) $\rho = 8$, (b) $\rho = 10$, (c) $\rho = 11$, (d) $\rho = 12$, (e) $\rho = 22$, and (f) $\rho = 23$. The inset figure shows the failure sequence.

To explain the decreasing trend of A_1/A_2 upto $\rho = 10$ in Figure 2.20 (a), we refer to the stress strain plots of $\rho = 8$ & 10 shown in Figure 2.21 (a) and (b). We see that although the area A_1 increases with aspect ratio, the total toughness A_2 also increases. This makes the ratio A_1/A_2 lesser than the preceding value (see Figure 2.18 to find the definition of A_1 and A_2).

Now, we look at why there is an increasing trend in A_1/A_2 plot from $\rho = 11$. Let us consider the failure sequence for the aspect ratios $\rho = 10$ & 11. It can be seen from Figure 2.21 (b) and (c) that the failure sequence changes to 'PF after VIF' from 'HIF after VIF' at $\rho = 11$. This makes a kink in the A_1/A_2 plot (Figure 2.20 (a)) at $\rho = 11$. Moreover, it can be found that the kinks in the A_1/A_2 plot occur at the same aspect ratio of the kinks in the plots of strength at the second failure (See Figure 2.14 (a)), since the toughness depends on the strength.

The plot of A_1/A_2 is found to end at an aspect ratio of 22, indicating no contribution from the first failure for $\rho > 22$. This is so because beyond an aspect ratio of 22, the first failure itself is platelet failure, which leads to the composite failure and there will not be any other preceding failure to contribute to the toughness. The strength plot shown in Fig 2.14 (a), also ends at the same aspect ratio, owing to the aforementioned reason. It is now evident that the trend of the toughness contribution from the first failure, i.e., A_1/A_2 curves, is highly dependent on the failure sequences and the modes.

2.4.4.2 Stairwise staggered models

It is observed from Figure 2.20 (b) that the toughness contribution from first failure is first decreasing and then increasing after a particular aspect ratio, for stairwise staggered models. We draw the stress-strain plots for the stairwise staggered model in a very similar manner to that of regularly staggered model, for explaining the overall pattern depicted by the A_1/A_2 plot in the case of stairwise staggered composites also.

First, we look into the reason for the decreasing trend. For this purpose, the stress-strain curves are plotted for a chosen set of values of aspect ratios in a stairwise staggered model with $\frac{\sigma^p_{critical}}{\tau^m_{critical}} = 10$, as shown in Figure 2.22.Similar to the case of regular staggered composites, here also it is observed that as the aspect ratio increases, both the areas A_1 and A_2 increases with A_2 increasing at a faster rate, making the value of A_1/A_2 lesser than the preceding value.

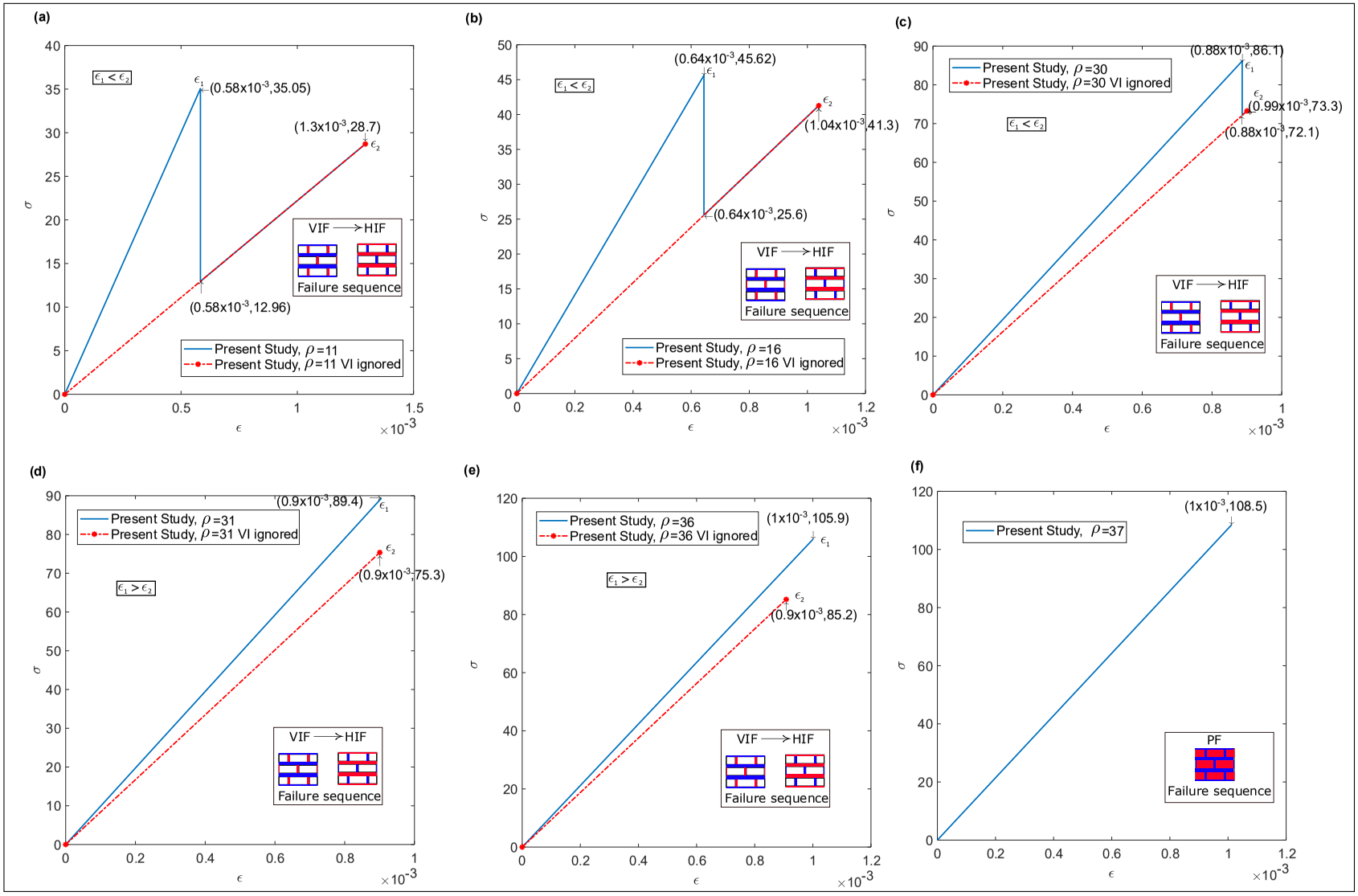

Figure 2.22: Variation of stress-strain plots for stairwise staggered model with $\frac{\sigma^p_{critical}}{\tau^m_{critical}} = 10$ for aspect ratios: (a) $\rho = 11$, (b) $\rho = 16$, (c) $\rho = 30$, (d) $\rho = 31$, (e) $\rho = 36$, and (f) $\rho = 37$. The inset figure shows the failure sequence; ϵ_1 and ϵ_2 represents the strains at the first and the second failures, respectively.

Now, to check the reason for the increasing trend of A_1/A_2 for aspect ratios beyond 30.7, the failure sequences are probed. The failure sequence is observed to be 'HIF after VIF' which is the same for all the chosen values of aspect ratios. However, when the strain at the first failure (ϵ_1) and that for the second failure (ϵ_2) are compared, it is observed that ϵ_1 is greater than ϵ_2 for models with $\rho > 30.7$, whereas for $\rho < 30.7$, ϵ_1 is less than ϵ_2. We also see that ϵ_1 increases with the aspect ratio, which increases the toughness contribution from first failure, thus causing the increasing trend of A_1/A_2 plot beyond $\rho = 30.7$. The area computation for cases with $\epsilon_1 > \epsilon_2$ is explained in detail, in Figure 2.24.

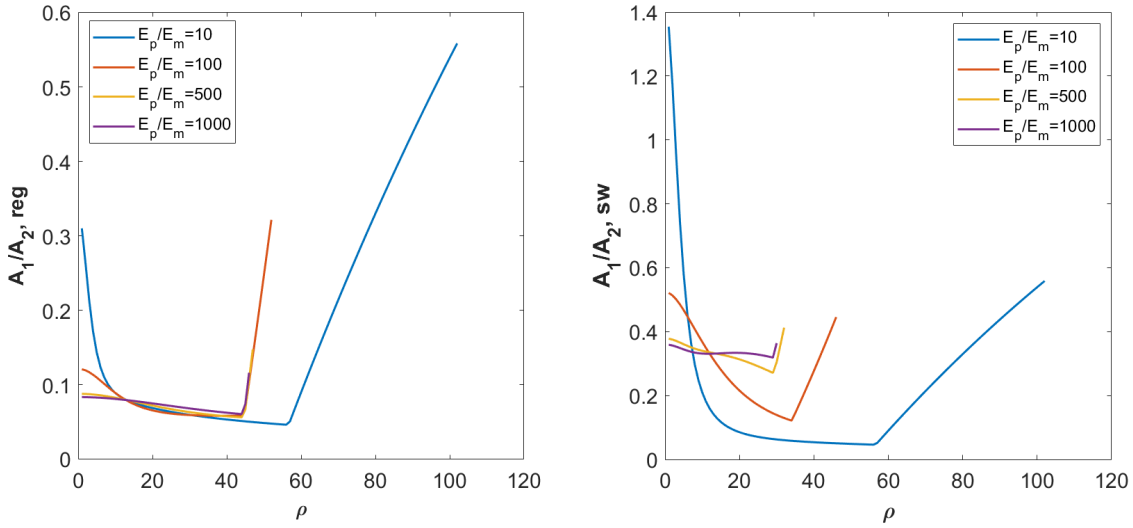

Figure 2.23: Variation of toughness contribution from the first failure expressed as A_1/A_2 (increase in toughness while considering the first failure and toughness due to the second failure ignoring vertical interface) for materials with different E_p/E_m in (a) regular staggered model (b) stairwise staggered model. (The link to the Matlab scripts for reproducing this figure can be found here)

The variation of the toughness ratio A_1/A_2 for different E_p/E_m ratios is depicted in Figure 2.23. It can be seen that both the plots (regular and stairwise staggered models) show a similar trend, but the highest values decrease as the E_p/E_m ratio increases. It is also observed that the relative toughness contribution from the first failure is greater for a stairwise staggered model compared to that of the regular staggered model. These graphs (Figure 2.20 (a) and (b)) show that the toughness contribution from the first failure is significant for low aspect ratio composites, especially with a stairwise staggered arrangement. Therefore, it may be prudent to include the vertical interface in models used for analyzing such cases depending on the material and geometrical parameters.

The trend of the A_1/A_2 plots seems to depend upon the sequence of failure modes

and the variation of failure stresses and strains w.r.t the aspect ratio. It can be seen that the A_1/A_2 plots follow a decreasing trend w.r.t aspect ratio initially, but the contribution of toughness from A_1 in comparison to A_2 increases with an increase in the aspect ratio beyond a certain point. To explain the role of variation of failure stresses and strains with change in aspect ratios in A_1/A_2 plots, consider the point $\rho = 80$ in Figure 2.23 (a) as an example. The stress-strain graph for this particular point is drawn as shown in Figure 2.24.

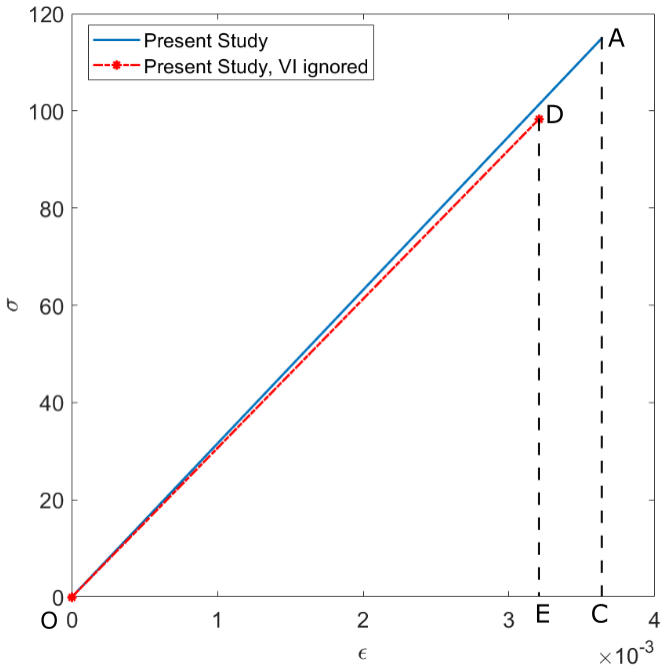

Figure 2.24: Stress (σ) - strain (ϵ) plot for regular staggered model with $E_p/E_m = 10$, $\rho = 80$.

It can be seen that the strain at first failure (ϵ_1, at point A) is greater than the strain obtained using the VI ignored model (ϵ_2, at point D), which is different from that of the schematic diagram shown in Figure 2.18. In such cases, the contribution from the inclusion of the first failure is obtained by taking the differences between the areas OAC and ODE.

2.5 Case Study

So far, we have analyzed the effect of variation of major material properties parameters like the Young's moduli ratio (E_p/E_m) and normal strength ratio ($\sigma^p_{critical}/\tau^m_{critical}$) on the mechanical properties like stiffness, strength, and toughness of the staggered composites. However, for a realistic analysis approach, a case study using some available materials'

properties is essential. This will be useful to elucidate the applicability of the present analysis in real life. To carry out the case study, five different sets of material properties adopted for the numerical/experimental studies (Askarinejad et al., 2018; Nukala and Simunovic, 2005; Yang et al., 2019) as shown in Table 2.1 are chosen for examining the failure modes.

Table 2.1: Mechanical Properties of different sets of materials used as brick and mortar phases for the numerical analysis (Askarinejad et al., 2018; Nukala and Simunovic, 2005; Yang et al., 2019)

Material -Sets	Modulus of elasticity (E) in GPa		Strength of the material in MPa		
	Brick Phase (E_p)	Mortar Phase (E_m)	Brick Phase	Mortar Phase	
			Tensile Strength $\sigma^p_{critical}$	Tensile Strength $\sigma^m_{critical}$	Shear Strength $\tau^m_{critical}$
1	1.2	0.00067	40	1	0.576
2	100	0.2	200	20	11.52
3	220	1.1	3250	30	17.3
4	220	3	3250	40	23.1
5	100	4	200	20	11.52

The material properties are chosen after examining the different types of materials adopted for computational and experimental works in these recent research works. Also, they are arranged in decreasing order of platelet to matrix Young's moduli ratio (E_p/E_m) for convenient discussion of the results. Here also, we identify the sequence of failure modes and find out the different mechanical properties corresponding to these failure modes. This is done by plotting the three non-dimensional numbers $\frac{\sigma^m_{critical}}{\sigma^m_{max}}$, $\frac{\tau^m_{critical}}{\tau^m_{max}}$, and $\frac{\sigma^p_{critical}}{\sigma^p_{max}}$ against the aspect ratio of platelets which is varied from 1 to 120 for the selected five material sets.

The trend of the graphs depends on the material properties, and we observe that VIF occurs at lower aspect ratios for all material sets. For instance, see the representative graph for set-1 shown in Figure 2.10. Note that for the ratio $\frac{\sigma^p_{critical}}{\sigma^p_{max}}$, a horizontal line is obtained with y-value as unity since the maximum stress experienced in a platelet is its normal strength.

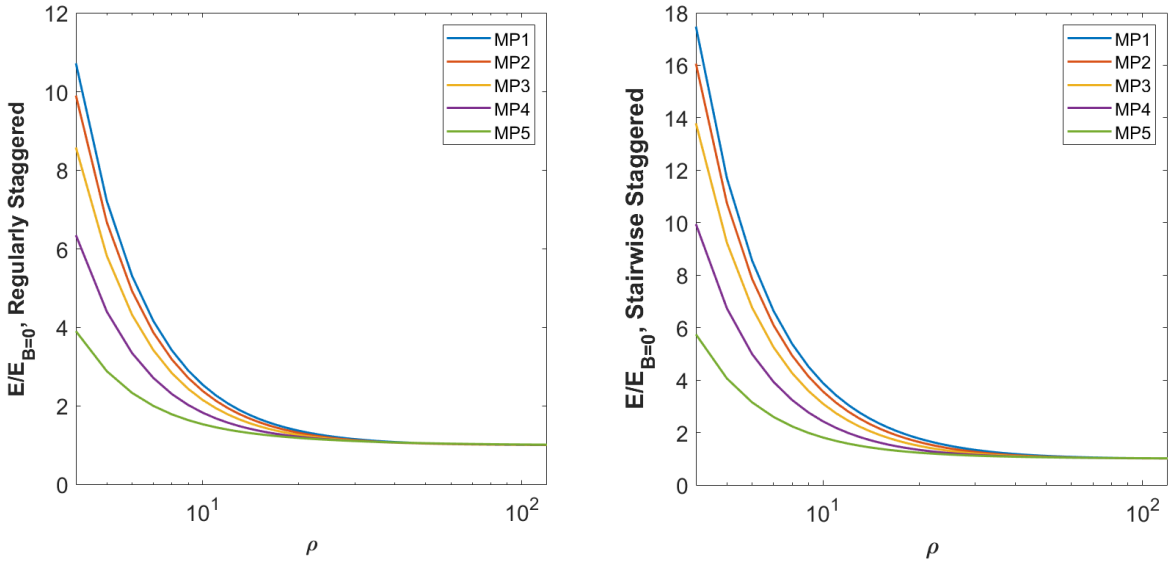

Figure 2.25: Variation of ratio between stiffness before and after first mode of failure of (a) regularly and (b) stairwise staggered composite; w.r.t the platelet aspect ratio (ρ). (The link to the Matlab scripts for reproducing this figure can be found here)

The variation of the ratio between the Young's modulus before and after the first failure with platelet aspect ratio, for different sets of material properties followed a same trend as obtained in 2.4.1. Figure 2.25 shows the variation of the ratio between the Young's modulus before and after the first failure with platelet aspect ratio, for different sets of material properties. Here, the log scale is implemented in the x-axis so as to appreciate the difference between the curves at lower aspect ratios.

We can observe from Figure 2.25 that for a regular staggered composite, the maximum value of stiffness before failure (E) as 10.7, 9.9, and 8.6 times (material-set 1, 2 and 3) the stiffness after failure ($E_{B=0}$), whereas for the stairwise staggered composite it ranges between 17.5 and 16 times (material-set 1 and 2). The models of material-sets with the lowest value of stiffness ratio are the ones with the lowest platelet to matrix Young's moduli ratio ($E_p/E_m = 25$). The stiffness ratio is seen to increase with increase in the E_p/E_m ratio, with the highest range of values for material-set 1 ($E_p/E_m = 1791.045$). For both the staggering types, the stiffness ratios for all material-sets are observed to converge and follow a constant trend (less than 1.03) above an aspect ratio around 100.

Figure 2.26 shows the normalized strength of regular and stairwise staggered composites before first failure (σ') and it can be seen that the strength increases w.r.t the aspect ratio and the rate of increase of strength is reduced after reaching a certain point. The strength at first failure (σ') seems to be maximum at intermediate aspect ratios, which is attributed

to the existence of a critical aspect ratio at which the strength is maximum (Zhang et al., 2010). It can also be observed that the strength at first failure decreases as the E_p/E_m ratio of the material-sets decreases.

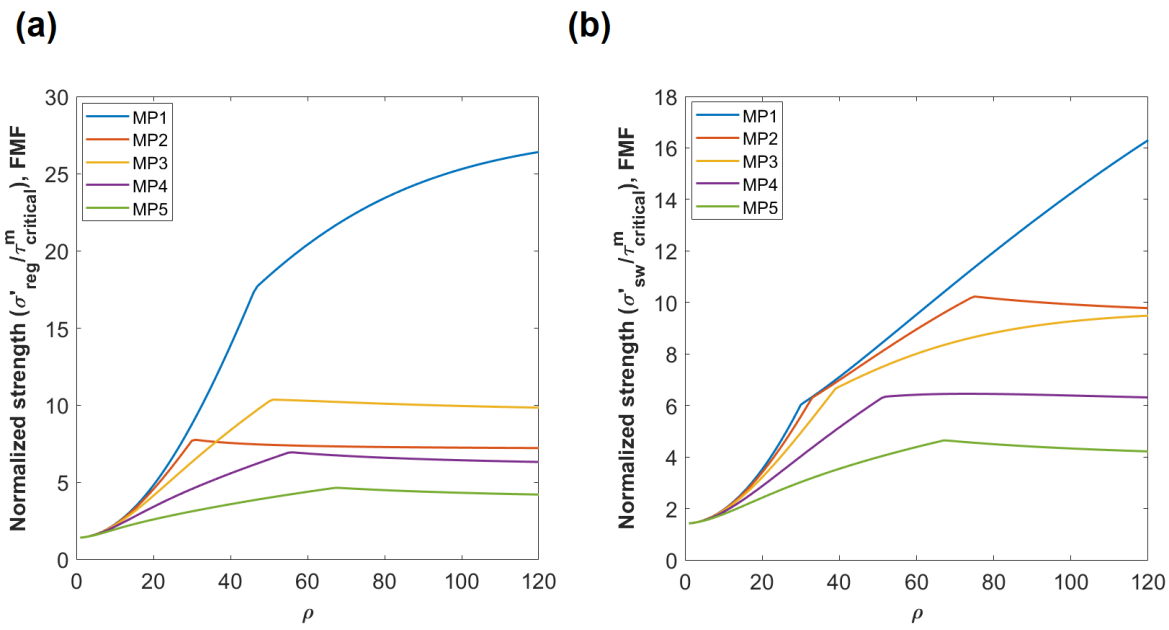

Figure 2.26: Variation of normalized strength of (a) Regularly and (b) Stairwise Staggered Composite, at first failure; with platelet aspect ratio (ρ). (The link to the Matlab scripts for reproducing this figure can be found here)

At the second failure, the strength(σ'') is computed for regular and stairwise staggered composites for all material-sets and the results are plotted against the platelet aspect ratio in Figure 2.27. For material-set 2 in regular staggered configuration, a kink is observed at $\rho = 19$ which is due to the change in the failure sequence from horizontal interface failure to platelet failure after vertical interface failure.

Figure 2.28 shows the ratio of strengths at the first and second failures for regular and stairwise staggered composites. It gives an idea about the decrease in strength at the second failure with respect to the strength at the first failure. For all material sets in a regular staggered model, the upper limit of strength at the first failure is observed to be about 3.5 to 4 times the strength at the second failure, whereas it is about 8 to 10 times for a stairwise staggered model. However, note that this is applicable for very low aspect ratios only. The strength at the first failure is higher than that at the second failure for aspect ratios less than around 3 and 8, respectively, for regular and stairwise staggered models.

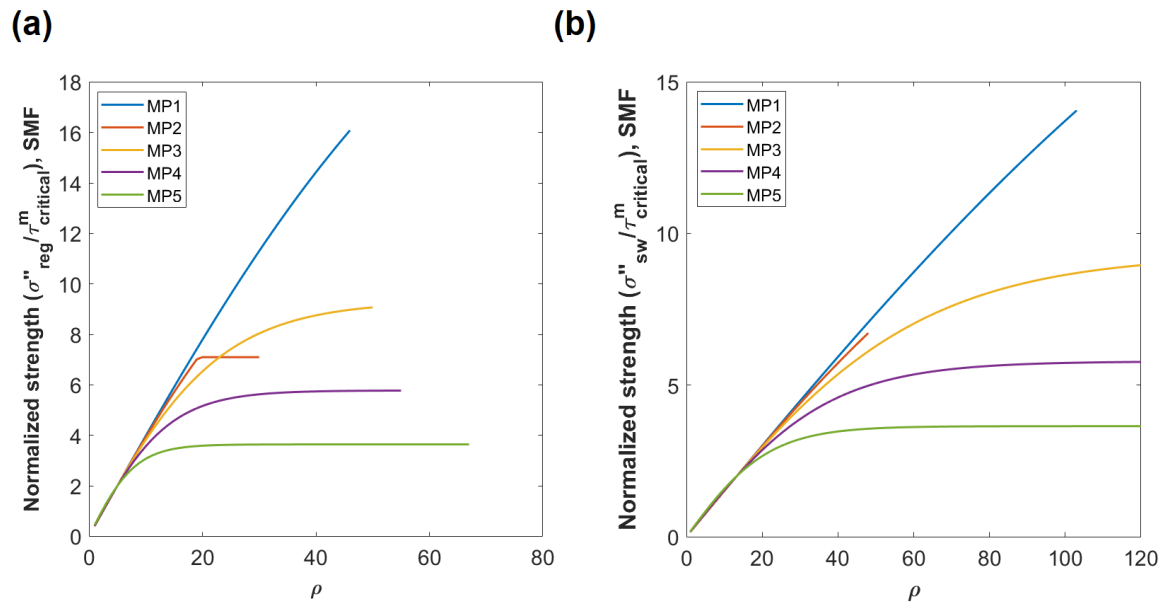

Figure 2.27: Variation of normalized strength of (a) Regularly and (b) Stairwise Staggered Composite, at second failure; with platelet aspect ratio (ρ). The plots are drawn for aspect ratios up to which platelet or horizontal interface failure does not occur first. (The link to the Matlab scripts for reproducing this figure can be found here)

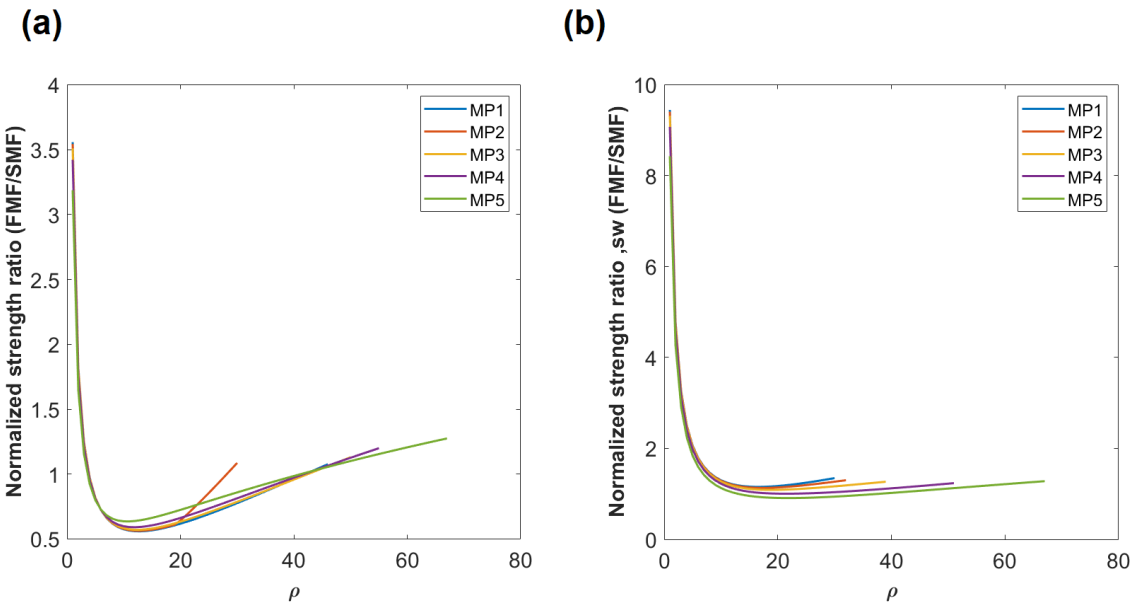

Figure 2.28: Variation of normalized strength Ratio between first and second failures, in (a) Regularly and (b) Stairwise Staggered Composite; with platelet aspect ratio(ρ). (The link to the Matlab scripts for reproducing this figure can be found here)

Figure 2.29 shows the variation of A_1/A_2 with aspect ratio for regular and stairwise staggered models with different material sets. In the regular staggered configuration, the highest value of A_1/A_2 (56.7%) is observed for material set - 5 at an aspect ratio of 67. In the chosen range of aspect ratios (1 to 120), for the stairwise staggered model, the contribution from the first failure is observed to be around 57.6 % for material set-5 at an aspect ratio of 67. Also, for both regular and stairwise staggered models, a reasonably good range of values of A_1/A_2 is observed for even lower aspect ratios. For example, at $\rho = 6$, A_1/A_2 is observed to be around 12.9% and 54.7% respectively, for regular and stairwise configurations with material set-5.

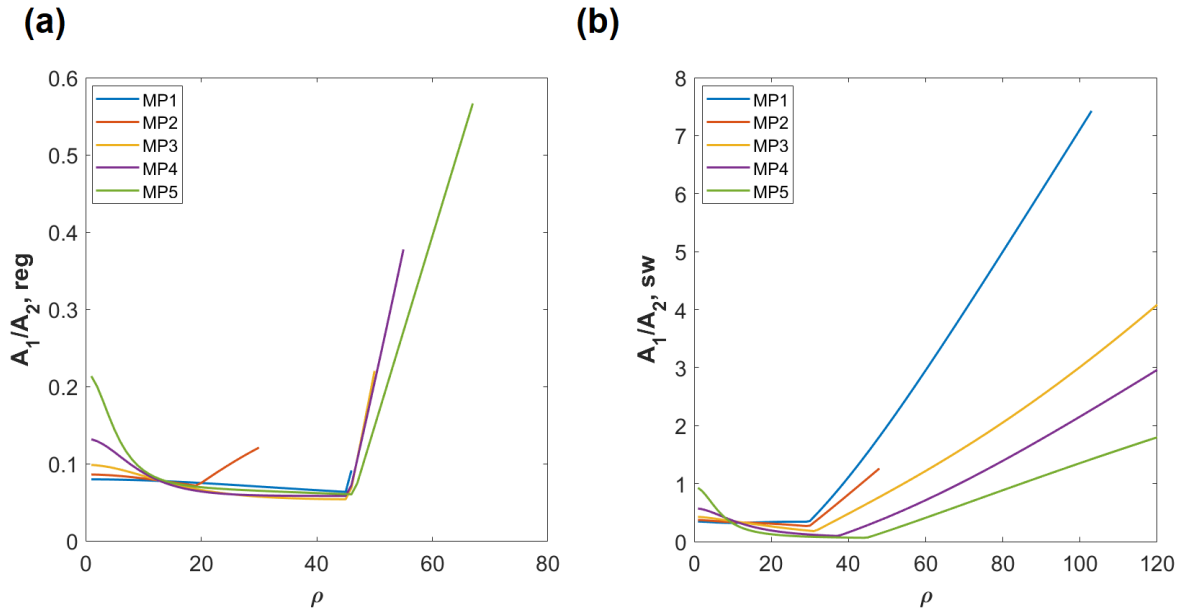

Figure 2.29: Variation of toughness contribution from first failure expressed as A_1/A_2 (increase in toughness while considering the first failure and toughness due to second failure ignoring vertical interface) for different materials in (a) regular staggered model (b) a stairwise staggered model. (The link to the Matlab scripts for reproducing this figure can be found here)

A decreasing trend of toughness with increasing aspect ratio was reported by (Kim et al., 2018) in their experimental studies, for a regular staggered composite. Here, we observe a similar trend for an initial range of values of aspect ratios and the contribution of toughness from the first mode of failure is observed to be higher for stairwise staggered composite when compared to that of regularly staggered composite. Also, the trend of the A_1/A_2 curve is observed to be similar to that of the parametric studies. The kinks are attributed to the change in sequence of failures as well as the variation of failure stresses

and strains with respect to the material properties and aspect ratio.

The vertical interface failure which is ignored in a TSC model is found to contribute to the increase in toughness and it is clearly indicated by the area ratio plots. It can be seen from Figure 2.29 (a) and (b) that the inclusion of the first of failure in the analysis of toughness has a significant contribution at lower aspect ratios. While designing a bio-inspired composite, toughness is regarded as a crucial factor. Researchers have pointed out that high toughness is achieved by sacrificing the stiffness of the composite (Lei et al., 2012a). Therefore, including contribution from the first mode of failure can give a more accurate estimation of toughness, which can help to effectively optimize the other properties like stiffness and strength, especially for lower aspect ratios.

The yielding and large deformations at the interfaces between the composite contribute to the toughness, which is not considered in the present study. Yet, the studies based on elastic assumptions give reasonable approximations of the mechanical properties of bio-inspired composites (Kim et al., 2018; Zhang et al., 2010). Also, even though advanced fracture mechanics methods are available to compute the work of fracture of brittle materials, the area under the stress-strain curve still gives a good estimation of the toughness (Lei et al., 2012b; Zhang et al., 2010). Moreover, the present study results are useful for conducting a first-cut analysis to estimate the mechanical properties even if a plastic deformation occurs in the composite.

2.6 Conclusion

In the present study, the effect of various failure modes and sequences on the mechanical properties of bio-inspired structures are found out. To accomplish these, the equations for evaluating the stiffness and the normal and shear stresses along the platelet and matrix interface, respectively, are developed for a stairwise staggered composite using the modified shear lag model. The developed model shows a good agreement with the FE results. Different possible modes of failure for stairwise and regularly staggered models are then identified using the existing and developed equations. From the failure studies, vertical interface failure - failure in the matrix between the short edge of the platelets is found to occur first in most cases.

After vertical interface failure, the stairwise staggered composites are observed to possess lesser stiffness than regularly staggered composites for low ranges of aspect ratios and a given Young's moduli ratio of platelet to the matrix. However, the composite stiffness is seen to be independent of the strength ratio of the platelet and matrix.

Another important conclusion obtained is the significance of the contribution of toughness from the failure of the matrix at the vertical interface between platelets. We found that the contribution to the toughness from this failure is proportional to the platelet aspect ratio.

The results from the case study show a good agreement with the parametric studies. Moreover, it can be inferred from the case study that the variation in failure sequence can indeed affect the stress-strain values, thereby affecting the toughness contribution from the first failure.

The scientific value of this work is that it could find out the sequence of failure modes and quantify the resulting mechanical properties like stiffness, strength, and toughness of a staggered structure after failure, w.r.t the one before failure. In other words, if the material properties (Young's moduli, Poisson's ratio, normal and shear strengths of the platelet and matrix) and geometric properties (volume fraction, aspect ratio, width, and overlap ratio of the platelet) are known, it is possible to quickly find out how much strength or toughness the model possess after failure, compared to the one before failure. Thus, this research could pave the way to obtain more reliable data on strength and toughness in the field of bio-inspired composite design.

The results from the current Chapter could also be used in the design of a bio-inspired stairwise staggered model for different values of n. Also, it could aid the development of bio-inspired hierarchical models with stairwise staggered configurations, which is a possible extension of the current work. Also, the present study is done on the assumption that the materials are linearly elastic. The flexible matrix's deformation is vital in achieving overall toughness, and its detailed analysis is left for future studies.

The current Chapter dealt with a single hierarchical model in which the failure sequences and its influences over the mechanical properties were studied in detail. In the following chapters, we focus on the investigation of mechanical properties of non-self-similar two hierarchical staggered composites. We analyse a two hierarchical non-self-similar model in the next Chapter after which it is generalized in the subsequent Chapters.

Chapter 3

Mechanical Properties of Non-self-similar Two-hierarchical Bio-inspired Composites

There are many examples of hierarchical structures in nature such as teeth, antler, bone, and nacre which point to the possibility of creating new bio-inspired structures with superior mechanical properties. In this Chapter, the analysis of mechanical properties of unidirectional bio-inspired composites with two levels of non-self-similar hierarchical structures is done using an existing popular model called Tension-Shear chain (TSC) model. The analytical equations of Young's modulus are validated using Finite Element Analysis which is implemented using Python scripting. The two hierarchical composites discussed in this Chapter are seen to maintain a reasonable strength with very high toughness compared to that of the single hierarchical composites and may be used for applications where more toughness is required rather than strength. Moreover, the optimum aspect ratios at the first and second levels of hierarchies are evaluated in this study and a comparison of maximum toughness that can be achieved in a particular configuration is also made. These studies could be useful in the design and development of tough bio-inspired composites. We formulate and analyse the equations required to compute the mechanical properties of a non-self-similar 2H bio-inspired composite.

3.1 Introduction

The biological composite system found in natural materials is a result of optimization by the million years of evolution of animals so as to safeguard their soft tissues from external loads arising from predator bites or the enormous hydro-static pressure occurring in the ocean (Tran et al., 2017). A classic example of natural structural material is timber. Timber acquires high strength through its composite structure composed of cellulose fibers and

soft lignin (Okumura and De Gennes, 2001). The structure of nacre, as we discussed in the previous Chapters, staggered with a brick-and-mortar (B-and-M) arrangement comprising of 95% stiff platelets (inclusions) and 5% soft matrix, results in a surprising improvement in strength and toughness in tension compared to the stiff platelet (Barthelat and Espinosa, 2007; Okumura and De Gennes, 2001). The mineral platelets in nacre impart the desired stiffness to support these biological systems mechanically, whereas the protein absorbs as well as dissipates an enormous amount of fracture energy (Gao et al., 2004). Researchers have come up with many reasons for the superior mechanical properties of the biological composites, which range from the nano-sized constituents, the high aspect ratio of the platelet, optimum ratios of Young's moduli of platelet and matrix, the property of the interface, the type of staggering in the structure (Dong et al., 2019; Ji and Gao, 2004a; Mathiazhagan and Anup, 2016a; Mirzaeifar et al., 2015; Studart, 2012). Therefore, while modeling the mechanical properties of a biological composite, say the micro-mechanical model of bone, shall essentially include the structural information on the shapes and sizes of mineral crystals as well as their orientation and pattern with respect to the matrix (collagen) framework (Wagner and Weiner, 1992). Of the different types of structural arrangement of these mineral crystals/platelets in biological composites, the most observed ones are regular and stairwise staggering, owing to their overall optimized mechanical properties, compared to other types (Zhang et al., 2010). For example, the platelet configuration in nacre and bone are examples of regular and stairwise staggering, respectively (Chao et al., 2021; Landis, 1996; Landis et al., 1996; Lei et al., 2012b).

Many researchers have proposed bio-inspiration as a tool to realize materials with superior mechanical properties (Chen et al., 2019; Mao et al., 2016; X Gu et al., 2016; Yin et al., 2021). Several research works have investigated the factors affecting the final properties of the biological composites, enabling them to adopt similar conditions to realize synthetic bio-inspired composites (Gu et al., 2017; Kim et al., 2018; Li et al., 2012; Martínez-Vázquez et al., 2021; Melaibari et al., 2021; Tran et al., 2017; Wu et al., 2019). Gao et al. (2017) have demonstrated a technique to replicate the properties of naturally occurring nacre (even superior mechanical performance compared to that of nacre) with a three-dimensional and large bulk artificial nacre using a bottom-up approach of assembling the pre-fabricated nacre mimetic films. It has been proved that a polymer (nacre-like) that is additively manufactured can well out-perform its constituents in terms of impact resistance (Gu et al., 2016). An optimization for balancing the flexibility and penetration resistance of a bio-inspired composite has been studied by Greco et al. (2020), and it was found that using the microstructural parameters such as aspect ratio and volume fraction, it is possible

to tailor the penetration resistance of the composite as a function of flexibility.

Several limitations and shortcomings of the existing composite designs are rectified by motivation from their respective natural counterparts' designs. In many of the natural composite materials, the essential properties such that high values of strength, stiffness, and toughness are achieved simultaneously through a discontinuous architecture called a 'brick-and-mortar' structure, made up of stiff inclusions arranged in a soft matrix as we already discussed in the previous Chapters (Barthelat and Rabiei, 2011; Pimenta and Robinson, 2014). Also, the ductility limitations faced by continuous fiber composites could be overcome by adopting the aforementioned discontinuous architecture observed in natural composites. For this, the composite shall be designed and modeled with due consideration given to the material microstructure and the effect of discontinuities (Begley et al., 2012).

There have been only a limited number of researches done on bio-inspired composites from a global hierarchical point of view (Bargmann et al., 2013; Dimas and Buehler, 2012; Li and Ji, 2020; Sen and Buehler, 2011; Xu et al., 2015; Yao and Gao, 2008). The study by Bargmann et al. (2013) focused on modeling dental enamel revealed that the hard platelet aspect ratio could regulate the optimization of fracture energy and fracture strength. Their findings have important implications for the design of bio-inspired artificial fiber-reinforced composite materials as the hard platelet aspect ratio can be used as a key design parameter. Dimas and Buehler (2012) demonstrated that a brick and mortar-type distribution of stiff and soft phases results in a more efficient utilization of materials in the presence of a crack. It was also reported by them that a continuous soft phase oriented at an angle was found to hinder the catastrophic propagation of fractures.

Another work by Sen and Buehler (2011) investigated the fracture mechanics of hierarchical structures comprised of up to four self-similar levels of hierarchy using an atomistically informed in silico mesoscale model yielding direct insights into hierarchical materials' fracture behavior. Through computational experiments, they demonstrated that multiple hierarchy length scales in the material increase the defect-tolerance length scale by dissipation of large loads through the initiation and arrest of cracks at different length scales. This behavior stands in contrast to single hierarchy materials, which would experience shattering due to the propagation of a single crack throughout the material. The mechanical properties of self-similar hierarchical materials were described by Yao and Gao (2008), using multi-scale cohesive laws. According to their findings based on models mimicking gecko and bone, designing a hierarchical material with multi-scale cohesive laws from the bottom up can result in flaw insensitivity at unattainable size scales for traditional non-hierarchical materials.

The number of studies conducted so far is even smaller when it comes to the case of non-self-similar hierarchical structures (An et al., 2014; Henry and Pimenta, 2021). The study by An et al. (2014) involved a theoretical examination of the mechanical characteristics of bio-inspired composite materials with a non-self-similar hierarchical structure. Their findings suggest that incorporating non-self-similar hierarchical designs could enhance the energy storage capabilities of the composites, resulting in improved resilience. Furthermore, compared to systems exhibiting a self-similar hierarchy, the non-self-similar hierarchical composites exhibited increased pull-out work, thereby enhancing fracture resistance and improving damage tolerance Henry and Pimenta (2021) found that self-similarity of the reinforcing units at the two hierarchical levels is not necessary for hierarchical failure mechanisms to occur in hierarchical discontinuous composites. Their results showed that removing the self-similarity constraint can lead to new microstructures with increased performance (strain, stress, damage diffusion) compared to the standard self-similar microstructure.

From the discussions done so far, we find that though bio-inspired composites have been proposed, most of them are limited to a single hierarchy. Moreover, there doesn't seem to be any studies particularly focussed on the mechanical properties of a two hierarchical composite with different defined configurations at the two different levels of hierarchy, which makes it an area still to be explored in the field of design of bio-inspired composites.

The solutions obtained are analyzed by varying the platelet aspect ratios at the first and second levels of hierarchy and keeping the strength ratio of platelet to matrix a constant. Also, a comparative study of the properties of 2H composites with single hierarchical bio-inspired composites is included in Section 3.3. An analysis for finding out the optimum configuration: aspect ratio of platelet at different levels of hierarchy, number of rows of platelets in each period that the design shall possess to achieve maximum toughness is also done in this section. The results are verified in Section 3.4 by conducting a Finite Element Analysis using the commercially available software package ABAQUS (SIMULIA, 2022). We summarize and conclude the study in Section 3.5.

3.2 Mechanical Properties of Two Hierarchical Composites based on Tension Shear Chain Model

In this section, we develop the expressions for various mechanical properties of non-self-similar 2H RS and 2H SR composites. Figure 3.1 depicts the schematic illustrations of

the models adopted for the studies, 2H RS and 2H SR structures. In Figure 3.1(b), the zoomed view of the platelet of the 2H RS composite is shown which is a stairwise staggered composite. Similarly, the schematic illustration of regularly staggered composite structure which is incorporated as platelet in 2H SR composite is shown in Figure 3.1 (d).

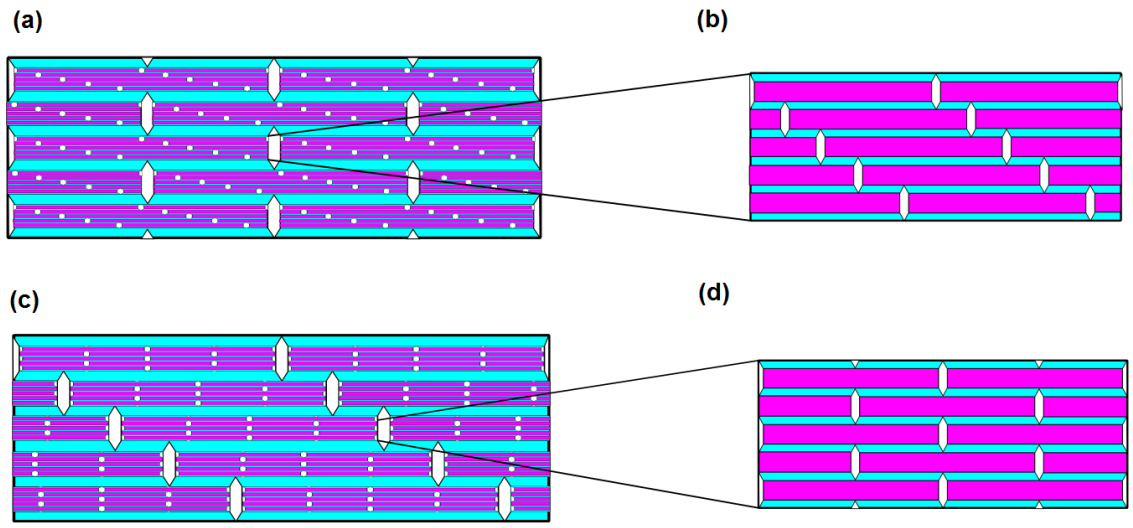

Figure 3.1: (a) Two Hierarchical Regularly Staggered Composite made with Stairwise Staggered Composite as platelet (2H RS) (b) Zoomed view of platelet with Stairwise Staggered Structure (c) Two Hierarchical Stairwise Staggered Composite made with Regularly Staggered Composite as platelet (2H SR) (d) Zoomed view of platelet with Regularly Staggered Structure.

In all the cases we start with the expressions available for different single hierarchical composites developed by Zhang et al. (2010) based on the tension shear chain (TSC) model and thereafter use them to develop the expressions for 2H composites. The main reason for using the TSC model in the present study for hierarchical structures is its simplicity and reasonable accuracy. When involved with multiple hierarchies, the shear lag model with vertical interface present would result in more complex formulations and increase the computational time. The following mechanical properties are analyzed: stiffness, strength, strain, and toughness. We consider regularly staggered structures with an overlap ratio of $1/2$ only. Here, the overlap ratio refers to the ratio of overlapped length of platelet to full length of a platelet.

3.2.1 Stiffness

For a regularly staggered composite with an overlap ratio of 0.5, the modulus of elasticity E_R is given by (Zhang et al., 2010) as,

$$E_R = \frac{\phi_R E_p}{\frac{4}{3} + \frac{4}{3\alpha_R}} \tag{3.1}$$

where,

$$\alpha_R = \frac{\phi_R \rho_R^2 G_m}{3(1-\phi_R)E_p} \tag{3.2}$$

is a parameter which combines the effects of platelet volume fraction of the regularly staggered composite ϕ_R and aspect ratio of platelet in the regularly staggered composite ρ_R, as well as the shear modulus of matrix G_m and Young's modulus of platelet E_p. Similarly, for a stairwise staggered composite with the number of platelets in each period as *n*, the modulus of elasticity E_S is given by (Zhang et al., 2010) as,

$$E_S = \frac{\phi_S E_p}{\frac{n(3n-4)}{3(n-1)^2} + \frac{n^2}{3(n-1)\alpha_S}} \tag{3.3}$$

where α_S is a parameter which combines the effects of platelet volume fraction ϕ_S and aspect ratio ρ_S, as well as the matrix and platelet elastic moduli G_m and E_p,

$$\alpha_S = \frac{\phi_S \rho_S^2 G_m}{3(1-\phi_S)E_p} \tag{3.4}$$

The stiffness, E_{RS} of a 2H RS composite is found out by substituting Eq. (3.3) for E_P in Eq. (3.1) and the obtained expression for E_{RS} is normalized by dividing it by $E_P\phi_R\phi_S$ (since the volume fraction for the 2H composite is $\phi_R\phi_S$) as,

$$\frac{E_{RS}}{E_P\phi_R\phi_S} = \frac{1}{(\frac{4}{3} + \frac{4}{3\alpha_{RS}})(\frac{n(3n-4)}{3(n-1)^2} + \frac{n^2}{3(n-1)\alpha_S})} \tag{3.5}$$

where,

$$\alpha_{RS} = \frac{\phi_S \rho_S^2 G_m \left(\frac{n(3n-4)}{3(n-1)^2} + \frac{n^2}{3(n-1)\alpha_S}\right)}{3(1-\phi_R)\phi_S E_P} \tag{3.6}$$

Similarly, the stiffness, E_{SR} of a 2H SR composite is found out by substituting Eq. (3.1) for E_P in Eq. (3.3) and the obtained expression for E_{SR} is normalized by dividing it by $E_P\phi_R\phi_S$ as,

$$\frac{E_{SR}}{E_P\phi_R\phi_S} = \frac{1}{(\frac{4}{3}+\frac{4}{3\alpha_R})(\frac{n(3n-4)}{3(n-1)^2}+\frac{n^2}{3(n-1)\alpha_{SR}})} \tag{3.7}$$

where,

$$\alpha_{SR} = \frac{\phi_S\rho_S^2 G_m\left(\frac{4}{3}+\frac{4}{3\alpha_R}\right)}{3\left(1-\phi_S\right)\phi_R E_P} \tag{3.8}$$

3.2.2 Strength

The average stress occurring in a composite when the maximum shear stress in the matrix reaches the shear strength of the matrix $\tau^m_{critical}$ or the normal stress in the platelet reaches the strength of the platelet $\sigma^p_{critical}$ is referred to as the composite strength (Zhang et al., 2010). The composite strength of a regularly staggered composite is given by (Zhang et al., 2010) as,

$$\sigma^R_{critical} = \begin{cases} \phi_R\sigma^p_{critical}\frac{\rho_R}{2\rho'_{critical}} & \text{if } \rho_R \le \rho'_{critical} \\ \phi_R\sigma^p_{critical}\frac{1}{2} & \text{if } \rho_R > \rho'_{critical} \end{cases} \tag{3.9}$$

where,

$$\rho'_{critical} = \frac{\sigma^p_{critical}}{\tau^m_{critical}} \tag{3.10}$$

is the critical aspect ratio separating matrix failure $\rho_R \le \rho'_{critical}$ from platelet failure $\rho_R > \rho'_{critical}$

The composite strength of a stairwise staggered composite is given by (Zhang et al., 2010) as,

$$\sigma^S_{critical} = \begin{cases} \phi_S\sigma^p_{critical}\frac{n-1}{n}\frac{\rho_S}{\rho''_{critical}} & \text{if } \rho_S \le \rho''_{critical} \\ \phi_S\sigma^p_{critical}\frac{n-1}{n} & \text{if } \rho_S > \rho''_{critical} \end{cases} \tag{3.11}$$

where,

$$\rho''_{critical} = (n-1)\frac{\sigma^p_{critical}}{\tau^m_{critical}} \tag{3.12}$$

is the critical aspect ratio separating matrix failure $\rho_S \leq \rho''_{critical}$ from platelet failure $\rho_S > \rho''_{critical}$

The strength, σ_{RS} of a two hierarchical regularly staggered composite with stairwise staggered composites as platelets is found out by substituting Eq. (3.11) for $\sigma^p_{critical}$ in Eq. (3.9) and the obtained expression for $\sigma^{RS}_{critical}$ is normalized by dividing it by $\sigma^P_{critical}\phi_R\phi_S$ as,

$$\frac{\sigma^{RS}_{critical}}{\sigma^p_{critical}\phi_R\phi_S} = \begin{cases} \frac{\rho_{RS}}{2\phi_S\frac{\sigma^p_{critical}}{\tau^m_{critical}}} & \text{if } \rho_{RS} \leq \rho'_{RS,critical} \\ \frac{\rho_S}{2n\frac{\sigma^p_{critical}}{\tau^m_{critical}}} & \text{if } \rho_{RS} > \rho'_{RS,critical} \; and \; \rho_S \leq \rho''_{critical} \\ \frac{n-1}{2n} & \text{if } \rho_{RS} > \rho'_{RS,critical} \; and \; \rho_S > \rho''_{critical} \end{cases} \tag{3.13}$$

where, ρ_{RS} and $\rho'_{RS,critical}$ are respectively the aspect ratio and its critical value for a 2H RS composite. $\rho'_{RS,critical}$ is given by,

$$\rho'_{RS,critical} = \begin{cases} \frac{\phi_S\rho_S}{n} & \text{when } \rho_S \leq \rho''_{critical} \\ \frac{(n-1)\phi_S\sigma^p_{critical}}{n\tau^m_{critical}} & \text{when } \rho_S > \rho''_{critical} \end{cases} \tag{3.14}$$

Similarly, the strength of a two hierarchical stairwise staggered composite with regularly staggered composites as platelets, σ_{SR} can be found out by substituting Eq. (3.9) for $\sigma^p_{critical}$ in Eq. (3.11) and the obtained expression for $\sigma^{SR}_{critical}$ is normalized by dividing it by $\sigma^P_{critical}\phi_R\phi_S$ as,

$$\frac{\sigma^{SR}_{critical}}{\sigma^p_{critical}\phi_R\phi_S} = \begin{cases} \frac{\rho_{SR}}{n\phi_R\frac{\sigma^p_{critical}}{\tau^m_{critical}}} & \text{if } \rho_{SR} \leq \rho''_{SR,critical} \\ \frac{(n-1)\rho_R}{2n\frac{\sigma^p_{critical}}{\tau^m_{critical}}} & \text{if } \rho_{SR} > \rho''_{SR,critical} \; and \; \rho_R \leq \rho'_{critical} \\ \frac{n-1}{2n} & \text{if } \rho_{SR} > \rho''_{SR,critical} \text{ and } \rho_R > \rho'_{critical} \end{cases} \tag{3.15}$$

where, ρ_{SR} and $\rho''_{SR,critical}$ are respectively the normal and critical aspect ratios of 2H SR composite. Here, $\rho''_{SR,critical}$ is given by,

$$\rho''_{SR,critical} = \begin{cases} \frac{(n-1)\phi_R\rho_R}{2} & \text{when } \rho_R \leq \rho'_{critical} \\ \frac{(n-1)\phi_R\sigma^p_{critical}}{2\tau^m_{critical}} & \text{when } \rho_R > \rho'_{critical} \end{cases} \tag{3.16}$$

3.2.3 Failure Strain

The optimal structural arrangement should influence not only stiffness and strength but also the failure strain $\epsilon^{RS}_{critical} = \sigma^{RS}_{critical}/E_{RS}$ and energy storage capacity $w^{RS}_{critical}=(\sigma^{RS}_{critical})^2/2E_{RS}$. The failure strain is normalized by the platelet failure strain $\epsilon^P_{critical} = \sigma^P_{critical}/E_P$ and is obtained for a 2H RS composite from Eq. (3.5) and Eq. (3.13) as,

$$\frac{\epsilon^{RS}_{critical}}{\epsilon^p_{critical}} = \begin{cases} \frac{\rho_{RS}}{2\phi_S\frac{\sigma^p_{critical}}{\tau^m_{critical}}}\left(\frac{4}{3}+\frac{4}{3\alpha_{RS}}\right)\left(\frac{n(3n-4)}{3(n-1)^2}+\frac{n^2}{3(n-1)\alpha_S}\right) & \text{if } \rho_{RS} \leq \rho'_{RS,critical} \\ \frac{\rho_S}{2n\frac{\sigma^p_{critical}}{\tau^m_{critical}}}\left(\frac{4}{3}+\frac{4}{3\alpha_{RS}}\right)\left(\frac{n(3n-4)}{3(n-1)^2}+\frac{n^2}{3(n-1)\alpha_S}\right) & \text{if } \rho_{RS} > \rho'_{RS,critical} \text{ and } \rho_S \leq \rho''_{critical} \\ \frac{n-1}{2n}\left(\frac{4}{3}+\frac{4}{3\alpha_{RS}}\right)\left(\frac{n(3n-4)}{3(n-1)^2}+\frac{n^2}{3(n-1)\alpha_S}\right) & \text{if } \rho_{RS} > \rho'_{RS,critical} \text{ and } \rho_S > \rho''_{critical} \end{cases} \tag{3.17}$$

Similarly, the normalized failure strain for a 2H SR composite is obtained from Eq. (3.7) and Eq. (3.15) as,

$$\frac{\epsilon^{SR}_{critical}}{\epsilon^p_{critical}} = \begin{cases} \frac{\rho_{SR}}{n\phi_R\frac{\sigma^p_{critical}}{\tau^m_{critical}}}\left(\frac{4}{3}+\frac{4}{3\alpha_R}\right)\left(\frac{n(3n-4)}{3(n-1)^2}+\frac{n^2}{3(n-1)\alpha_{SR}}\right) & \text{if } \rho_{SR} \leq \rho''_{SR,critical} \\ \frac{(n-1)\rho_R}{2n\frac{\sigma^p_{critical}}{\tau^m_{critical}}}\left(\frac{4}{3}+\frac{4}{3\alpha_R}\right)\left(\frac{n(3n-4)}{3(n-1)^2}+\frac{n^2}{3(n-1)\alpha_{SR}}\right) & \text{if } \rho_{SR} > \rho''_{SR,critical} \text{ and } \rho_R \leq \rho'_{critical} \\ \frac{n-1}{2n}\left(\frac{4}{3}+\frac{4}{3\alpha_R}\right)\left(\frac{n(3n-4)}{3(n-1)^2}+\frac{n^2}{3(n-1)\alpha_{SR}}\right) & \text{if } \rho_{SR} > \rho''_{SR,critical} \text{ and } \rho_R > \rho'_{critical} \end{cases} \tag{3.18}$$

3.2.4 Energy Storage Capacity

The energy storage capacity (or toughness), of a 2H RS composite is found out using the formula,

$$w_{critical}^{RS} = \frac{(\sigma_{critical}^{RS})^2}{2E_{RS}} \tag{3.19}$$

The obtained $w_{critical}^{RS}$ is normalized by that of $\phi w_{critical}^{p}$ which is given by,

$$\phi w_{critical}^{p} = \frac{\phi {\sigma_{critical}^{p}}^2}{2E_p} \tag{3.20}$$

Thus, the normalized value of energy storage capacity of a 2H RS composite is obtained as,

$$\frac{w_{critical}^{RS}}{\phi_R \phi_S w_{critical}^{p}} = \begin{cases} \frac{\rho_{RS}^2}{4\phi_S^2 (\frac{\sigma_{critical}^{p}}{\tau_{critical}^{m}})^2} \left(\frac{4}{3} + \frac{4}{3\alpha_{RS}}\right) \left(\frac{n(3n-4)}{3(n-1)^2} + \frac{n^2}{3(n-1)\alpha_S}\right) & \text{if } \rho_{RS} \leq \rho'_{RS,critical} \\ \frac{\rho_{RS}^2}{4n^2 (\frac{\sigma_{critical}^{p}}{\tau_{critical}^{m}})^2} \left(\frac{4}{3} + \frac{4}{3\alpha_{RS}}\right) \left(\frac{n(3n-4)}{3(n-1)^2} + \frac{n^2}{3(n-1)\alpha_S}\right) & \text{if } \rho_{RS} > \rho'_{RS,critical} \text{ and } \rho_S \leq \rho''_{critical} \\ \frac{(n-1)^2}{4n^2} \left(\frac{4}{3} + \frac{4}{3\alpha_{RS}}\right) \left(\frac{n(3n-4)}{3(n-1)^2} + \frac{n^2}{3(n-1)\alpha_S}\right) & \text{if } \rho_{RS} > \rho'_{RS,critical} \text{ and } \rho_S > \rho''_{critical} \end{cases} \tag{3.21}$$

The normalized value of energy storage capacity of a 2H SR composite also can be obtained as,

$$\frac{w_{critical}^{SR}}{\phi_R \phi_S w_{critical}^{p}} = \begin{cases} \frac{\rho_{SR}^2}{n^2 \phi_R^2 (\frac{\sigma_{critical}^{p}}{\tau_{critical}^{m}})^2} \left(\frac{4}{3} + \frac{4}{3\alpha_R}\right) \left(\frac{n(3n-4)}{3(n-1)^2} + \frac{n^2}{3(n-1)\alpha_{SR}}\right) & \text{if } \rho_{SR} \leq \rho''_{SR,critical} \\ \frac{(n-1)^2 \rho_R^2}{4n^2 (\frac{\sigma_{critical}^{p}}{\tau_{critical}^{m}})^2} \left(\frac{4}{3} + \frac{4}{3\alpha_R}\right) \left(\frac{n(3n-4)}{3(n-1)^2} + \frac{n^2}{3(n-1)\alpha_{SR}}\right) & \text{if } \rho_{SR} > \rho''_{SR,critical} \text{ and } \rho_R \leq \rho'_{critical} \\ \frac{(n-1)^2}{4n^2} \left(\frac{4}{3} + \frac{4}{3\alpha_R}\right) \left(\frac{n(3n-4)}{3(n-1)^2} + \frac{n^2}{3(n-1)\alpha_{SR}}\right) & \text{if } \rho_{SR} > \rho''_{SR,critical} \text{ and } \rho_R > \rho'_{critical} \end{cases} \tag{3.22}$$

3.3 Results and Discussions

Here, we illustrate the effect of aspect ratio (ρ) on the mechanical properties by considering a representative case of moduli ratio of $E_p/G_m = 1000$ and volume fractions at the first

and second levels of hierarchy $\phi_S = \phi_R = 0.5$. Note that the effective platelet volume fraction for the 2H composites is $\phi_R\phi_S$ and the results are normalized with this value. The number of platelets in a period for the stairwise staggered structure, n is kept as 5. Note that the applicability of the present study depends on the approximate valid regions of the TSC model, which can be identified using the aspect ratio ranges introduced by (Chen et al., 2009) and (Liu et al., 2011).

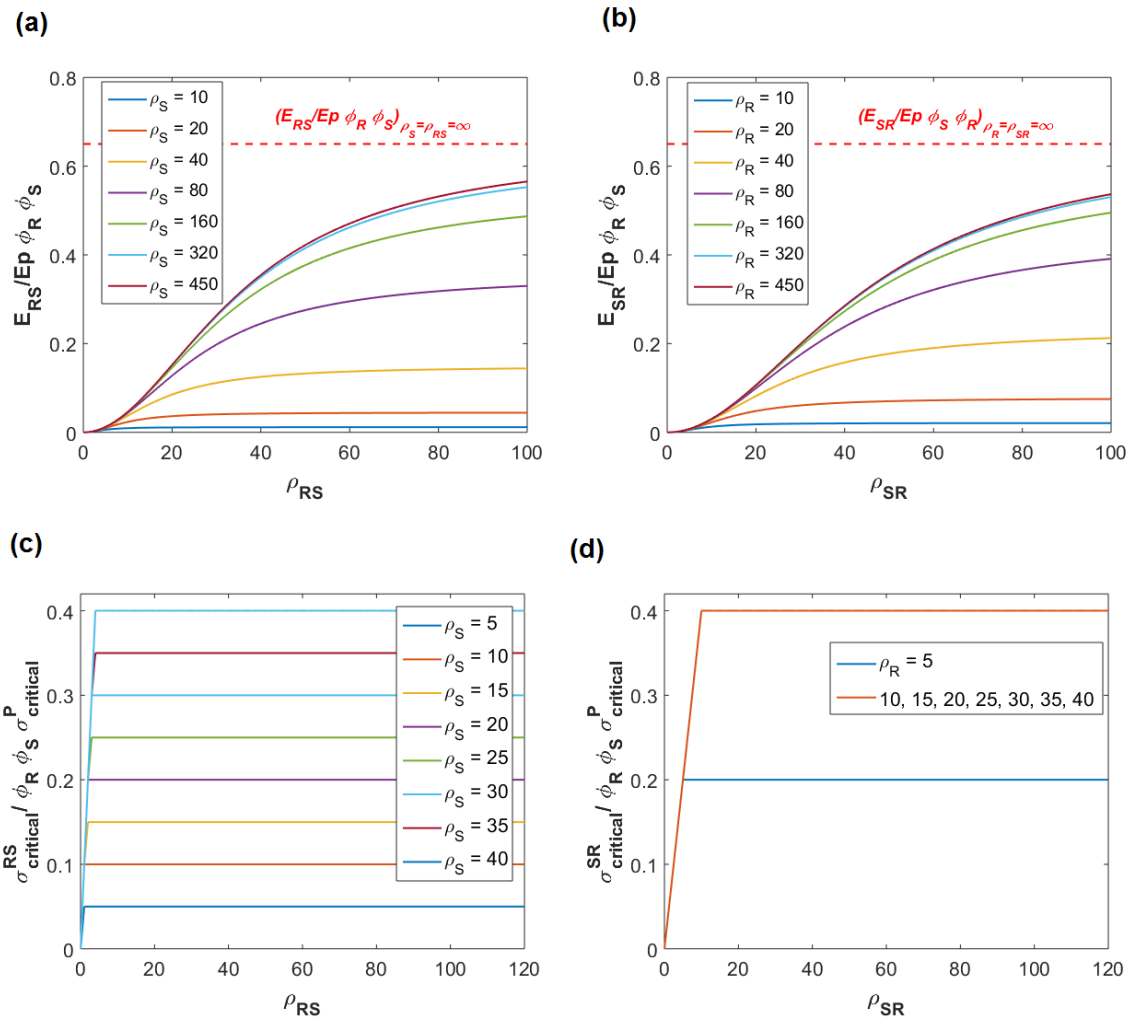

Figure 3.2: Variation of normalized Young's modulus of (a) 2H RS composite with platelet aspect ratio for different values of ρ_{RS} varying from 10 to 100, (b) 2H SR composite with platelet aspect ratio for different values of ρ_{SR} varying from 10 to 100, (c) Variation of normalized strength of 2H RS composite with platelet aspect ratio (ρ_{RS}) for different values of ρ_S varying from 5 to 40, and (d) 2H SR composite with platelet aspect ratio (ρ_{SR}) for different values of ρ_R varying from 5 to 40; $E_p/G_m = 1000$, $\sigma^p_{critical}/\tau^m_{critical} = 10$ and $n = 5$ (The link to the code for reproducing this Figure can be found here)

Figure 3.2 (a) shows the variation of Young's modulus of the 2H RS composite with respect to the platelet aspect ratio (ρ_{RS}) for different values of the platelet aspect ratio of the stairwise staggered composite in the first hierarchical level (ρ_S). It can be seen that Young's modulus increases with an increase of ρ_{RS} as well as ρ_S. After reaching a particular value of ρ_{RS} Young's modulus tends to attain a constant value. The rate of increase in Young's modulus with increasing values of ρ_S also shows a decreasing trend.

A similar pattern can be observed for the 2H SR composite also as shown in Figure 3.2 (b). The x-axis limit for both Figure 3.2 (a) and (b) are kept as 100 so as to capture the lower values of Young's modulus at lower values of aspect ratios. As the aspect ratio increases in both levels of hierarchy, the normalized stiffness converges to a limit stiffness of 0.65, which is obtained by substituting the terms corresponding to $\rho = \infty$ in Equations 3.5 and 3.7.

The stiffness of the platelets decreases with hierarchy. Though at the first level, the stiffness ratio is $1 : 1000$, at the second level, the stiffness ratio is much lesser since the matrix modulus remains the same. For example, consider a 2H SR model. Here, say, $E_p/G_m = 1000$ at the first level of the hierarchy, and the aspect ratio is 10. This gives, in the second level of the hierarchy, the $E_R/G_m \approx 12$ where E_R is the stiffness of the regular staggered composite, which is the platelet in the second level of hierarchy. Also, with increasing levels of hierarchy the matrix material tends to influence the mechanical properties of the composite more even for self-similar hierarchical materials (Sen and Buehler, 2011; Zhang et al., 2011). This could be because with increasing hierarchy, the matrix influences even the platelet properties at that higher level.

Figure 3.2 (c) shows the variation of the strength of the 2H RS composite with platelet aspect ratio (ρ_{RS}) for different values of the platelet aspect ratio of the stairwise staggered composite in the first hierarchical level (ρ_S). The ratio of the strength of mineral platelet (at the first level of hierarchy) to the matrix strength, $\sigma^p_{critical}/\tau^m_{critical}$ is taken to be 10. It is seen that the strength increases with an increase in ρ_{RS} as well as ρ_S, and remains a constant on reaching the critical values for both ρ_{RS} as well as ρ_S. Here, these critical values of aspect ratios in the second level of the hierarchy, $\rho'_{RS,critical}$ and $\rho''_{SR,critical}$ are 4 and 10 respectively. In Figure 3.2 (c) and (d), an x-axis limit of 120 is chosen since it can show both the increasing and then constant y-values trends conveniently.

In Figure 3.2 (d), the normalized strength of 2H SR composites for a set of aspect ratios (ρ_R) greater than 10 is seen to be the same. This is because the strength remains the same beyond the critical aspect ratio in the first level of hierarchy. The maximum strength always depends on the critical aspect ratio of the composite in the first level of the hierarchy. For

2H RS and 2H SR composites, the critical aspect ratios in the first level of the hierarchy are found to be 10 and 40, respectively, for the representative properties chosen. It can also be observed that the critical aspect ratio at the second level of hierarchy for 2H composites for aspect ratios beyond the critical aspect ratio in the first level of the hierarchy are 4 and 10 respectively for 2H RS and 2H SR composites. Thus, the aspect ratios beyond the critical aspect ratios in both levels of hierarchy will result in identical and constant curves of strength. This implies that the maximum strength that can be achieved by both 2H RS and 2H SR composites are capped at a value of 0.4, which is lesser than that of the strengths of regularly and stairwise staggered composites.

Figure 3.3(a) shows the variation of the normalized critical strain of the 2H RS composite with respect to the platelet aspect ratio in the second hierarchical level (ρ_{RS}) for different values of the platelet aspect ratio of the stairwise staggered composite in the first hierarchical level (ρ_S). Here, it can be seen that for lesser values of ρ_{RS}, maximum values of strain are observed for all cases of ρ_{RS}. It can also be seen that when ρ_S is increased, the values of critical strain converge to a constant value. The variation of the normalized critical strain of 2H SR composite is shown in Figure 3.3 (b), in which a kink can be observed, which is attributed to the stairwise pattern in the second level of hierarchy. In Figure 3.3 (a) and (b), the x-axis limit is set as 120 so as to capture the decreasing trend of y-values for up to x-values of around 40 and uniform y-values beyond that.

Figure 3.3 (c) shows the variation of normalized energy storage capacity of the 2H RS composite with platelet aspect ratio (ρ_{RS}) for different values of the platelet aspect ratio of the stairwise staggered composite in the first hierarchical level (ρ_S). We observe that the toughness decreases with an increase in both ρ_{RS} and ρ_S. It is also seen that the curves show a trend of converging towards a constant value when ρ_S is increased. Figure 3.3 (d) shows that the toughness of the 2H SR composite increases initially, but after reaching a peak value it tends to decrease. As ρ_R is increased the curves are seen to converge as in 2H RS composites. Moreover, the maximum value of toughness is obtained for a combination of critical aspect ratios in both levels of hierarchy.

Note that Figure 3.3 (c) is drawn to capture the difference with respect to the aspect ratio in the first level of hierarchy, which does not show the peak point of the graph. Moreover, the shape of the graphs seems to be dictated by the variable that is used in the x-axis, and a change of variable (for example in the case of 2H RS composites, interchanging ρ_{RS} and ρ_R) produces a different shape as shown in Figure 3.4. The y-limit of the graph is set to 45 in Figure 3.3 (c) to capture the difference with respect to the aspect ratio in the first level of the hierarchy, which ignores the peak point of the graph.

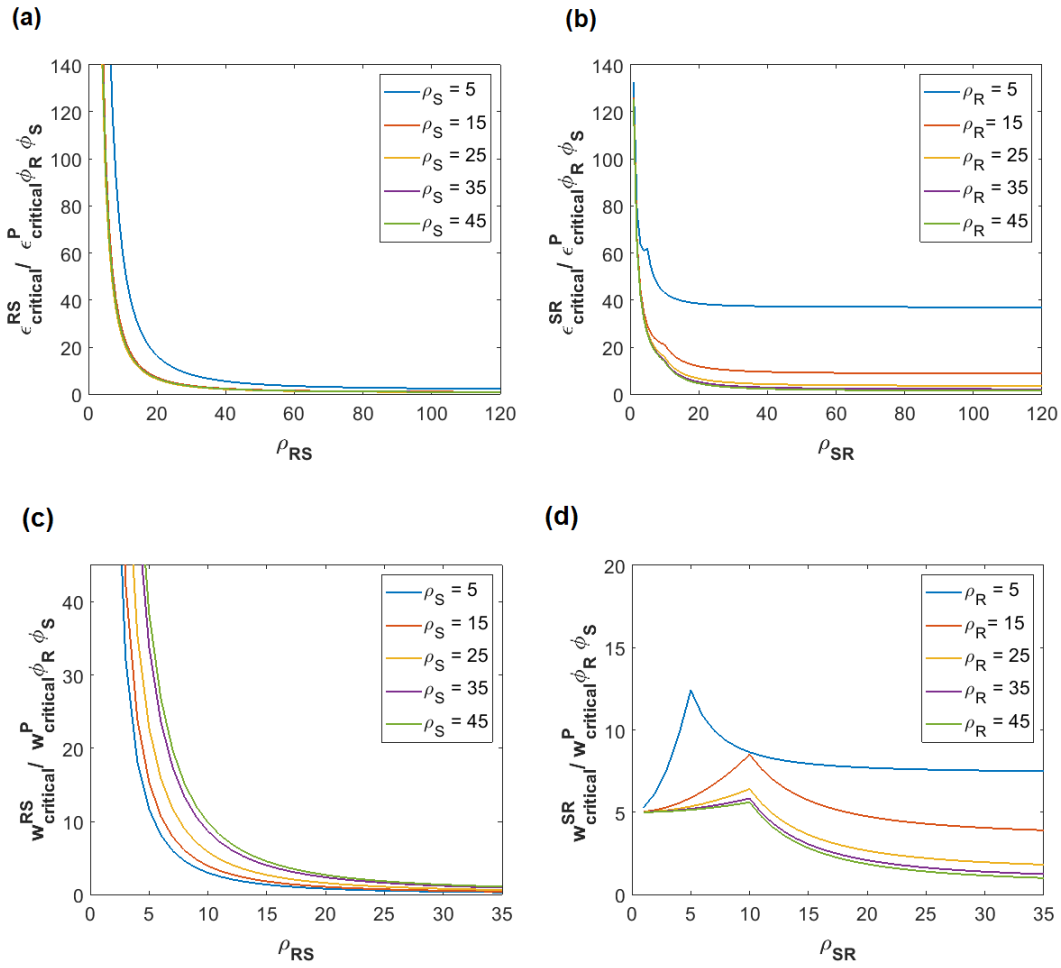

Figure 3.3: Variation of normalized critical strain of (a) 2H RS composite with platelet aspect ratio (ρ_{RS}) for different values of ρ_S varying from 5 to 45 , and (b) 2H SR composite with platelet aspect ratio (ρ_{SR}) for different values of ρ_R varying from 5 to 45 (c) Variation of normalized energy storage capacity of 2H RS composite with respect to platelet aspect ratio (ρ_{RS}) for different values of ρ_S varying from 5 to 45 , and (d) 2H SR composite with respect to platelet aspect ratio (ρ_{SR}) for different values of ρ_R varying from 5 to 45; $E_p/G_m = 1000$, $\sigma^p_{critical}/\tau^m_{critical} = 10$ and $n = 5$ (The link to the code for reproducing this Figure can be found here)

The relevant graph without y-limit is provided as shown in Figure 3.4 (a). Probably, the shape of the graphs seems to be dictated by the variable that is used in the x-axis. For example, for an RS composite, if instead of ρ_{RS}, ρ_S is used in the x-axis with different curves drawn for different ρ_{RS}, the effect is similar to that of a stairwise staggered composite as shown in Figure 3.4 (b). To depict the varying trend of y-values for x-values up to a range of 15 to 20 after which the y-values tend to remain uniform, an x-limit of 35 is chosen in Figure 3.3 (c) and (d).

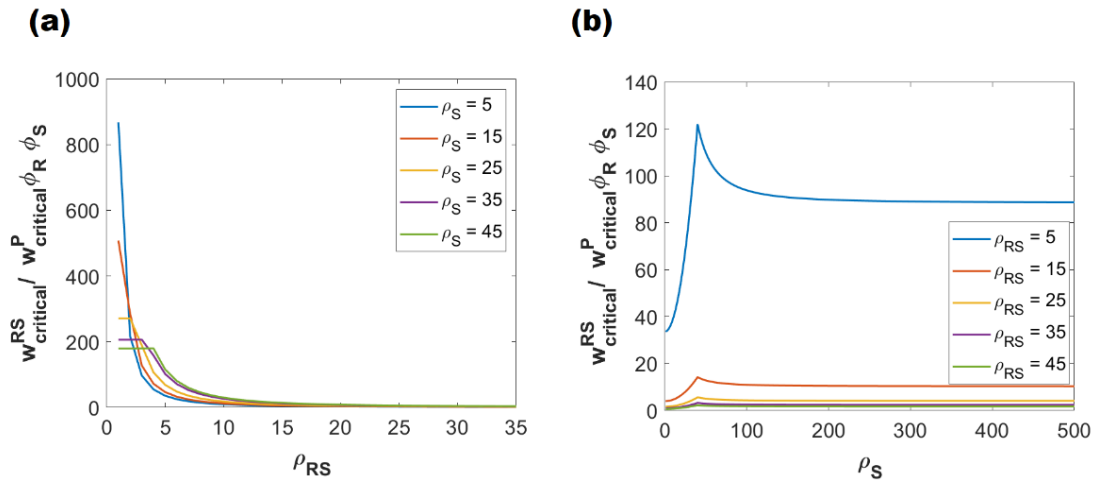

Figure 3.4: Variation of normalized energy storage capacity of 2H RS composite with respect to (a) platelet aspect ratio at 2H (ρ_{RS}) for different values of platelet aspect ratio at 1H (ρ_S) varying from 5 to 45 (without y-lim); (b) platelet aspect ratio at 1H (ρ_S) for different values of platelet aspect ratio at 2H (ρ_{RS}) varying from 5 to 45

The comparison of the above graphs for 2H bio-inspired composites with that of a unidirectional composite with regularly staggered platelet distribution shows that for $\rho_S > 100$, the stiffness of the 2H RS composite approaches to that of the regularly staggered composite. Moreover, the maximum normalized strength of the 2H RS composites (0.4) seems to be marginally lesser than that of a regularly staggered composite (0.5) (Zhang et al., 2010). The toughness of 2H composites are much higher compared to that for unidirectional nanocomposite with regularly staggered platelet distribution, but this increment is confined to a smaller range of aspect ratios at the first level of hierarchy.

The 2H RS and 2H SR composites consist of a stairwise staggered structure in the first or second level of the hierarchy, where the number of platelets per period is n. This design parameter could influence the mechanical properties. We investigate the dependence in toughness and strength of 2H RS and 2H SR composites on this parameter. For this purpose, we vary the aspect ratio, and find the maximum value of toughness for each n, while keeping all other parameters fixed. We consider two cases: unconstrained and with imposing a lower limit value for normalized stiffness (2% that of platelet) in the analysis. When we fix the value of n for both hierarchical levels in SR and RS combinations, the maximum toughness occurs at the critical aspect ratios at both levels. Therefore, we find out the maximum toughness value (at the critical aspect ratio) for both SR and RS composites. The strength of the composite for the same combination of n and aspect ratios is also found

out. The procedure is repeated for each value of n, varying from 2 to 10 to investigate the effect of n on the strength and toughness.

Figure 3.5 (a) and (b) show the maximum toughness and corresponding strengths obtained for models without imposing a lower value of normalized stiffness and it can be seen that for 2H RS composites, the maximum toughness is achieved for $n = 2$, but the normalized strength at that point is the least which is only 0.2.

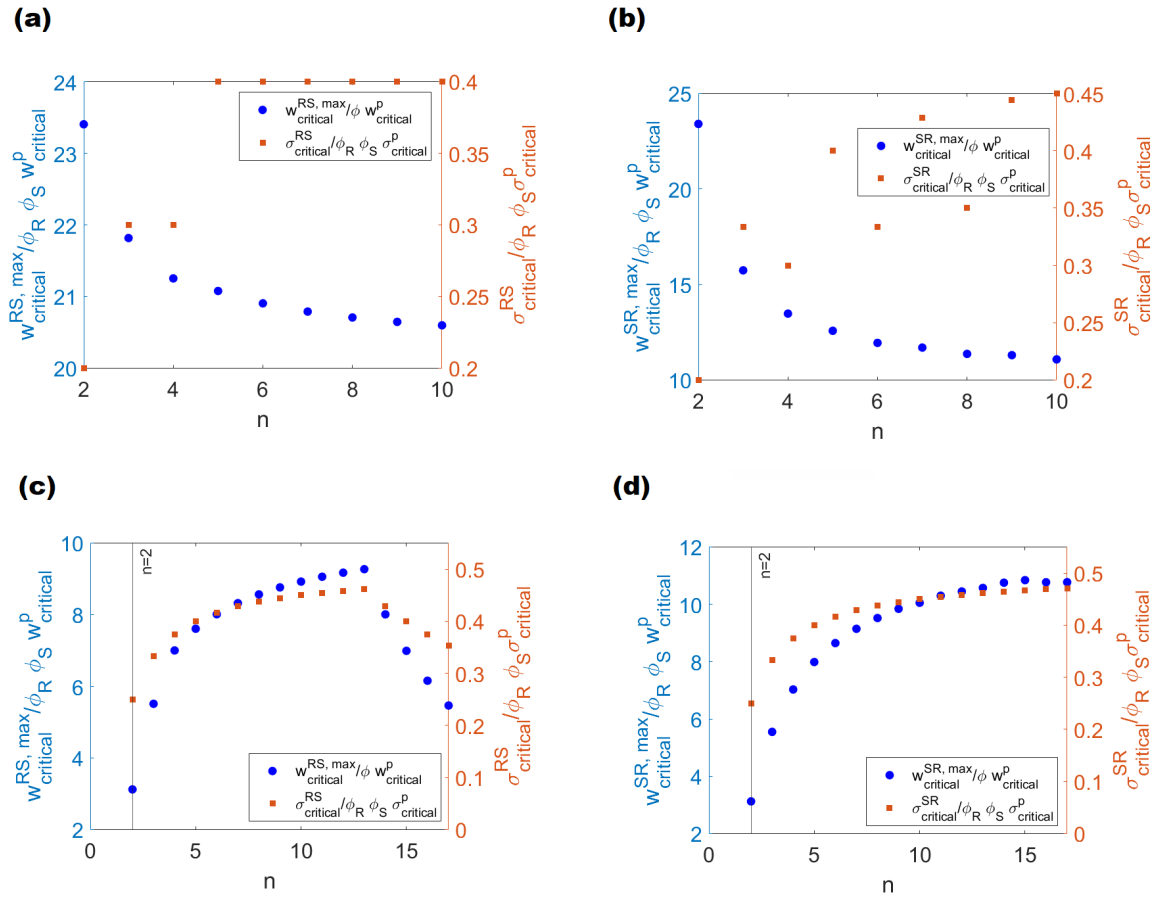

Figure 3.5: Normalized strength vs normalized maximum toughness for (a) Two Hierarchical Regularly Staggered Model with Stairwise Staggered Model as platelet (2H RS) (see Table 3.1 for the corresponding data of aspect ratios), (b) Two Hierarchical Stairwise Staggered Model with Regularly Staggered Model as platelet (2H SR) (see Table 3.1 for the corresponding data of aspect ratio), (c) 2H RS model with a minimum normalized stiffness of 2%, (d) 2H SR model with a minimum normalized stiffness of 2%; the aspect ratios chosen corresponds to the one required to obtain the maximum toughness. $E_p/G_m = 1000$, $\sigma^p_{critical}/\tau^m_{critical} = 10$ for all models.

It can be well understood from Figure 3.5 (a) that the point corresponding to $n = 3$ can be considered as an optimal point where we can obtain toughness as high as 21.82 with a strength of 0.3. With further increase in n, it is seen that the toughness decreases whereas the strength increases and gets capped at a value of 0.4. The variation of maximum toughness for 2H SR composites also shows a decreasing trend as that of 2H RS composites, but the strength shows an oscillating trend which can be well explained by equation 3.16. Figure 3.5 (c) and (d) show the results for models with a minimum normalized stiffness of 2% that of the platelet. It can also be seen from Figure 3.5 (c) and (d) that the strength and toughness increase first with the number of platelets in a period (n) and decreases after reaching a peak value when the minimum stiffness criterion is imposed.

Here, it would be worthwhile to compare self-similar and non-self similar models. Self-similar hierarchical structures with regularly staggered arrangement is a special case of 2H RS and 2H SR composite with the period, $n = 2$. For the case of unrestricted stiffness, (Figure 3.5 (a) and (b)) it can be seen that the non-self-similar models possess higher strength but lower toughness. However, for the case where the stiffness of the hierarchical composite is restricted to a minimum value of at least 2% of the platelet (similar to RSM), non-self similar models provide both higher toughness and strength. For example, the maximum normalized toughness is observed to be 9.272 at n=13 and 10.84 at n=15 (around three times higher than that of the self-similar model) for 2H RS and 2H SR models respectively at n=10 with a corresponding normalized strength of approximately 0.46 for both the models.

From the comparison of the normalized toughness and normalized strength values for n= 2 and n= 5 in Figure 3.5 (a), and (b), we found that non-self-similar 2H composites can indeed provide increased strength than self-similar 2H composites with reasonable toughness for unconstrained stiffness. From Figure 3.5 (c) and (d) we found that non-self-similar 2H composites can provide both higher toughness and strength than self-similar 2H composites for cases with constrained stiffness. Therefore, while designing 2H bio-inspired composites, non-self-similarity could be an important design consideration.

Table 3.1 shows the combination of aspect ratios required at the first and second levels of hierarchy to produce maximum toughness in the 2H RS and 2H SR composites with the corresponding strength. It can be seen that the aspect ratio combinations for a 2H RS composite show an increasing trend while an oscillating trend is observed for the case of the aspect ratio in the first level of hierarchy for 2H SR composites. For both the 2H composites, the maximum toughness is observed to be decreasing when the number of platelets in each period (n) is increased. It can also be seen that 2H RS composites are

capable of achieving more toughness and strength. But, as mentioned earlier, the normalized Young's modulus values corresponding to the maximum toughness will be extremely small. Therefore, when the stiffness is also considered, both the 2H composites give almost equal maximum toughness and strength as explained in Figure 3.5 (c), and (d).

Table 3.1: Combination of aspect ratios at the first and second levels of hierarchy in 2H composites to obtain maximum toughness and corresponding strength

Number of platelets in each period (n)	2H RS				2H SR			
	Maximum normalized toughness	ρ_S	ρ_{RS}	Normalized strength at maximum normalized toughness	Maximum normalized toughness	ρ_R	ρ_{SR}	Normalized strength at maximum normalized toughness
2	23.4044	8	2	0.2	23.4044	8	2	0.2
3	21.8167	18	3	0.3	15.7407	10	5	0.3333
4	21.2533	24	3	0.3	13.4756	8	6	0.3
5	21.0778	40	4	0.4	12.5778	10	10	0.4
6	20.9056	48	4	0.4	11.9437	8	10	0.3333
7	20.7906	56	4	0.4	11.6984	10	15	0.4286
8	20.7084	64	4	0.4	11.3683	8	14	0.35
9	20.6467	72	4	0.4	11.3025	10	20	0.4444
10	20.5986	80	4	0.4	11.0822	10	23	0.45

3.4 Comparison of Analytical results with Finite Element Results

In this section, the obtained results for Young's modulus for 2H composites are validated by conducting a Finite Element Analysis (FEA) using the commercially available Finite Element Package ABAQUS (SIMULIA, 2022). The FEA is carried out for 2H RS as well as 2H RS composites as follows:

3.4.1 2H RS Composites

For this, a Representative Volume Element (RVE) of the stairwise staggered composite was created with an E_p/G_m ratio of 1000 for different volume fractions and aspect ratios of the

platelet. The Poisson's ratios of platelet and matrix are set as 0.22 and 0.49 respectively. The following procedure is adopted for finding the properties of 2H RS composites by finite element (FE) simulation. The properties of the SSM at the first level of the hierarchy are found out first. To find out the properties of the 2H RS composite, the platelets in the RSM at the second level of the hierarchy are modeled with orthotropic material properties as that obtained from the analysis of the SSM at the first level of hierarchy.

Figure 3.6 shows the quad dominated meshing and the boundary conditions (BC) applied to the Finite FE models of the TSC RVEs used for the static analysis of 2H RS composites. The SSM and RSM as shown in Figure 3.6 are meshed with 5,042 and 2,048 numbers of quadrilateral shaped CPE4R elements respectively, with linear geometric order. The mesh dependency study for a regular staggered model is provided in Appendix F, which showed that the stress variation with change in mesh size is very less. Periodic boundary conditions (PBC) and symmetric boundary conditions (SBC) were applied in SSM and RSM respectively at the highlighted boundaries (excluding the removed matrix region) as depicted in Figure 3.6 for finding the stiffness matrix coefficients.

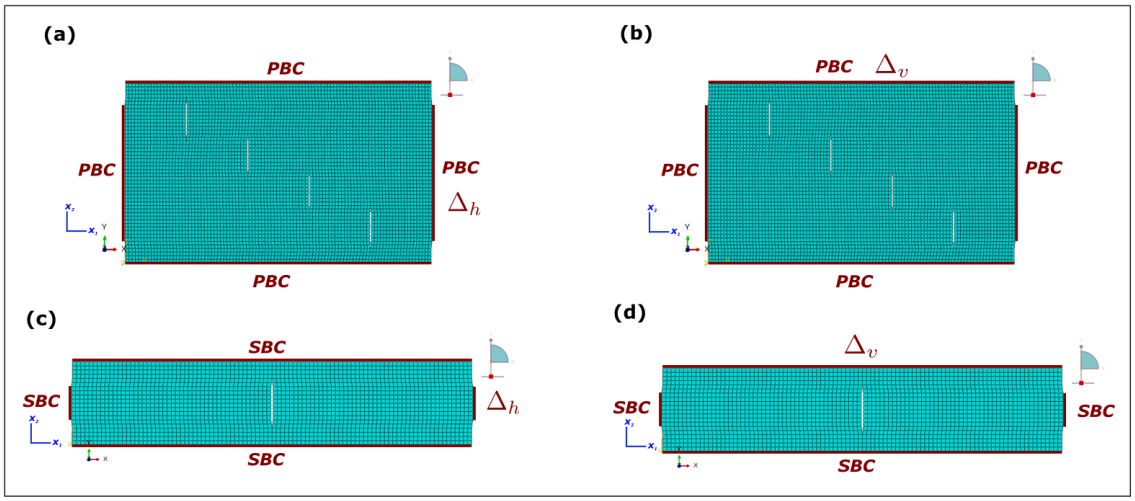

Figure 3.6: TSC FE models with highlighted boundary conditions (BC) applied for static analysis of 2H RS composite having 80% volume fraction of platelets with a platelet aspect ratio of 12, (a) SSM model in the first level of hierarchy for finding Q_{11} & Q_{12}, (b) SSM model in the first level of hierarchy for finding Q_{22}, (c) RSM model in the second level of hierarchy for finding Q_{11} & Q_{12}, (d) RSM model in the second level of hierarchy for finding Q_{22}; PBC, SBC, Δ_h, Δ_v represent the periodic and symmetric boundary conditions, horizontal and vertical displacements respectively.

For an orthotropic lamina with plane stress conditions and coordinate directions x_1 and x_2 as shown in Figure 3.6, we have the stress $\{\sigma\}$ - strain $\{\epsilon\}$ relationship as (Gibson,

2016),

$$\begin{Bmatrix} \sigma_{11} \\ \sigma_{22} \\ \sigma_{12} \end{Bmatrix} = \begin{bmatrix} Q_{11} & Q_{12} & 0 \\ Q_{12} & Q_{22} & 0 \\ 0 & 0 & Q_{66} \end{bmatrix} \begin{Bmatrix} \epsilon_{11} \\ \epsilon_{22} \\ \epsilon_{12} \end{Bmatrix} \tag{3.23}$$

Displacement in horizontal direction (Δ_h) was applied to compute the stiffness matrix coefficient Q_{11} and Q_{12}. To determine Q_{22}, displacement was applied in the vertical direction (Δ_v). Considering the model to be in plane-strain, the stiffness matrix [Q] and thereafter the compliance matrix [S] is obtained by manipulating the ABAQUS output database (Gibson, 2016; SIMULIA, 2022).

A finite RVE as shown in Figure 3.6 (a) is enough to simulate a bulk material for evaluating the material properties of an SSM provided that periodic boundary conditions are used (Wu et al., 2014). For finding Q_{11} and Q_{12}, the periodic boundary conditions are applied such that the strain along the x_2 direction, $\epsilon_{22} = 0$. Similarly, for finding Q_{22}, periodic boundary conditions are imposed to keep the strain along the $x_1$direction, $\epsilon_{11} = 0$.

Another FE model is built and subjected to shear by applying a point load (P) at the top corners and keeping bottom edges arrested from moving in the horizontal directions as shown in Figure 3.7. The nodes in the top edge are constrained such that the difference between displacements along the x_1-direction (u_1) of two successive nodes is zero. The shear modulus is found out by using $G_{12} = \frac{2PW_{rve}}{L_{rve}\delta_1}$ where, L_{rve} and W_{rve} are the length and width of the model respectively and δ_1 is the resulting magnitude of deflection in x_1-direction as marked in Figure 3.7 (a) (Sun and Vaidya, 1996). The length and width of the TSC SSM RVE shown in Figure 3.7 (b) is given by,

$$L_{rve} = h_m + L; \quad W_{rve} = n(v_m + b) \tag{3.24}$$

where, L, b, h_m, and v_m are the length and width of platelet and thickness of matrix between two columns of platelets, and thickness of matrix between two rows of platelets respectively.

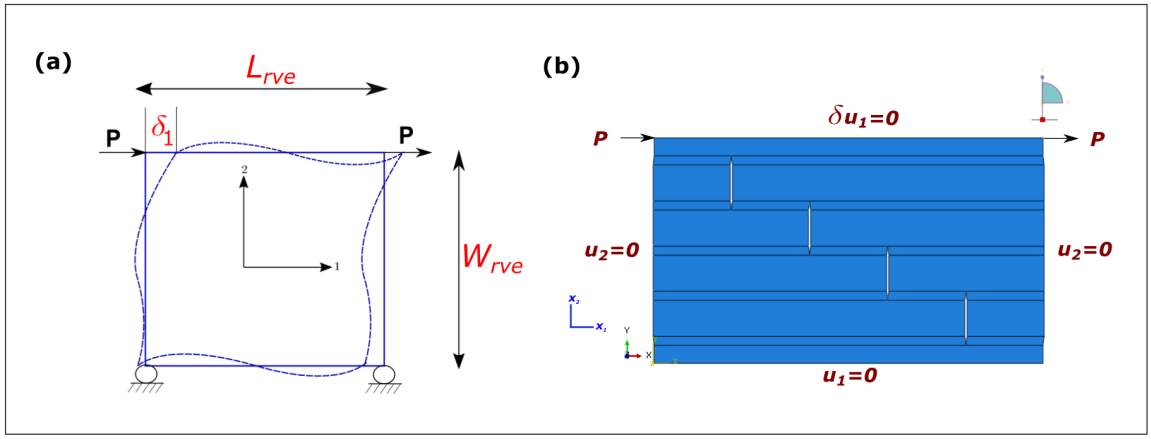

Figure 3.7: Boundary conditions applied for finding G_{12} (a) Schematic diagram (Adapted with permission from (Sun and Vaidya, 1996)), L_{rve}, W_{rve} & δ_1 represent the length and width of the RVE and the resulting magnitude of deflection along x_1 direction respectively, (b) SSM model in the first level of hierarchy with the applied boundary conditions, $u_1, u_2, \delta u_1$ represent the displacements along x_1 and x_2 directions and difference in u_1 between two adjacent nodes, respectively.

In the present study, it is assumed that the thickness of the matrix between two columns is one-fourth of that between two rows of platelets and can be found out by solving the following equation for given values of volume fraction (ϕ), L and b.

$$\phi = \frac{nLb}{L_{rve}W_{rve}} = \frac{Lb}{(h_m + L)(v_m + b)} \tag{3.25}$$

The same procedure is repeated with suitable symmetric boundary conditions for an RVE of a regularly staggered composite (as shown in Figure 3.6 (c) and (d)) with orthotropic platelet properties as that obtained from the previous results. The obtained results from FE analysis are tabulated as shown in Table 3.2, and compared with analytical results. It is seen that the results from Finite Element Analysis (FEA) hold a reasonably good agreement with the proposed analytical model, especially for larger aspect ratios. For 2HRS composites, the maximum error (5.6%) is observed for the model with a volume fraction 90% and an aspect ratio of 12, whereas the error is observed to be least (0.55%) for the model having volume fraction 80% and an aspect ratio of 30. Note that in general, for the TSC model, the analytical values though in good agreement with FE results, could be higher or lower depending on aspect ratio, volume fraction and type of arrangement (whether SSM or RSM) (Ji and Gao, 2004a; Lei et al., 2012b).

It can be seen that the maximum error is 5.63% in the computations, and decreases with an increase in the aspect ratio. Also, the error is observed to be greater in the second

level of the hierarchy, which is attributed to the orthotropic properties of the platelets at the second hierarchy (the analytical model is based on isotropic materials for platelets and matrix). The errors are accumulated, but the errors with opposite signs when accumulated get reduced to an extent. This leads to a lower error in the second level of hierarchy in some cases (for example, $\phi = 0.8,\ \rho = 30$), since the error from the first level of the hierarchy is canceled out to an extent in the second level of hierarchy.

Table 3.2: Comparison of analytical and FE results of stiffness, E_{RS} of a 2H RS composite (The link to the python scripts for reproducing these values can be found here)

Volume Fraction (ϕ)	Aspect Ratio	Young's modulus of Composite (MPa)			
		First Hierarchy (SSM)		Second Hierarchy (2H RS)	
		Finite Element Analysis	Analytical Method	Finite Element Analysis	Analytical Method
0.8	12	458.74	466.8	197.34	207.88
	18	934.24	938.28	413.82	429.66
	30	1970.22	1943.1	941.63	946.85
0.9	12	1046.46	1055.6	498.39	528.15
	18	1927.45	1915.4	976.97	1008.9
	30	3376.3	3285.6	1923.82	1889.4

3.4.2 2H SR Composites

Here, we describe the FE model of 2H SR composites. Fig. 3.9 shows the boundary conditions applied in the finite element representative volume element (RVE) of the stairwise and regular staggered composites at the first and second levels of hierarchies respectively. Symmetric boundary conditions (SBC) are applied for computing the stiffness matrix coefficients of the regular staggered model (RSM) in the first level of the hierarchy, as shown in Fig. 3.9 (a) and (b). To find the shear modulus of the RSM in the first hierarchy, the regular staggered FE model was subjected to shear by applying a point load at the top corners with the bottom edges arrested from moving in the horizontal directions as shown in Fig. 3.10. In Fig. 3.10, the difference between u_1 of two successive nodes is set to zero.

The above procedure is repeated with suitable periodic boundary conditions for the stairwise staggered RVEs. For this, orthotropic material properties are assigned to the platelets at the second level of hierarchy, using the data obtained from the analysis of the

RSM at the first level of hierarchy. The obtained results from FE analysis are then compared with analytical results.

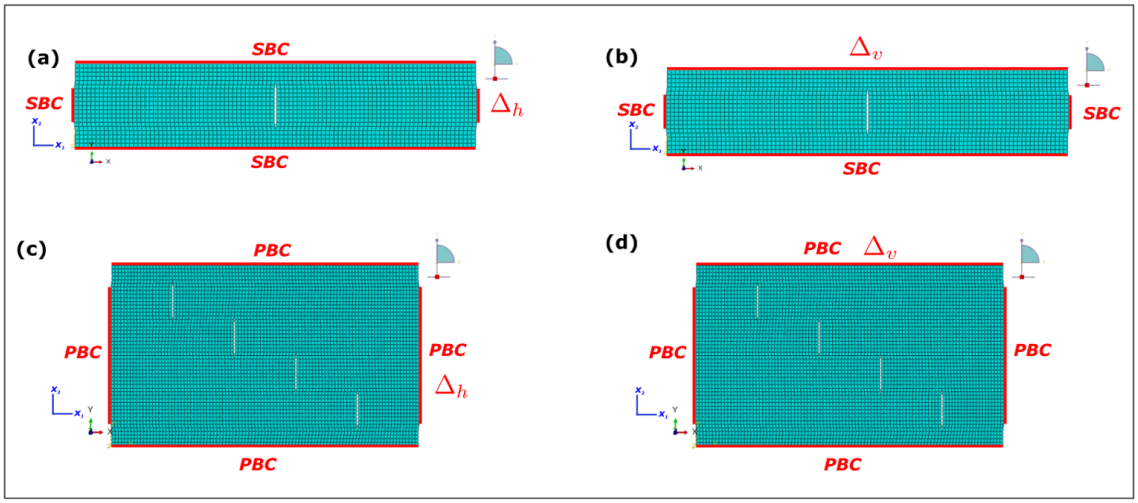

Figure 3.9: TSC FE models with highlighted boundary conditions (BC) applied for static analysis of 2H SR composite having 80% volume fraction of platelets with a platelet aspect ratio of 12, (a) Regular staggered model (RSM) in the first level of hierarchy for finding Q_{11} & Q_{12}, (b) RSM model in the second level of hierarchy for finding Q_{22} (c). Stairwise staggered model (SSM) model in the second level of hierarchy for finding Q_11 & Q_{12}, d. SSM model in the second level of hierarchy for finding Q_{22}; PBC, SBC, Δh, ΔV represent the periodic and symmetric boundary conditions, horizontal and vertical displacements respectively.

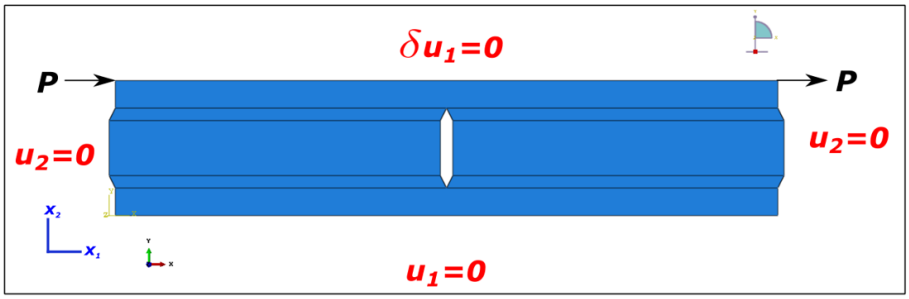

Figure 3.10: Boundary conditions applied for the computation of shear modulus (G12) of the RSM u_1, u_2, δu_1 represent the displacements in the directions x_1 and x_2 directions and difference in u_1 between two adjacent nodes, respectively.

For carrying out the FE analysis, the material properties of platelet and matrix are chosen such that the ratio of Young's modulus of platelet (E_p) to the shear modulus of matrix

(G_m) is 1000. The Poisson's ratio of platelet and matrix were set as 0.22 and 0.49 respectively. Three different aspect ratios ($\rho = 12, 18, 30$) were chosen for two sets of platelet volume fractions ($\phi = 0.8, 0.9$).

Table 3.3: Comparison of FE and analytical results of stiffness, E_{SR} of a 2H SR composite

Volume Fraction (ϕ)	Aspect Ratio	Young's modulus of Composite (MPa)			
		First Hierarchy (RSM)		Second Hierarchy (2H SR)	
		Finite Element Analysis	Analytical Method	Finite Element Analysis	Analytical Method
0.8	12	671.01	676.51	204.02	246.62
	18	1261.41	1267	428.63	502.11
	30	2299.7	2290.9	955.94	1069.3
0.9	12	1416.75	1425.4	502.65	602.9
	18	2329.54	2329	975.15	1127.16
	30	3509.71	3448	1877.12	2033.7

The obtained results are tabulated as shown in Table 3.3. It can be seen that the FE results hold an excellent agreement with the analytical results at the first level of hierarchy for all the models. The results in the second level of hierarchy indicates that the FEA yields a slightly lesser approximation of stiffness compared to the analytical results. This may be attributed to the orthotropic properties applied in the FEA which is not considered in the derivations of the analytical equations selected for the comparison. It is also seen that the error between the analytical and FE results decreases as the aspect ratio increases, for both sets of volume fractions chosen.

3.5 Conclusion

In this Chapter, two non-self similar hierarchical bio-inspired composites, Two Hierarchical Regularly Staggered composite with Stairwise Staggered composite as platelet (2H RS) and Two Hierarchical Stairwise Staggered composite with Regularly Staggered composite as platelet (2H SR) were analyzed. From the results and discussions, it can be concluded that the two hierarchical non-self similar composites conceived in the present study possess much higher toughness than single hierarchical regular staggered (RSM) and stairwise staggered models (SSM) available in literature (Zhang et al., 2010).

When using two levels of non-self-similar hierarchy, the toughness can be amplified by a factor of more than 20 while keeping the strength at 20% of the platelet. However,

these values induce a substantial reduction of elastic stiffness (less than 1% of the platelet stiffness). Even if the minimum stiffness is set to 2% of the platelet, the toughness gain is still greater than 10 times regardless of the staggered arrangement in the first or second level of hierarchy. Moreover, non-self-similar composites seem to have much better strength while possessing similar toughness to that of self-similar 2H composites. Therefore, these results will be useful to enhance the toughness properties of a 2H composite by reducing the decrease in strength when compared to that of a self-similar structure (Zhang et al., 2011).

The FE analysis results of Young's moduli show a sufficient match with the analytical model. The values of platelet aspect ratios at the first and second levels of hierarchy required to achieve maximum toughness in a 2H composite are also generated by comparing the different combinations. It is also seen that both the configurations i.e., 2H RS and 2H SR are capable of producing an equal range of maximum toughness and strength for a particular minimum stiffness.

It can be found from the present study as well as other research works on self-similar hierarchical structures that the stiffness gets reduced whenever a new level of the hierarchy is introduced (Sen and Buehler, 2011; Zhang et al., 2011). One way to address this problem is to have stiffer platelets at the basic level. This enables the hierarchical structure to possess a reduced, but acceptable stiffness at the same time. Therefore, it may not be possible to retain the stiffness at the first level of hierarchy for the second level of the hierarchy. However, the minimization of reduction in stiffness when moving up from a level of the hierarchy is a problem to be addressed.

The results from the present Chapter could aid the development of novel bio-inspired composites with two hierarchical non-self-similarity, which can outperform other types of bio-inspired composites for certain combinations of strength, toughness, and stiffness. The FE analysis in this Chapter is done by assigning the obtained results of the first-level staggered composites to the platelets modeled with orthotropic material properties in the second hierarchy level. Furthermore, the analyses are conducted based on the TSC model, wherein the vertical interface (VI) is disregarded for the sake of simplicity. However, an analysis of hierarchical composites that incorporates the vertical interface utilizing a modified shear lag model is left for future studies. A multi-scale finite element model could give more information about the stress distributions inside the hierarchical composite, which is done in the following Chapter.

Chapter 4

Stress Analysis of 2H Non-self-similar Staggered Composites using FEA

In this Chapter, the failure analysis of the 2H non-self-similar staggered composites is conducted using Finite Element Analysis (FEA). Here, the stress distributions in a two hierarchical (2H) non-self-similar bio-inspired composite with regular and stairwise staggering, respectively, at the first and second levels of hierarchy (SR) with that of the models with single hierarchy is compared.

4.1 Introduction

Even though the studies have found various properties that can be mimicked to obtain a bio-inspired composite, it has still been impossible to get an artificial material as perfect as its natural inspiration. For this, researchers are still exploring the optimum parameters of the different factors affecting the final properties of a bio-inspired composite.

A few researchers have made efforts to employ Finite Element Analysis (FEA) on bio-inspired single hierarchical staggered composites (Maghsoudi-Ganjeh et al., 2021; Yang et al., 2019). Yang et al. (2019) have done a numerical validation to support the strength predicting model put forward by them for regular as well as random staggered models. Their FEA and analytical findings demonstrate a linear relationship between the strength increase and the platelet volume fraction. Using simulations as well as experiments, Mirzaeifar et al. (2015) conducted a comparison of stress distributions in materials possessing varying numbers of self-similar hierarchies. The findings revealed that materials with higher hierarchy levels exhibited a more uniform stress distribution in the uncracked region. The FE analysis of multi-scale models of non-self-similar hierarchical structures is an area that is still to be looked into.

In this Chapter, we conduct a Finite Element (FE) analysis using the commercially available software ABAQUS (SIMULIA, 2022) to compare the variation of stresses in a nacre inspired two hierarchical (2H) non-self-similar composite with that of the staggered composites with one hierarchy: regular staggered and stairwise staggered composites.

4.2 Methodology

Fig. 4.1 shows the schematic diagram of a 2H stairwise staggered composite with regular staggered composite as platelet (SR). For the present study we approximate the model for a reasonable toughness with a platelet volume fraction of 80% and the material properties as shown in Table 4.1. This is done by finding out the aspect ratio required for the maximum toughness and corresponding strength that can be obtained for a set of platelet and matrix material properties. The procedure for analysis as explained in Chapter 3, Section 3.3, Figure 3.5 is used for the determination of required aspect ratios at the first and second levels of hierarchy. The geometry details of the 2H SR model are shown in Table 4.2. The number of platelets in a period n is chosen as 5 for the present study.

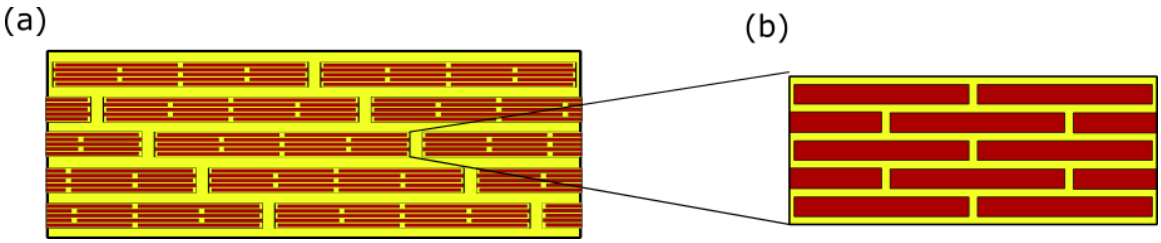

Figure 4.1: Schematic representation of (a) Two hierarchical (2H) stairwise staggered composite ($n = 5$) composed of regular staggered composite platelets (SR) (b) zoomed view of the platelet which is a regular staggered model (RSM)

The material properties for the platelet and matrix are assigned the same as that of the widely used materials for experimental works on bio-inspired composites: Verowhite and Agillus 30, respectively (See Table 4.1) (Mirzaeifar et al., 2015; Patpatiya et al., 2022).

The details of geometry and meshing adopted for the models is given in Table 4.2. We conduct a 3D simulation here so as to get a closer look to the possible outcomes of an experimental simulation. The 3D models of the composites for the three configurations (2H

SR, SSM, and RSM) with an out of plane thickness of 5 mm are developed in ABAQUS (SIMULIA, 2022). The meshing is done using the 3D element type C3D8R which is an eight noded linear brick element.

Table 4.1: Material Properties adopted for the FEA

Part	Material	Young's modulus (MPa)	Poisson's ratio	Strength (MPa)
Platelet	Verowhite	2600	0.33	47.5 (normal)
Matrix	Agillus 30	0.56	0.49	0.67 (shear)

Table 4.2: Geometry and mesh details of the FE model

Model	Volume fraction	Platelet aspect ratio	Meshing element	
			Type	No. of elements
2H SR	0.8	20 (first level of hierarchy), 32 (second level of hierarchy)	C3D8R	375555
SSM		32		397790
RSM		20		104670

The dimensions of the model are fixed such that the minimum thickness of the interface is kept as 1 mm, owing to the resolution of the commercially available multi jet 3D printer (Mirzaeifar et al., 2015). Once the minimum interface thickness is fixed, the other dimensions are computed by using the volume fraction and aspect ratio.

Fig. 4.2 shows the FE models of the 2H SR, stairwise staggered, and the regular staggered composites with the details of the applied boundary conditions on the four edges. We apply a displacement $\Delta_h = 0.01$ with periodic boundary conditions (PBC) at all edges, for the 2H SR and the stairwise staggered model (SSM) (Figure 4.2 (a) & (b)) owing to the periodicity of the stairwise staggering. For the simple regular staggered model (RSM), symmetric boundary conditions are applied at the top, bottom, and left edges, with a displacement of $\Delta_h = 0.01$ at the right edge, as shown in Fig. 4.2 (c).

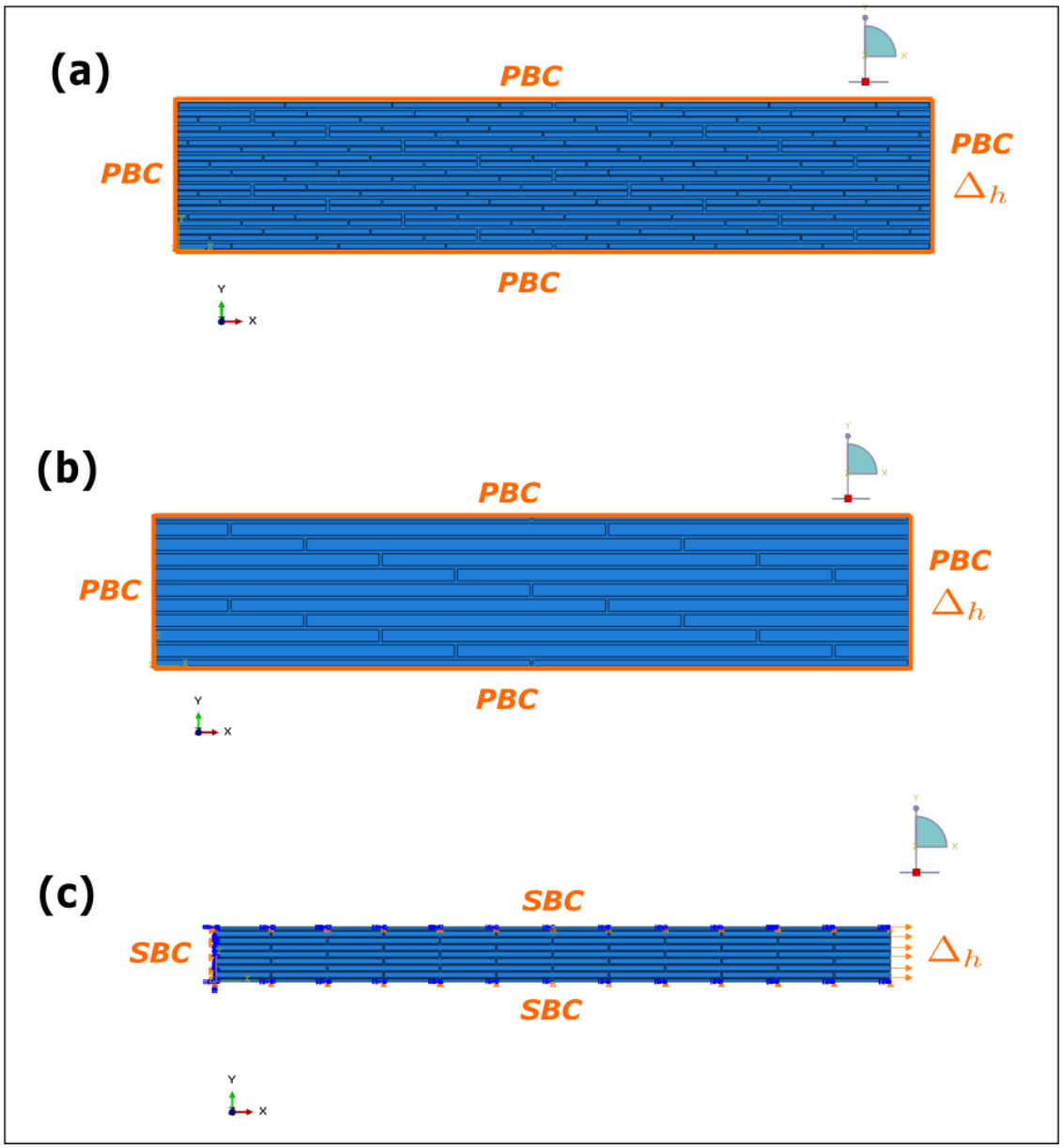

Figure 4.2: Boundary conditions applied in different models (a) 2H SR model with Periodic Boundary Conditions (PBC) at top, bottom, left and right edges with a displacement along x-direction $\Delta_h = 0.01$ at the right edge; (b) stairwise staggered model with PBCs at top, bottom, left and right edges with a displacement along x-direction $\Delta_h = 0.01$ at the right edge; (c) regular staggered model with Symmetric Boundary Conditions (SBC) at top, bottom and left edges, with a displacement along x-direction $\Delta_h = 0.01$ at the right edge

4.3 Result and Discussions

The stress contours obtained for σ_{11} (normal stress along x-direction) from the Output Data Base (ODB) of the three models are shown in Figure 4.3. It can be observed from Figure 4.3 that the the normal stress distribution in a 2H SR composite (Figure 4.3 (a)) is uniform when compared with that of the simple stairwise staggered (Figure 4.3 (b)) or regular staggered model (Figure 4.3 (c))

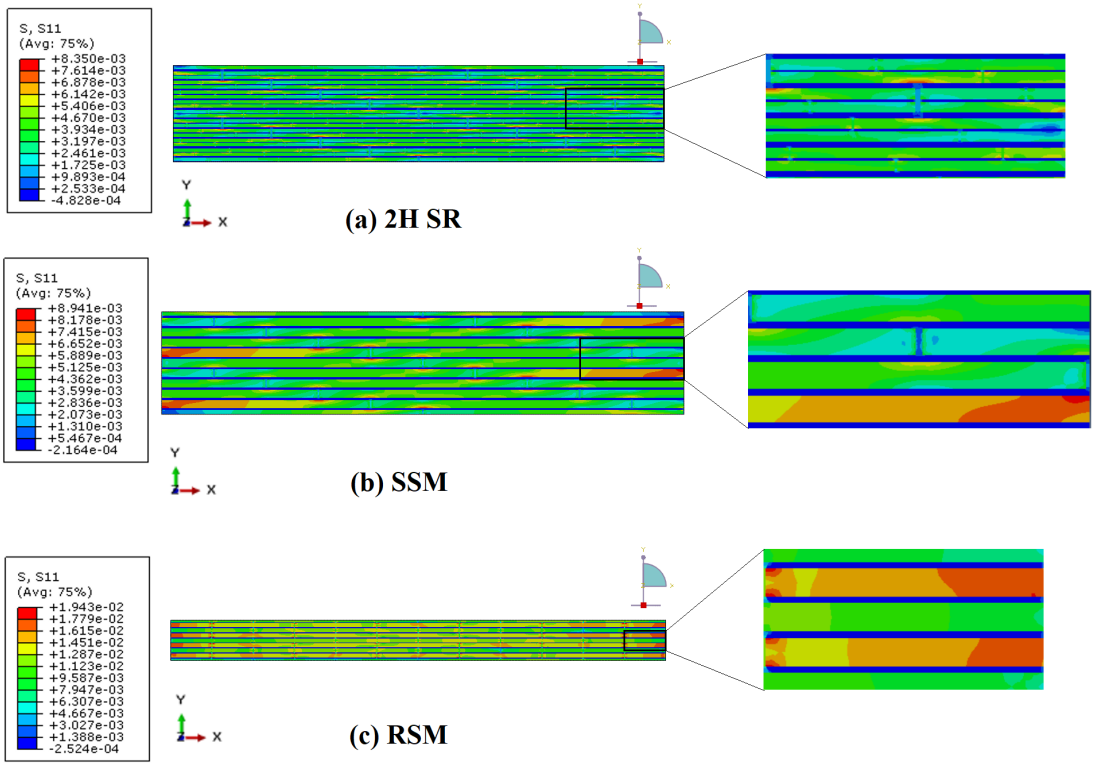

Figure 4.3: σ_{11} (normal stress along x-direction) contours obtained from the Output Data Base (ODB) for (a) 2H SR model, (b) SSM, and (c) RSM

Also, stress concentrations are observed towards the end of the models in the single hierarchical staggered models with stairwise and regular staggering configurations (Figure 4.3 (b) and (c)), where as it is reduced to a great extent in the 2H SR model (Figure 4.3 (a)).

The contours obtained for the shear stress in the three models are shown in Figure 4.4. The shear stress distribution in the 2H SR model (Figure 4.4 (a)) is observed to be a combination of the shear stress distributions observed in the stairwise staggered model (Figure 4.4 (b)) and the regular staggered model (Figure 4.4 (c)). However, in the 2H SR model,

more uniform shear stress distribution and lesser regions with high stress concentrations are observed than in the other models with a single hierarchy.

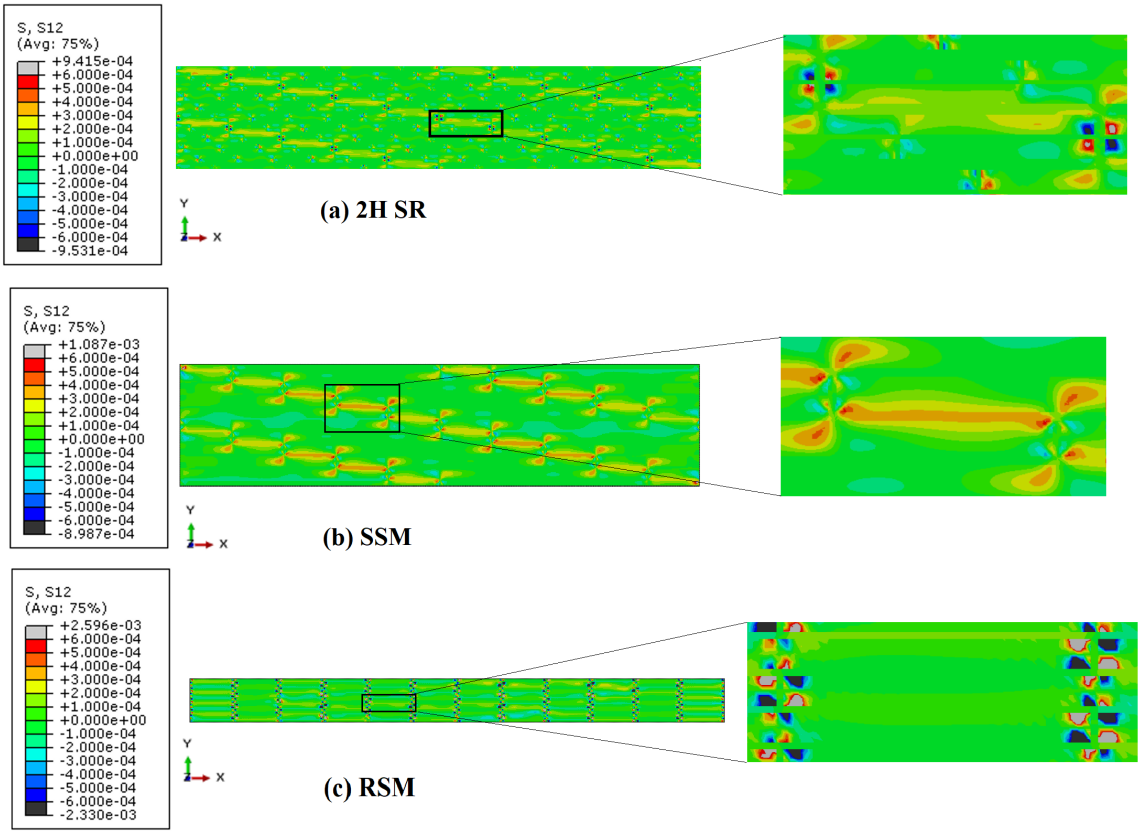

Figure 4.4: τ_{12} (shear stress) contours obtained from the Output Data Base (ODB) for (a) 2H SR model, (b) SSM, and (c) RSM

The shear stress (τ_{12}) contour of the stairwise staggered model (Figure 4.4 (b)) shows that the regions with more shear stresses are at the platelet matrix horizontal interface and at the corner regions. But, in a regular staggered model (Fig 4.4 (c)), maximum shear stress is observed to be at the platelet corner regions.

The results show that the introduction of multiple hierarchy could cap the stress concentrations which are observed in single hierarchical structures. The studies on self-similar hierarchical composites done by Mirzaeifar et al. (2015) also shows a similar result. In the work by Mirzaeifar et al. (2015), digital image correlation (DIC) was utilized to observe the strain distributions on various regular staggered composite specimens with increasing levels of self-similar hierarchy. Through the analysis of strain distributions, their research showcased the evident impact of the hierarchical structure in effectively distributing strain and stress within the material. The hierarchical arrangement could also impart more defect

tolerance to the structures (Sen and Buehler, 2011).

The stress analysis findings by Yang et al. (2019) indicate that in regular staggered composites, the matrix experiences greater magnitudes of normal and shear stresses at the platelet end with a shorter overlap. In our present study, we have observed higher levels of normal stress at the ends of single hierarchical regular staggered models. This phenomenon is particularly evident in the alternating rows of half platelets, where the overlap is shorter. Furthermore, in the case of single hierarchical composites, the variation in shear stress is found to be concentrated at the corners. Conversely, for the stairwise staggered one hierarchical model, the shear stress is found to be higher in the horizontal interface region.

4.4 Conclusion

From the results and discussion of the present study, it can be concluded that the hierarchical arrangement of platelets could reduce the stress concentrations significantly and assure a more uniform stress distribution inside the structure, compared to the structures with one hierarchy. This can help the structure to withstand impact loads, and improve the defect tolerance.

The current study will be extremely useful in the multi-scale modelling and simulation of bio-inspired hierarchical staggered structures subjected to various loads. Also, this could provide a reasonably good approximation of results which can be used as a preliminary estimation before conducting experimental works.

The stress distributions inside a multi-scale two hierarchical non-self-similar is analysed through FE analysis in the current Chapter. Now, we now generalize optimize the analytical formulations for the mechanical properties of two hierarchical composites in the following Chapter.

Chapter 5

Generalization and Optimization of 2H Bio-inspired Non-self-similar Staggered Composites

Bio-inspired composites are often considered as ideal candidates in the field of light and innovative structures, which the world is in need of. In order to develop a bio-inspired composite with fine mechanical properties, it is required to study all the possible factors which are responsible for the superior mechanical properties of a biological composite. The hierarchical arrangement and the staggering pattern of the platelets inside the matrix are major factors affecting the final properties of such composite materials. The generalization of parameters in a hierarchical structure could be beneficial in finding out the optimum parameters responsible for the maximum desirable mechanical properties in a bio-inspired composite. In this Chapter, we formulate a novel generalized model for a stairwise staggered (which is regarded as one of the patterns mostly found in nature due to its optimized properties) two hierarchical bio-inspired composite, and we optimize the model for a tailored design according to the stiffness, strength, and toughness requirements. The developed model can evaluate self-similar as well as non-self-similar configurations, and the analytical results from the studies show a good agreement when compared with the models of specific known designs from the literature. Also, the ternary plots obtained from optimization show that the number of platelets in a period at the first and second levels of hierarchy are the key parameters other than the volume fractions and the critical aspect ratios, controlling the final properties of the two hierarchical composites.

5.1 Introduction

Many devices and equipments are conceived based on natural structures. For example, the thin shell structural elements we see nowadays are developed based on eggshells, which is a biological composite (Shu et al., 2020). Nacre, bone, and bamboo are a few examples of biological composites which are well known for their superior mechanical properties, compared to their basic constituents (Currey, 1977; Fratzl et al., 2004; Mathiazhagan and Anup, 2016a,b; Meyers et al., 2008; Murali et al., 2011; Wegst et al., 2015).

Some of the major reasons behind the exceptional mechanical properties of biological composites include the peculiar micro-structure of constituents at the elementary level, the very small size of the constituents (of the order of nanometers), the hierarchical structure, optimum aspect ratio (length to width ratio) of the platelet, and the optimum Young's moduli ratio of platelet and matrix (Anup et al., 2007; Ji and Gao, 2004b; Kim et al., 2018; Maghsoudi-Ganjeh et al., 2021; Saroj et al., 2019).

In Figure 5.1 (b), the arrangement of platelets inside a matrix can be observed, which is generally called a brick-and-mortar or masonry-slurry or platelet and matrix structure. The brick/masonry/platelet refers to the rigid element, and the mortar/slurry/matrix refers to the relatively soft element. The concepts of staggerings, self-similar, and non-self-similar hierarchies have already been discussed in the previous Chapters. Bone is regarded as a 7-level self-similar hierarchical structure composed of mineral crystals and protein An et al. (2014); Gupta et al. (2006); Rho et al. (1998); Wagner and Weiner (1992). Examples of non-self-similar biological composites include the dental enamel, the scales of alligator gars, and turtle carapaces Achrai and Wagner (2013); Spears (1997); Yang et al. (2013).

An et al. (2014) reported that the non-self-similar hierarchical composites possess enhanced fracture resistance and damage tolerance compared to a self-similar composite structure. Only a few works in open literature discuss about hierarchical bio-inspired composites Henry and Pimenta (2021); Mirzaeifar et al. (2015); Sen and Buehler (2011); Tseng et al. (2017).

The experimental and simulation studies by Mirzaeifar et al. (2015); Sen and Buehler (2011) show that the hierarchical arrangement is a key factor contributing to the defect-tolerant property of a composite. Here, the defect-tolerant property refers to the ability to take up more loads, even if the material structure contains some initial flaws or cracks. They found that the more the hierarchical levels, the higher the uniformity in the stress distribution in the uncracked domain of the materials. Also, the studies by Zhang et al. (2011) point out the existence of an optimum level of structural hierarchy, beyond which

the toughness of a composite reduces. So, there exist various design guidelines for different parameters in a composite.

The requirement of appropriate mechanical properties according to the situations where the composite material is intended to use leads to the need for optimization. In most cases, having all properties at a higher end may not be necessary, but conditions can be imposed according to the requirements. Multi-objective optimization is a method in which a model can be optimized for multiple properties with some set conditions. The multi-objective optimization done by Barthelat (2014) deals with the simultaneous optimization of stiffness, strength, and toughness for a simple regular staggered bio-inspired composite. In the abovementioned work, comprehensive design guidelines were formulated for optimizing mechanical properties and applied to a model with material and structural properties of nacre, and it was found that, indeed, nacre possesses an optimized design.

In Chapter 3, the equations to compute the mechanical properties of two hierarchical (2H) non-self-similar composites with regular and stairwise staggerings at the first and second levels of hierarchy and vice versa were developed. The results from Chapter 3 show that non-self-similar composites undoubtedly possess better strength for a range of high toughness values when compared to the self-similar staggered composites.

Even though various studies exist on optimization of simple staggered models, a generalized model for a two hierarchical stairwise staggered structure and its optimization for different mechanical properties is not available in the open literature. In the present work, we propose a generalized model for a stairwise hierarchical structure based on the tension shear chain (TSC) model put forward by Gao et al. (2003). The optimization of the obtained generalized model of is done using multi-objective optimization technique. The methodology adopted for the study is explained in detail in Section 5.2. The obtained solutions are applied to get the ternary diagrams for optimization as discussed in Section 5.3. We conclude the investigation in Section 5.4.

5.2 Methodology

Figure 5.1 shows the schematic representation of a two hierarchical (2H) stairwise staggered composite composed of stairwise staggered composites as platelets (SS). This can be regarded as a non-self-similar model when the number of platelets in a period (the number of rows of platelets after which the pattern gets repeated) at the first and second levels of the hierarchy are different. Here, our objective is to develop equations to compute the mechanical properties such as Young's modulus, strain, strength and toughness of the composite.

Using a generalized model, it is possible to examine the effect of different material and geometric parameters such as the numbers of platelets in a period, the material property of matrix, the aspect ratio as well as the volume fraction of platelets at each level of hierarchy on these mechanical properties. The present study is carried out for a 2H SS model with the following parameters considered in the generalization (these variables can be varied at the first and second levels of hierarchy) study: (i) Number of platelets in a period (n), (ii) Aspect ratio of the platelet (ρ), (iii) Volume fraction (ϕ). In the resulting equations, the subscripts 1 and 2 denote the first and second levels of hierarchy, respectively. Also, we consider the same matrix material in the first and second levels of hierarchy to simplify the model.

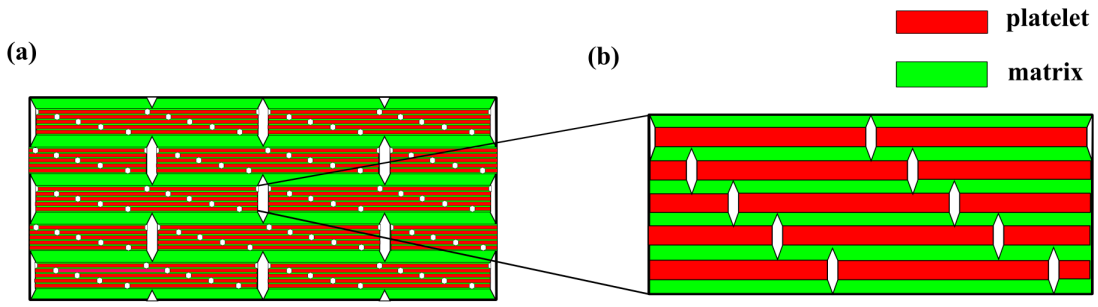

Figure 5.1: Schematic diagram of 2H TSC models: (a) 2H stairwise staggered composite made with stairwise staggered composite as reinforcing platelets (SS) (b) Zoomed view of platelet

We generalize the 2H SS composite model shown in Figure 5.1 (a), by deriving the equations to compute the mechanical properties such as stiffness, strength, and toughness. The stiffness of the stairwise staggered configuration (E_S) in a bio-inspired composite at the first level of hierarchy as shown in Figure 5.1 (b) is given by Zhang et al. (2010) as,

$$E_S = \frac{\phi_1 E_p}{\frac{n_1(3n_1-4)}{3(n_1-1)^2} + \frac{n_1^2}{3(n_1-1)\alpha_1}} \tag{5.1}$$

where,

$$\alpha_1 = \frac{\phi_1 \rho_1^2 G_i}{3(1-\phi_1)E_p} \tag{5.2}$$

G_i and E_p represent the shear modulus of the matrix and Young's modulus of platelet materials, respectively. For, the second level of the hierarchy, the equation for stiffness can

be written as,

$$E_{SS} = \frac{\phi_2 E_S}{\frac{n_2(3n_2-4)}{3(n_2-1)^2} + \frac{n_2^2}{3(n_2-1)\alpha_2}} \tag{5.3}$$

where,

$$\alpha_2 = \frac{\phi_2 \rho_2^2 G_i}{3(1-\phi_2)E_S} \tag{5.4}$$

Substituting E_S from Equation 5.1 in the equations of E_{SS} (Equation 5.3) and α_2 (Equation 5.4) and simplifying, we get the normalized stiffness of a 2H SS model as,

$$\frac{E_{SS}}{E_p \phi_1 \phi_2} = \frac{\left[3(n_2-1)^2 + \frac{n_2^2}{3(n_2-1)\alpha_2}\right]}{D n_2(3n_2-4)} \tag{5.5}$$

where,

$$D = \frac{n_1(3n_1-4)}{3(n_1-1)^2 + \frac{n_1^2}{3(n_1-1)\alpha_1}} \tag{5.6}$$

$$\alpha_2 = \frac{\phi_2 \rho_2^2 \frac{G_i}{E_p} D}{3(1-\phi_2)\phi_1} \tag{5.7}$$

The critical aspect ratio is referred to as that value of aspect ratio which separates the matrix failure from the platelet failure, which is given by Zhang et al. (2010) at the first level of hierarchy as,

$$\rho_{1,crit} = (n_1 - 1)\frac{\sigma^p_{critical}}{\tau^i_{critical}} \tag{5.8}$$

where $\sigma^p_{critical}$ and $\tau^i_{critical}$ represent the normal strength of platelet and shear strength of matrix, respectively. The strength of a stairwise staggered composite ($\sigma^S_{\text{critical}}$) is given by Zhang et al. (2010) as,

$$\sigma^{S}_{\text{critical}} = \begin{cases} \phi_1 \sigma^{p}_{\text{critical}} \frac{n_1 - 1}{n_1} \frac{\rho_1}{\rho_{1,\text{critical}}} & \text{if } \rho_1 \leq \rho_{1,\text{critical}} \\ \phi_1 \sigma^{p}_{\text{critical}} \frac{n_1 - 1}{n_1} & \text{if } \rho_1 > \rho_{1,\text{critical}} \end{cases} \tag{5.9}$$

Now, the critical aspect ratio at the second level of hierarchy can be computed by substituting Equation 5.9 for $\sigma^{p}_{\text{critical}}$ in Equation 5.8 as,

$$\rho_{2,critical} = \begin{cases} \frac{(n_2-1)\phi_1\rho_1}{n_1} & \text{if } \rho_1 \leq \rho_{1,critical} \\ \frac{(n_2-1)(n_1-1)\phi_1}{n_1} \frac{\sigma^{p}_{critical}}{\tau^{i}_{critical}} & \text{if } \rho_1 > \rho_{1,critical} \end{cases} \tag{5.10}$$

In a similar manner, the other properties are also found out. We get the normalized strength of the 2H SS model as,

$$\frac{\sigma^{SS}_{critical}}{\sigma^{p}_{critical}\phi_1\phi_2} = \begin{cases} \frac{\rho_2}{n_2\phi_1 \frac{\sigma^{p}_{critical}}{\tau^{m}_{critical}}} & \text{if } \rho_2 \leq \rho_{1,critical} \\ \frac{(n_2-1)\rho_1}{n_1 n_2 \frac{\sigma^{p}_{critical}}{\tau^{m}_{critical}}} & \text{if } \rho_2 > \rho_{2,critical} \; and \; \rho_1 \leq \rho_{1,critical} \\ \frac{(n_1-1)(n_2-1)}{n_1 n_2} & \text{if } \rho_2 > \rho_{2,critical} \text{ and } \rho_1 > \rho_{1,critical} \end{cases} \tag{5.11}$$

the normalized strain,

$$\frac{\epsilon^{SS}_{critical}}{\epsilon^{p}_{critical}} = \frac{\sigma^{SS}_{critical}}{\sigma^{p}_{critical}} / \frac{E^{SS}_{critical}}{E_p} \tag{5.12}$$

the normalized toughness,

$$\frac{w^{SS}_{critical}}{w^{p}_{critical}\phi_1\phi_2} = \left(\frac{\sigma^{SS}_{critical}}{\sigma^{p}_{critical}\phi_1\phi_2} \right)^2 / \frac{E^{SS}_{critical}}{E_p\phi_1\phi_2} \tag{5.13}$$

The newly formulated generalized model for a two hierarchical stairwise staggered (2H SS) model is able to predict the mechanical properties such as the Young's modulus, strength, strain, and toughness for any combinations of the variables in the first as well as the second levels of the hierarchy. Now, the need for optimization arises to find the most suitable combination of variables for achieving good strength and toughness with also an acceptable stiffness. For carrying out the optimization part, we follow a weighted product approach where a multi-objective function or the fitness can be defined as (Barthelat, 2014),

$$f_c = E_{c,norm}^m \sigma_{c,norm}^n w_{c,norm}^k \tag{5.14}$$

where, $E_{c,norm}, \sigma_{c,norm}$, and $w_{c,norm}$ are the normalized stiffness, normalized strength, and normalized toughness of the 2H SS composite respectively given by,

$$E_{c,norm} = \frac{E_{SS}}{E_p} \tag{5.15}$$

$$\sigma_{c,norm} = \frac{\sigma_{critical}^{SS}}{\sigma_{critical}^{p}} \tag{5.16}$$

$$w_{c,norm} = \frac{w_{critical}^{SS}}{\sigma_{critical}^{p} \gamma_{critical}^{m}} \tag{5.17}$$

Here, m, n, k are non dimensional indices such that $m + n + k = 1$. The indices can be modulated according to the emphasis given on particular properties. More the value of an index more will be the emphasis on the respective property. For example, if (m,n,k)= (0.3,0.3,0.4), an equal emphasis of 30 % is assigned for stiffness and strength, whereas toughness is given the greatest emphasis of 40 %. The optimum configurations can then be displayed in a ternary diagram in which all possible combinations of (m, n, k) can be represented.

It is to be noted that the normalization of composite properties is done with respect to the platelet properties for the case of stiffness and strength, whereas a hypothetical material having the strength of platelet and elongation of the matrix is considered for normalizing the toughness. This is done so as to keep the three parameters E_{norm}, σ_{norm}, and w_{norm} of the composite, platelet, and matrix between 0 and 1 (Barthelat, 2014).

5.3 Results and Discussion

The mechanical properties of 2H SS composites, as deduced from the preceding sections, are now used to investigate the impact of the period of staggering and subsequently, for the optimization of the mechanical properties as described below.

5.3.1 Effect of period of staggering on mechanical properties

Using the expressions obtained for the normalized mechanical properties viz. stiffness, strength, strain, and toughness for the 2H SS composites (Equations 5.5, 5.11, 5.12, and 5.13), plots are drawn to understand the variation of the properties with respect to the number of platelets in a period at the first and second levels of hierarchy. For this, we consider a set of representative material properties with the ratio of Young's modulus of platelet to shear modulus of the matrix, $E_p/G_i = 1000$, the volume fractions at the first and second levels of hierarchy, $\phi_1 = \phi_2 = 0.5$, and the platelet aspect ratio at the first and second levels of hierarchy, $\rho_1 = \rho_2 = 10$.

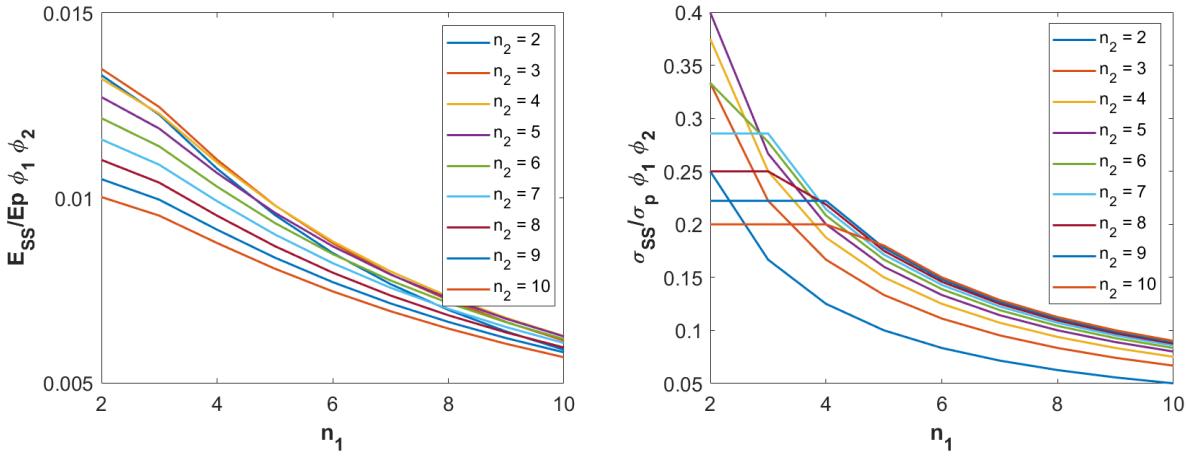

Figure 5.2: Variation of (a) normalized stiffness, and (b) normalized strength in a 2H SS composite with the number of platelets in a period at first and second levels of hierarchy (n_1, n_2). The values are plotted for $E_p/G_i = 1000$, $\sigma^p_{critical}/\tau^i_{critical} = 10$, $\phi_1 = \phi_2 = 0.5$, and $\rho_1 = \rho_2 = 10$. (The link to the Matlab scripts for reproducing this figure can be found here)

Figure 5.2 (a) shows the variation of normalized stiffness of 2H SS composite with respect to the number of platelets in a period at first and second levels of hierarchy (n_1 and n_2). From the plot, it can be seen that for a fixed value of aspect ratio and volume fractions at the first and second levels of hierarchy, the normalized stiffness decreases as n_1 and n_2 increases. The variation of normalized strength of 2H SS composite with n_1 and n_2 is shown in Figure 5.2 (b), from which a decreasing trend with n_1 is observed for each value of n_2. Also, the strength is seen to be increasing with an increase in n_2. The constant trend of the normalized stress graphs can be described by Equation 5.11; since the aspect ratio, volume fraction, and material properties are the same, a quadratic variation of stress

will be obtained according to the values of n_1 and n_2.

Figure 5.3 (a) and (b), show the variation of normalized strain and toughness respectively, for a 2H SS composite with n_1 for different values of n_2. We can see a similar trend for both the plots; the strain and toughness increase with the increase in n_1 whereas they decrease with the increase in n_2. This could be because toughness depends on stress and strain, both of which decrease with an increase in n_1 as we can see from Figure 5.2 (b).

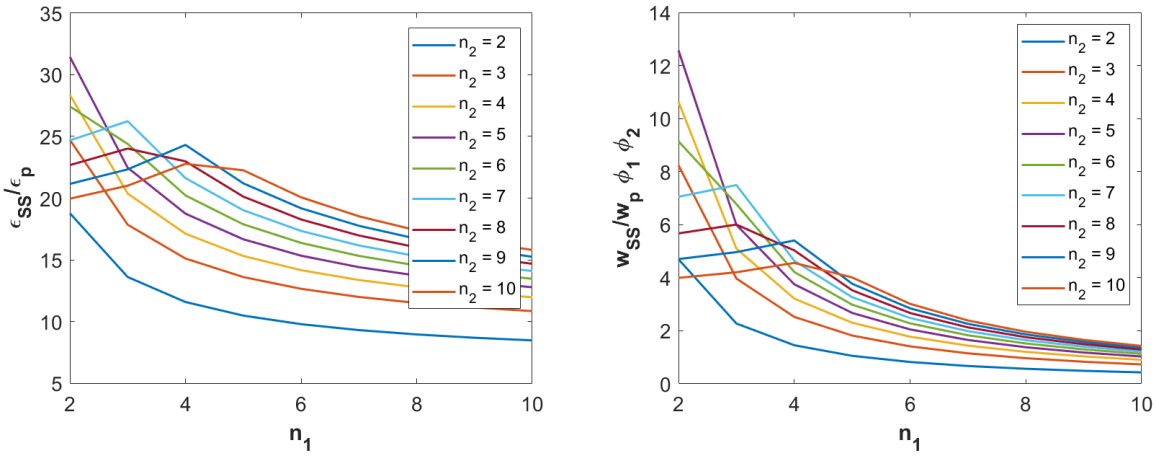

Figure 5.3: Variation of (a) normalized strain, and (b) normalized toughness in a 2H SS composite with the number of platelets in a period at first and second levels of hierarchy (n_1, n_2). The values are plotted for $E_p/G_i = 1000$, $\sigma^p_{critical}/\tau^i_{critical} = 10$, $\phi_1 = \phi_2 = 0.5$, and $\rho_1 = \rho_2 = 10$. (The link to the Matlab scripts for reproducing this figure can be found here)

The above results show the variation of mechanical properties with only two parameters, n_1 and n_2, while the other parameters, such as the volume fractions and aspect ratios at the first and second levels of hierarchy, were kept constant. To find the influence of variation of the other parameters and to start with the process of optimization, the maximum toughness for a particular combination of n_1 and n_2 is found out by comparing the values obtained for different sets of aspect ratios at the first and second levels of hierarchy. For this, the aspect ratios at the first and second levels of the hierarchy are varied from 1 to 120, and the maximum value of toughness obtained is found for a particular set of n_1 and n_2. Also, the corresponding values of stiffness and strength for the maximum toughness are also computed.

Figure 5.4 to 5.8 show the variation of maximum toughness and corresponding strength and stiffness with n_1 for $n_2 = 2$ to 10. It can be seen from the plots that the maximum toughness of the generalized 2H SS model decreases with n_1.

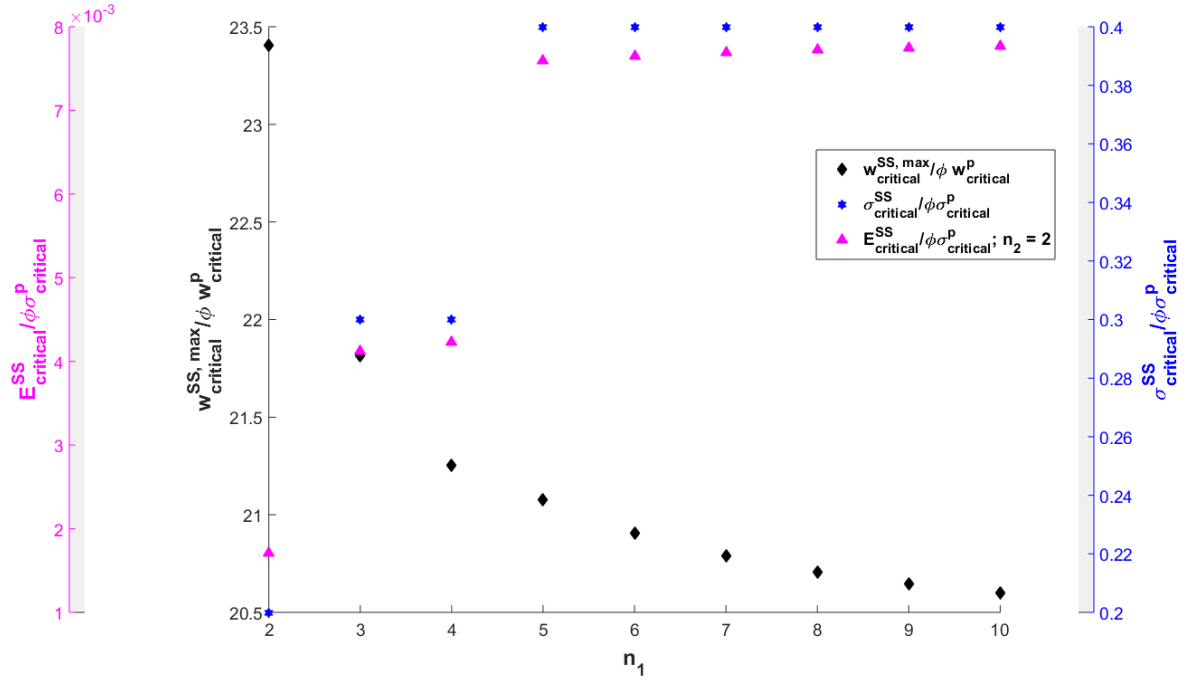

(a) $n_2 = 2$

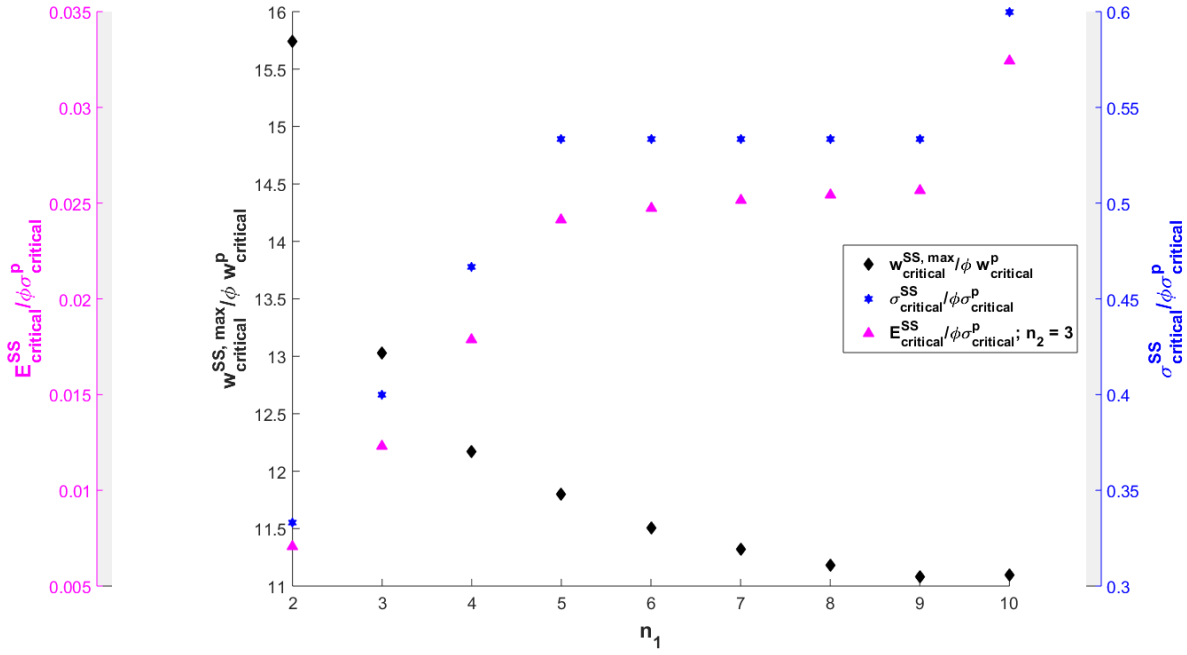

(b) $n_2 = 3$

Figure 5.4: Maximum normalized toughness with corresponding normalized strength and stiffness with n_1, for different values of n_2. ϕ represents the effective platelet volume fraction of the 2H SS composite which is equal to $\phi_1\phi_2$. The plots are drawn for $E_p/G_i = 1000$ and $\sigma^p_{critical}/\tau^i_{critical} = 10$. (The link to the Matlab scripts for reproducing this figure can be found here)

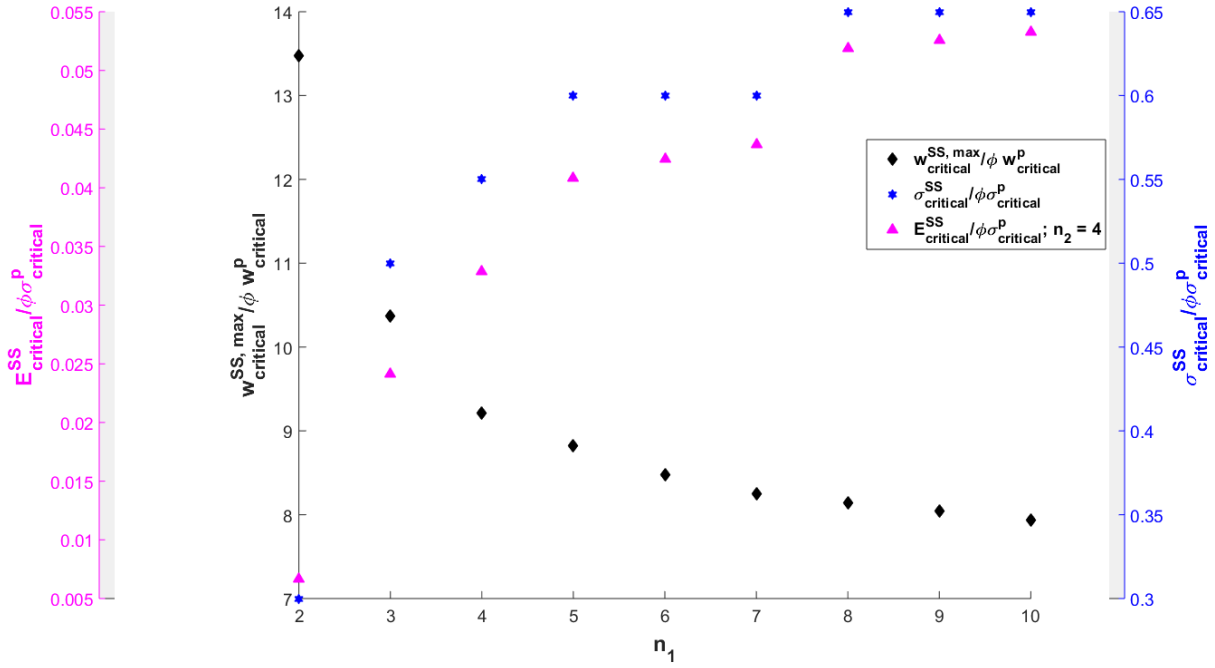

(a) $n_2 = 4$

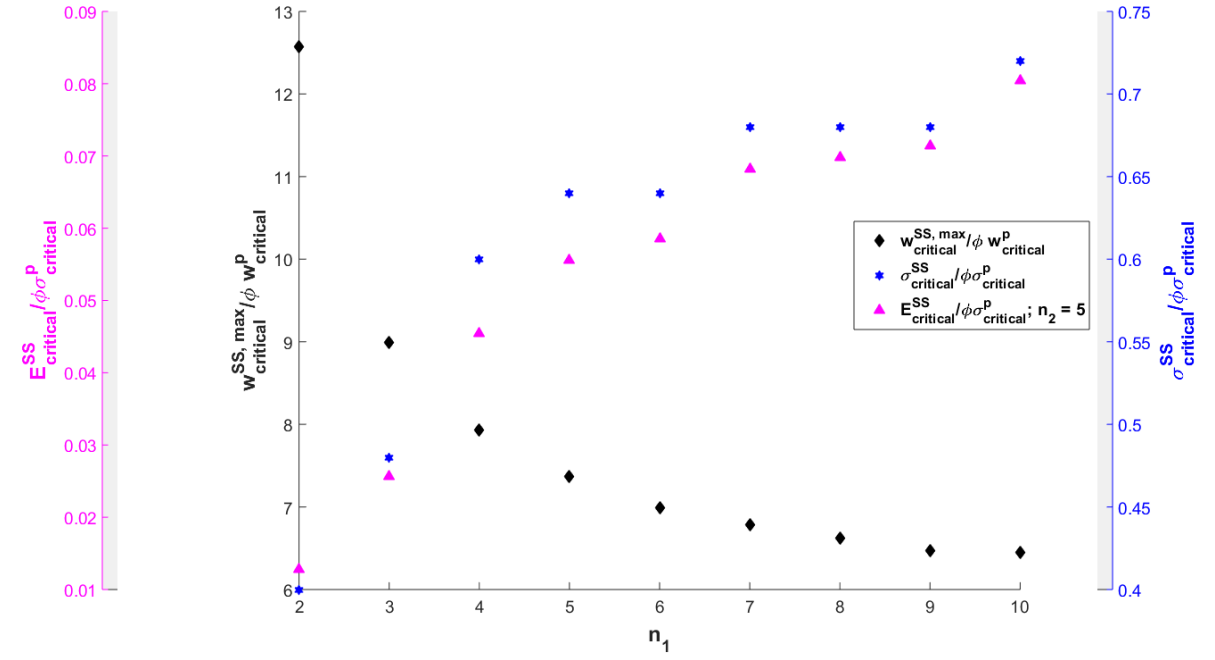

(b) $n_2 = 5$

Figure 5.5: Maximum normalized toughness with corresponding normalized strength and stiffness with n_1, for (a) $n_2 = 4$, and (b) $n_2 = 5$. ϕ represents the effective platelet volume fraction of the 2H SS composite which is equal to $\phi_1\phi_2$. The plots are drawn for $E_p/G_i = 1000$ and $\sigma^p_{critical}/\tau^i_{critical} = 10$. (The link to the Matlab scripts for reproducing this figure can be found here)

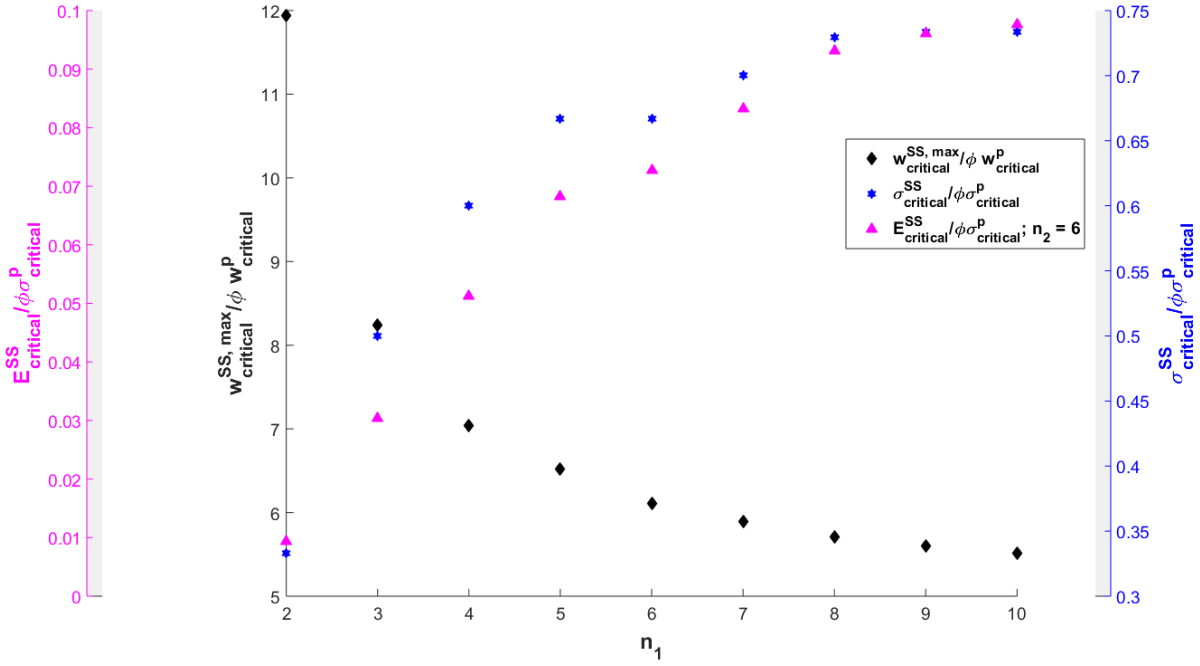

(a) $n_2 = 6$

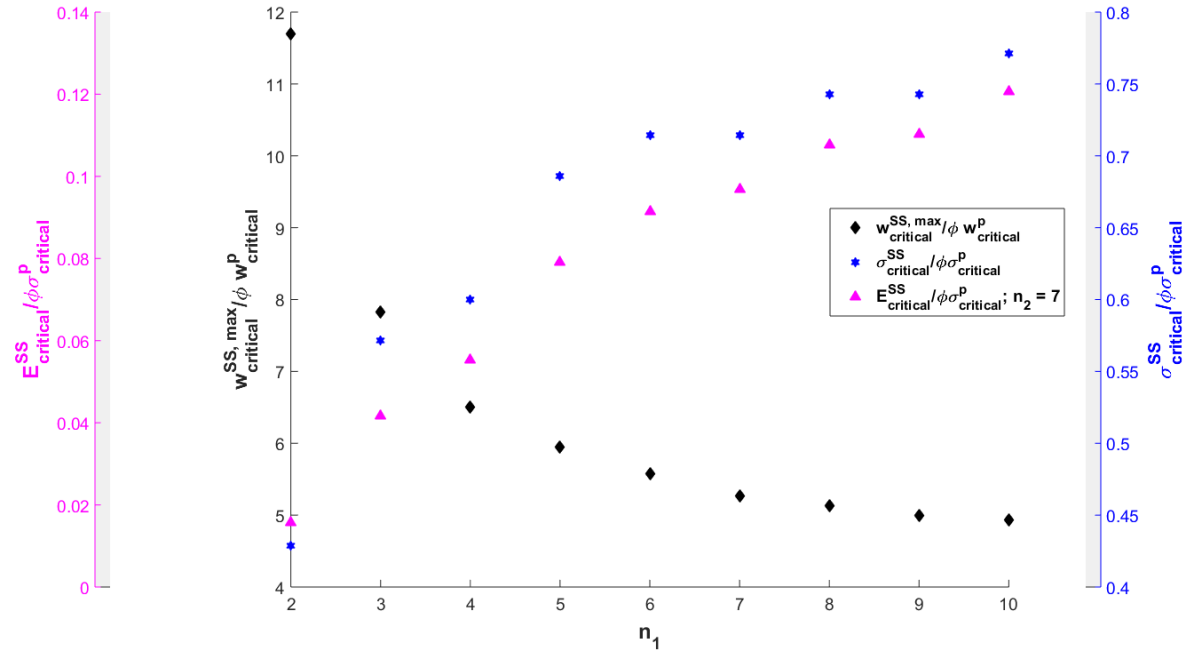

(b) $n_2 = 7$

Figure 5.6: Maximum normalized toughness with corresponding normalized strength and stiffness with n_1, for (a) $n_2 = 6$, and (b) $n_2 = 7$. ϕ represents the effective platelet volume fraction of the 2H SS composite which is equal to $\phi_1\phi_2$. The plots are drawn for $E_p/G_i = 1000$ and $\sigma^p_{critical}/\tau^i_{critical} = 10$. (The link to the Matlab scripts for reproducing this figure can be found here)

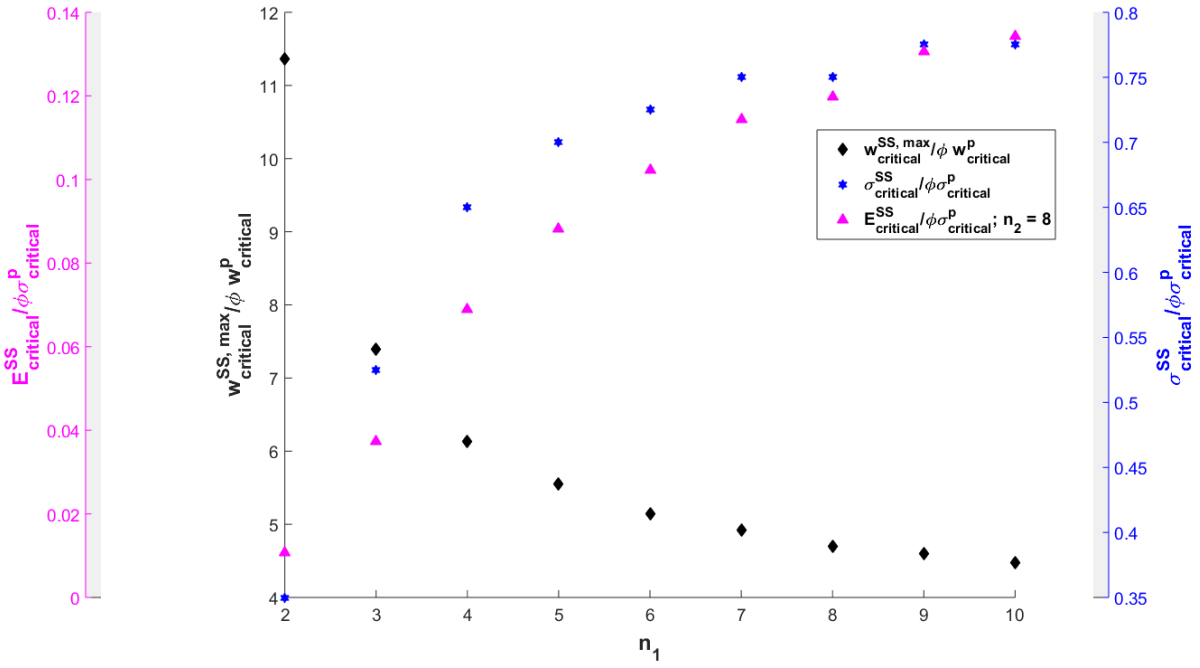

(a) $n_2 = 8$

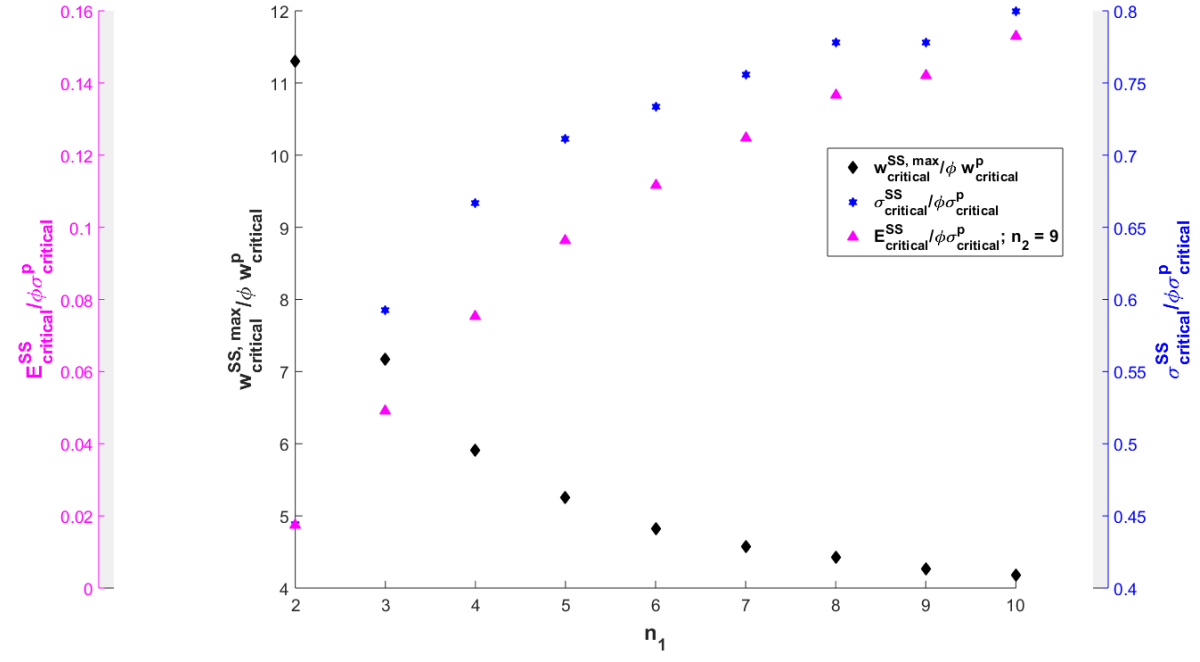

(b) $n_2 = 9$

Figure 5.7: Maximum normalized toughness with corresponding normalized strength and stiffness with n_1, for (a) $n_2 = 8$, and (b) $n_2 = 9$. ϕ represents the effective platelet volume fraction of the 2H SS composite which is equal to $\phi_1\phi_2$. The plots are drawn for $E_p/G_i = 1000$ and $\sigma^p_{critical}/\tau^i_{critical} = 10$. (The link to the Matlab scripts for reproducing this figure can be found here)

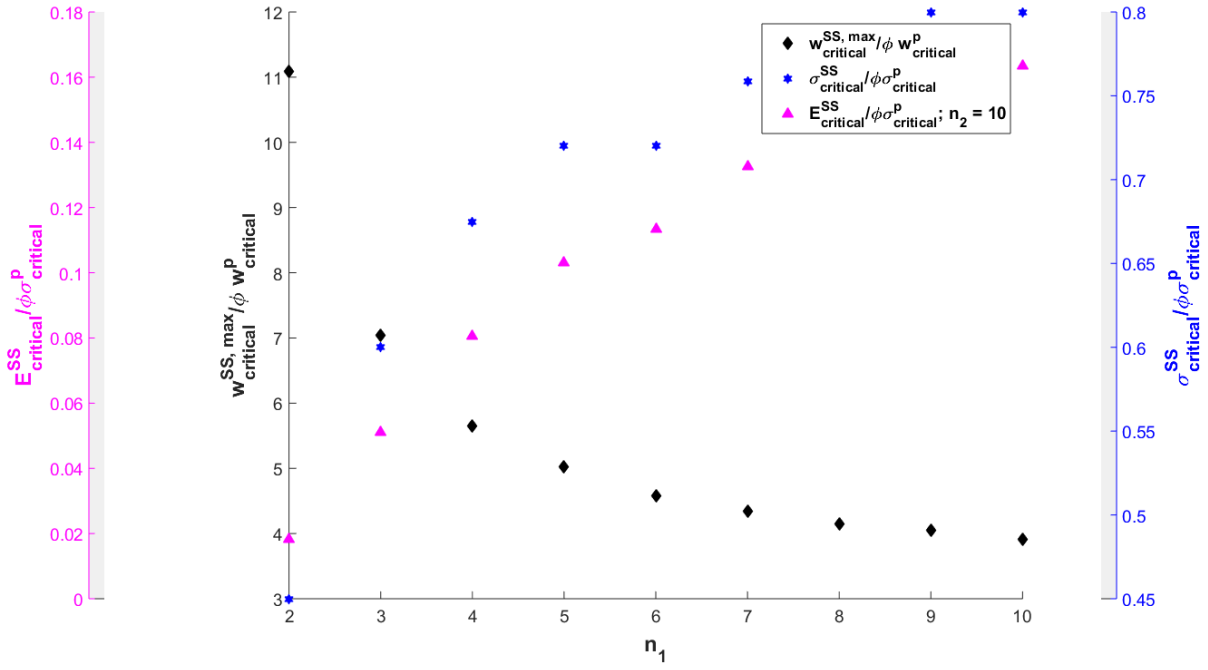

Figure 5.8: Maximum normalized toughness with corresponding normalized strength and stiffness with n_1, for $n_2 = 10$. ϕ represents the effective platelet volume fraction of the 2H SS composite which is equal to $\phi_1\phi_2$. The plots are drawn for $E_p/G_i = 1000$ and $\sigma^p_{critical}/\tau^i_{critical} = 10$. (The link to the Matlab scripts for reproducing this figure can be found here)

The results of the generalized model are seen to be matching with that obtained in Chapter 3 for 2H regular staggered model with stairwise staggered composite as platelets (2H RS), which can be regarded as a special case of the generalized 2H SS model with $n_2 = 2$. It is also observed from the plots that the maximum toughness decreases, whereas the corresponding strength and stiffness increase with an increase in n_2.

5.3.2 Optimization of the composite using fitness function and ternary diagrams

The need for optimization arises when we have several options for designing the hierarchical composite. Here the options refer to the range of platelet aspect ratios, the number of platelets in a period, and the platelet volume fraction. For example, if we have a particular set of materials for the platelet and matrix, the optimum configuration refers to that design in which we get the maximum properties we are looking for. Here we make use of the fitness function for the composite (Equation 5.14), which is a collection of the three

important mechanical properties: stiffness, strength, and toughness, for the optimization process.

The following variables involved in the fitness function for the composite given by Equation 5.14 are considered for the optimization: (i) volume fractions (ϕ_1, ϕ_2), aspect ratios (ρ_1, ρ_2), and the number of platelets in a period (n_1, n_2) at the first and second levels of hierarchy. The optimization is done by maximizing the fitness function for the composite using the '*fmincon*' function in MATLAB (The Mathworks, 2020) with default convergence criteria. It is observed that the fitness function for the composite (Equation 5.14) is an increasing function of volume fraction. Due to this, the optimized values obtained for maximized fitness function of the composite would converge at the upper limit of the volume fraction provided. As an alternative, we optimize the other variables by keeping the volume fractions constant.

The optimum values of aspect ratios at the first and second levels of hierarchy are chosen as the critical aspect ratios since the maximum strength in a two hierarchical structure is obtained for the critical aspect ratios in Chapter 3. Thus, for a particular volume fraction at the first and second levels of hierarchy, at the critical aspect ratios, we maximize the fitness function for the composite to optimize the remaining variables n_1, and n_2.

The maximized fitness function of the composite (f_c) is normalized with the fitness function of the matrix (f_i) which is given by,

$$f_i = E_{i,norm}^m \sigma_{i,norm}^n w_{i,norm}^k \tag{5.18}$$

where $E_{i,norm}, \sigma_{i,norm}$, and $w_{i,norm}$ are the normalized stiffness, normalized strength, and normalized toughness of the interface respectively which are given by, $E_{i,norm} = w_{i,norm} = \tau_i$, and $\sigma_{i,norm} = \sqrt{3}\tau_i$. These assumptions are made so as to confine the material selection for the matrix from a wide range.

Figure 5.9 (a) shows the variation of f_c/f_i in ternary diagrams for various combinations of m, n, and k obtained after maximizing f_c. The corresponding values of n_1 and n_2 are shown in Figure 5.9 (b), and (c). It can be observed from Figure 5.9 (a) that the transition boundary is shifting towards the right edge as the volume fraction increases. This indicates that more combinations of m, n,and k would give a higher range of values of f_c/f_i, as the volume fraction is increased.

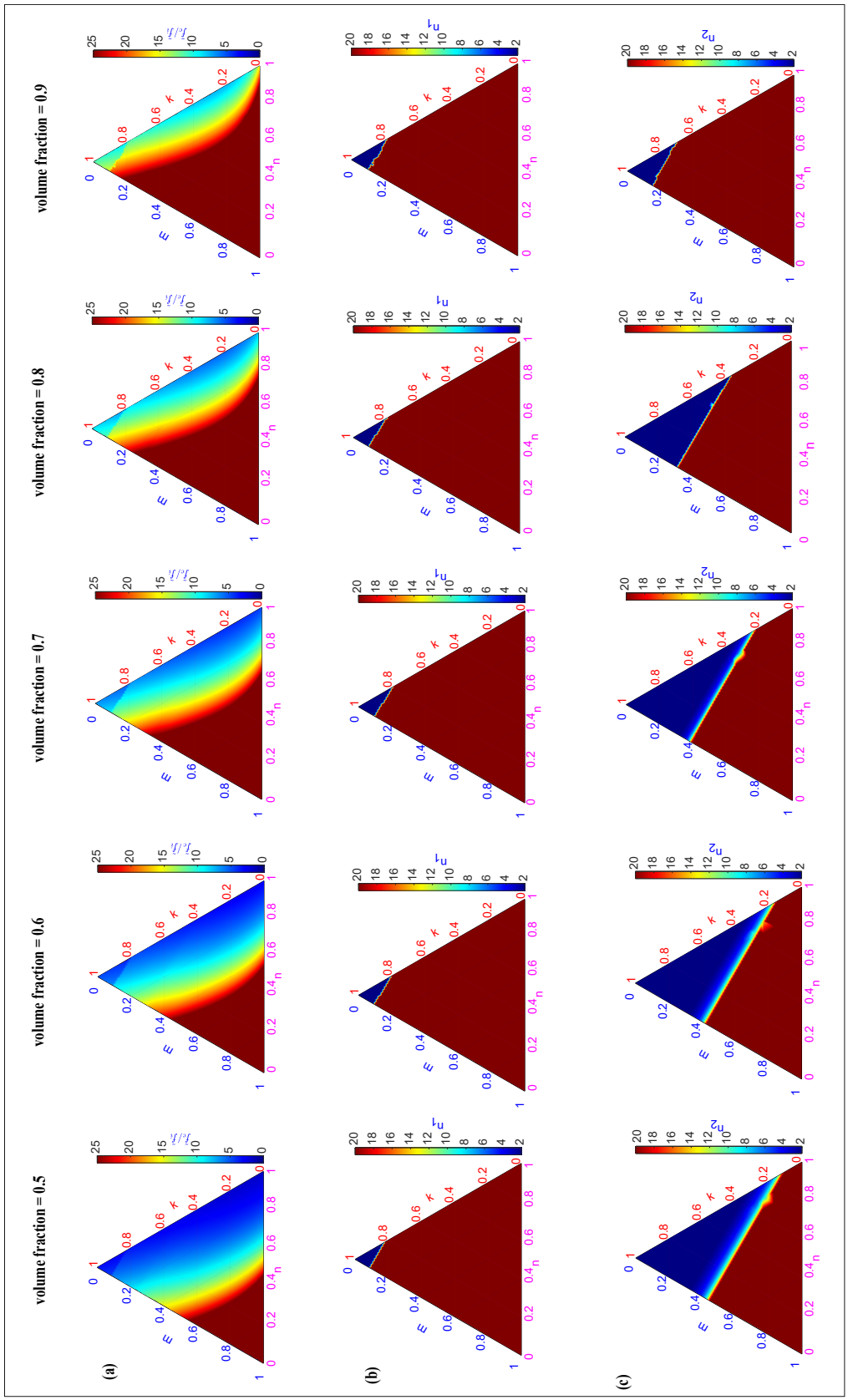

Figure 5.9: Variation of maximized f_c/f_i, corresponding n_1 and n_2 with increase in volume fraction. The plots are drawn for $E_p/G_i = 1000$ and $\sigma^p_{critical}/\tau^i_{critical} = 10$ (The link to the Matlab scripts for reproducing this figure can be found here)

From Figure 5.9 (b), it can be seen that the optimized value of n_1 is close to the upper bound (20) for a larger portion of the area in the ternary diagram, with only a slight variation as the volume fraction is increased. Also, a low value of n_1 is observed for combinations with high values of k and low values of m. This implies that if we need a 2H SS composite having high toughness ($k = 1$) with low stiffness ($m \approx 0$), a lower number of rows of platelets is sufficient in a period at the first level of hierarchy. For the remaining cases, including the ones for high stiffness ($m = 1$) and strength ($n = 1$), a higher number of rows of platelets are required in a period at the first hierarchy.

The transition boundaries in the ternary plots of n_2 shift towards the right and top with an increase in volume fraction as observed from Figure 5.9. This interprets that as volume fraction is increased, only a small range of combinations of m, n, and k near to the top vertex of the ternary diagram (high toughness and low stiffness) are possible with a lower number of rows of platelets in the second level of hierarchy. But, at low volume fractions, the regions with a lower number of rows of platelets increase. Also, it can be observed that more combinations of m, n, k have the upper bound of n_2 as the optimum value of the number of rows of platelets in a period in the second level of hierarchy as the volume fraction is increased.

Thus, the procedure for a quick design of a non-self-similar hierarchical composite using a set of platelet and matrix materials for a particular volume fraction can be summarized as follows. The optimum aspect ratio is first found out using Equations 5.8 and 5.10. Once the critical aspect ratios are obtained, the mechanical properties are maximized using the multi-objective function, and the ternary plots can be generated. Finally, according to the priorities of each mechanical property, viz. stiffness, strength, and toughness, assigned to the variables m, n, and k, respectively, the values of n_1 and n_2 can be chosen from the ternary diagrams.

As an example, consider 50% volume fraction at the first and second levels of hierarchy, with material properties such that $E_p/G_i = 1000$ and $\sigma^p_{critical}/\tau^i_{critical} = 10$. For a 2H SS composite with maximum stiffness, we can easily obtain the values of n_1 and n_2 by observing the values at the left corner in Figure 5.9 (b) and (c) as 20, and 20 respectively. To get the aspect ratio, these values can be substituted into Equations 5.8 and 5.10. Thus we get the four variables n_1, n_2, ρ_1, and ρ_2 required for the design of a 2H SS composite.

5.4 Conclusion

The generalization and optimization of a non-self-similar hierarchical bio-inspired composite are made in the present study. The major conclusions from the results and discussions of the current work can be summarized as follows: The strength of the non-self-similar two hierarchical composites (2H SS) for a given volume fraction and aspect ratio is independent of the number of platelets in a period at the second level of hierarchy. But, the maximum stiffness, as well as toughness for a 2H SS composite, is obtained when the number of platelets in a period at both levels of hierarchy are minima.

It can be concluded from the results and discussions that the design of a non-self-similar composite is influenced by the volume fraction, platelet aspect ratios, and the number of platelets at the first and second levels of hierarchy. The design can be done according to the required priorities of stiffness, strength, and toughness for a set of platelet and matrix materials easily with the aid of the ternary diagrams obtained from the optimization of the multi-objective fitness function for the composite.

This study could find its application as a design and optimization tool to estimate the range of mechanical properties that can be expected in a 2H non-self-similar composite for a given combination of platelet and matrix materials, and platelet volume fraction. Also, it can be used to tailor the 2H bio-inspired composite to meet requisites according to its intended purpose, as desired by the designer. The limitations of the present study include the non-consideration of factors such as the plasticity of materials and the uncertainty of the variables in the optimization problem. The influence of these factors is, however, left for future studies.

Chapter 6

Conclusions and Future Work

Throughout this study, we have delved into the depths of the research question on the mechanical properties of non-self-similar two hierarchical (2H) composites through literature review, data analyses, and discussions. This Chapter brings all the threads together and draw meaningful insights from the findings. The future scopes of the present study are also discussed.

6.1 Conclusions

The present study investigates the essential mechanical properties of non-self-similar two hierarchical composites by analytical as well as finite element analyses. The failure mechanisms and the influence of different sequences of failure over the stiffness, strength, and toughness of the staggered composites with a single hierarchy (1H) are studied in detail, first. Also, a novel analytical formulation to estimate the stresses in a stairwise staggered composite is formulated using shear lag model. The influence of failure sequences on the mechanical properties is compared for regular and stairwise staggered composites for various sets of material properties for the platelet and matrix, by conducting a case study.

An analytical model to predict the mechanical properties of two-hierarchical (2H) non-self-similar composites is developed using the tension shear chain (TSC) model. We adopt the TSC model for the formulation involving two hierarchy in the structure, owing to its simplicity and lesser computation time, compared to that of the shear lag model.

Finally, the various parameters in the first and second levels of hierarchy are generalized to obtain a generalized model for 2H non-self-similar bio-inspired composites. The generalized model is also optimized to get the configuration of a 2H composite for a given stiffness, strength, and stiffness, using ternary diagrams.

The major conclusions from the study are summarized as follows:

- Based on the failure analysis of single hierarchical regular staggered and stairwise staggered models, we find that the failure sequence has an important effect on the mechanical properties of bio-inspired composites. However, this effect is influenced by various geometrical and material parameters.
  - A significant contribution to the toughness from vertical the interface failure is observed for regular as well as stairwise staggered models.
- The 2H non-self-similar composites conceived in the present study are characterized with a greater toughness than single hierarchical regular staggered (RSM) and stairwise staggered models (SSM) available in literature (Zhang et al., 2010).
  - For a similar toughness, the non-self-similar composites seem to have more strength.
- The failure analysis using comparison of stress distribution show a significant reduction in the stress concentrations in two hierarchical composite, compared to the ones with single hierarchy, due to the hierarchical arrangement of platelets.
- The optimization results show that for a non-self-similar two hierarchical composites (2H SS) with a given volume fraction and aspect ratio, the strength is independent of the number of platelets in a period at the second level of hierarchy. However, a lower number of platelets in a period for both levels of hierarchy yielded maximum toughness and stiffness in a 2H SS composite.
  - The optimization results enable the user to tune the properties such as the stiffness, strength, and the toughness of the 2H SS bio-inspired composite according to the priorities and requirements, with the help of the ternary diagrams.

6.2 Scope for future work

The results from the thesis are promising and useful in the design of modern bio-inspired staggered composites. Also, the finite element analysis (FEA) methodology can be used for analysing a wide range of problems in the field of staggered composites. The following are the possible scopes for future works:

- Since the current analyses are done on the linearly elastic material assumptions, the effect of the flexible matrix's deformation is not captured. A detailed analysis considering the matrix deformation, as well as the cohesive behaviour of matrix interfaces can be done to get more realistic results.

- The optimization study can be extended for more than the two parameters (aspect ratio and number of platelets in one period), considered at present. The other parameters include the volume fractions in the first and second hierarchical levels, the overlap ratio of platelets, and different material combinations of platelet and matrix.

- Experimental studies can be conducted to verify the obtained results and get more in-depth details for the production of staggered composites.

- The study of the influence of factors like the waviness of the platelets, and randomness in the platelet distribution as observed in biological composites over the mechanical properties, is also a possible future direction of this work.

There exist different types of finite element methods which are found to be useful for the analysis. For example, the lattice spring models (LSM) can be used to obtain the information on the deformation, stress variation pattern, and fracture mechanism (Buxton et al., 2001; Chen et al., 2014; Dimas and Buehler, 2012; Ghimire et al., 2021; Libonati et al., 2017; Sen and Buehler, 2011). Another method is the extended finite element method (XFEM) which has an advantage of mesh independence, when compared to other conventional FEM methods (Belytschko, 1997; Goyal and Irizarry, 2016; Vellwock et al., 2018). In phase field method (PFM), unlike most of the standard methods of fracture mechanics, it used a predetermined crack path which is naturally described using thermodynamics-based dynamic models (Amor et al., 2009; Khaderi et al., 2014; Miehe et al., 2010). The cohesive zone modeling (CZM) can capture the interface failures which consist of the debonding of matrix from the platelet (Alfano et al., 2007; Singh et al., 2019). These approaches are of really beneficial for the validation of the failure analysis along with the experimental investigations, leaving room for future research.

Bibliography

N. Abid, M. Mirkhalaf, and F. Barthelat. Discrete-element modeling of nacre-like materials: Effects of random microstructures on strain localization and mechanical performance. *Journal of the Mechanics and Physics of Solids*, 112:385–402, 2018.

B. Achrai and H. D. Wagner. Micro-structure and mechanical properties of the turtle carapace as a biological composite shield. *Acta biomaterialia*, 9(4):5890–5902, 2013.

M. Alfano, F. Furgiuele, A. Leonardi, C. Maletta, and G. H. Paulino. Cohesive zone modeling of mode i fracture in adhesive bonded joints. *Key engineering materials*, 348:13–16, 2007.

H. Amor, J.-J. Marigo, and C. Maurini. Regularized formulation of the variational brittle fracture with unilateral contact: Numerical experiments. *Journal of the Mechanics and Physics of Solids*, 57(8):1209–1229, 2009.

B. An, X. Zhao, and D. Zhang. On the mechanical behavior of bio-inspired materials with non-self-similar hierarchy. *Journal of the mechanical behavior of biomedical materials*, 34:8–17, 2014.

S. Anup, S. Sivakumar, and G. Suraishkumar. Structural arrangement effects of mineral platelets on the nature of stress distribution in bio-composites. *COMPUTER MODELING IN ENGINEERING AND SCIENCES*, 18(2):145, 2007.

S. Askarinejad and N. Rahbar. Mechanics of bioinspired lamellar structured ceramic/polymer composites: Experiments and models. *International Journal of Plasticity*, 107: 122–149, 2018.

S. Askarinejad, H. A. Choshali, C. Flavin, and N. Rahbar. Effects of tablet waviness on the mechanical response of architected multilayered materials: Modeling and experiment. *Composite Structures*, 195:118–125, 2018.

H. Bai, F. Walsh, B. Gludovatz, B. Delattre, C. Huang, Y. Chen, A. P. Tomsia, and R. O. Ritchie. Bioinspired hydroxyapatite/poly (methyl methacrylate) composite with a nacre-mimetic architecture by a bidirectional freezing method. *Advanced Materials*, 28(1): 50–56, 2016.

S. Bargmann, I. Scheider, T. Xiao, E. Yilmaz, G. A. Schneider, and N. Huber. Towards bio-inspired engineering materials: Modeling and simulation of the mechanical behavior of hierarchical bovine dental structure. *Computational Materials Science*, 79:390–401, 2013.

F. Barthelat. Designing nacre-like materials for simultaneous stiffness, strength and toughness: Optimum materials, composition, microstructure and size. *Journal of the Mechanics and Physics of Solids*, 73:22–37, 2014.

F. Barthelat and H. Espinosa. An experimental investigation of deformation and fracture of nacre–mother of pearl. *Experimental mechanics*, 47(3):311–324, 2007.

F. Barthelat and R. Rabiei. Toughness amplification in natural composites. *Journal of the Mechanics and Physics of Solids*, 59(4):829–840, 2011.

F. Barthelat, C.-M. Li, C. Comi, and H. D. Espinosa. Mechanical properties of nacre constituents and their impact on mechanical performance. *Journal of Materials Research*, 21(8):1977–1986, 2006.

F. Barthelat, H. Tang, P. Zavattieri, C.-M. Li, and H. Espinosa. On the mechanics of mother-of-pearl: a key feature in the material hierarchical structure. *Journal of the Mechanics and Physics of Solids*, 55(2):306–337, 2007.

F. Barthelat, A. K. Dastjerdi, and R. Rabiei. An improved failure criterion for biological and engineered staggered composites. *Journal of The Royal Society Interface*, 10(79): 20120849, 2013.

M. R. Begley, N. R. Philips, B. G. Compton, D. V. Wilbrink, R. O. Ritchie, and M. Utz. Micromechanical models to guide the development of synthetic 'brick and mortar'composites. *Journal of the Mechanics and Physics of Solids*, 60(8):1545–1560, 2012.

T. Belytschko. Elastic crack growth in finite elements with minimal remeshing. *Int. J. Numer. Meth. Engrg.*, 40:1483–1504, 1997.

F. Bosia, T. Abdalrahman, and N. M. Pugno. Investigating the role of hierarchy on the strength of composite materials: evidence of a crucial synergy between hierarchy and material mixing. *Nanoscale*, 4(4):1200–1207, 2012.

G. A. Buxton, C. M. Care, and D. J. Cleaver. A lattice spring model of heterogeneous materials with plasticity. *Modelling and simulation in materials science and engineering*, 9(6):485, 2001.

F. Carosio, F. Cuttica, L. Medina, and L. A. Berglund. Clay nanopaper as multifunctional brick and mortar fire protection coating—wood case study. *Materials & Design*, 93: 357–363, 2016.

M. A. O. Carreño, E. N. A. Mireles, and E. Rocha-Rangel. Biologically inspired innovation: a review on structural materials and manufacturing. *Bioinspired, Biomimetic and Nanobiomaterials*, 11(3):86–100, 2022.

C. Chao, H. Guo, P. Yan, and L. Dong. Dynamic modulus of staggered nanocomposites with different distributions of platelets considering the interface stress effect. *Journal of Applied Mechanics*, 88(9), 2021.

B. Chen, P. Wu, and H. Gao. A characteristic length for stress transfer in the nanostructure of biological composites. *Composites Science and Technology*, 69(7-8):1160–1164, 2009.

H. Chen, E. Lin, and Y. Liu. A novel volume-compensated particle method for 2d elasticity and plasticity analysis. *International Journal of Solids and Structures*, 51(9):1819–1833, 2014.

S.-M. Chen, H.-L. Gao, X.-H. Sun, Z.-Y. Ma, T. Ma, J. Xia, Y.-B. Zhu, R. Zhao, H.-B. Yao, H.-A. Wu, et al. Superior biomimetic nacreous bulk nanocomposites by a multiscale soft-rigid dual-network interfacial design strategy. *Matter*, 1(2):412–427, 2019.

K. Cheng, P. She, H. Wang, Z. Wang, L. Zhang, X. Tang, L. Yuan, Y. Feng, X. Song, G. Pan, et al. A bio-inspired versatile free-standing membrane for oral cavity microenvironmental monitoring and remineralization to prevent dental caries. *Materials Horizons*, 2023.

J. Currey. Mechanical properties of mother of pearl in tension. *Proceedings of the Royal Society of London B: Biological Sciences*, 196(1125):443–463, 1977.

J. D. Currey. *The mechanical adaptations of bones*. Princeton University Press, 1984.

S. Deng, L. Tong, X. Li, J. Chu, M. Li, and D. Zou. Enhanced anti-corrosion/wear properties of mg alloy through a hierarchical bio-inspired self-healing composite coating. *Colloids and Surfaces A: Physicochemical and Engineering Aspects*, 658:130770, 2023.

L. S. Dimas and M. J. Buehler. Influence of geometry on mechanical properties of bio-inspired silica-based hierarchical materials. *Bioinspiration & biomimetics*, 7(3):036024, 2012.

L. Dong, C. Chao, and P. Yan. Effective modulus of biological staggered nanocomposites with interface stress effect. *Composites Part B: Engineering*, 2019.

A. Dutta and S. A. Tekalur. Crack tortuousity in the nacreous layer–topological dependence and biomimetic design guideline. *International Journal of Solids and Structures*, 51(2): 325–335, 2014.

H. D. Espinosa, J. E. Rim, F. Barthelat, and M. J. Buehler. Merger of structure and material in nacre and bone–perspectives on de novo biomimetic materials. *Progress in Materials Science*, 54(8):1059–1100, 2009.

S. F. Fischer, M. Thielen, R. R. Loprang, R. Seidel, C. Fleck, T. Speck, and A. Bührig-Polaczek. Pummelos as concept generators for biomimetically inspired low weight structures with excellent damping properties. *Advanced Engineering Materials*, 12(12): B658–B663, 2010.

P. Fratzl and R. Weinkamer. Nature's hierarchical materials. *Progress in materials Science*, 52(8):1263–1334, 2007.

P. Fratzl, H. Gupta, E. Paschalis, and P. Roschger. Structure and mechanical quality of the collagen–mineral nano-composite in bone. *Journal of materials chemistry*, 14(14): 2115–2123, 2004.

H. Gao. Application of fracture mechanics concepts to hierarchical biomechanics of bone and bone-like materials. *International Journal of Fracture*, 138(1):101–137, 2006.

H. Gao, B. Ji, I. L. Jäger, E. Arzt, and P. Fratzl. Materials become insensitive to flaws at nanoscale: lessons from nature. *Proceedings of the national Academy of Sciences*, 100 (10):5597–5600, 2003.

H. Gao, B. Ji, M. J. Buehler, and Y. Haimin. 'flaw tolerant nanostructures of biological materials. *Mech. Chem. Biosyst*, 1:37–52, 2004.

H.-L. Gao, S.-M. Chen, L.-B. Mao, Z.-Q. Song, H.-B. Yao, H. Cölfen, X.-S. Luo, F. Zhang, Z. Pan, Y.-F. Meng, et al. Mass production of bulk artificial nacre with excellent mechanical properties. *Nature communications*, 8(1):1–8, 2017.

A. Ghimire, Y.-Y. Tsai, P.-Y. Chen, and S.-W. Chang. Tunable interface hardening: Designing tough bio-inspired composites through 3D printing, testing, and computational validation. *Composites Part B: Engineering*, 215:108754, 2021.

R. F. Gibson. *Principles of composite material mechanics*. CRC press, 2016.

V. Goyal and E. Irizarry. Development of a combined cohesive and extended finite element method to predict delamination in composite structures. In *57th AIAA/ASCE/AHS/ASC Structures, Structural Dynamics, and Materials Conference*, page 0987, 2016.

F. Greco, L. Leonetti, A. Pranno, and S. Rudykh. Mechanical behavior of bio-inspired nacre-like composites: A hybrid multiscale modeling approach. *Composite Structures*, 233:111625, 2020.

G. X. Gu, M. Takaffoli, A. J. Hsieh, and M. J. Buehler. Biomimetic additive manufactured polymer composites for improved impact resistance. *Extreme Mechanics Letters*, 9:317–323, 2016.

G. X. Gu, M. Takaffoli, and M. J. Buehler. Hierarchically enhanced impact resistance of bioinspired composites. *Advanced Materials*, 29(28):1700060, 2017.

X. Guo and H. Gao. Bio-inspired material design and optimization. In *IUTAM Symposium on Topological Design Optimization of Structures, Machines and Materials: Status and Perspectives*, pages 439–453. Springer, 2006.

H. S. Gupta, J. Seto, W. Wagermaier, P. Zaslansky, P. Boesecke, and P. Fratzl. Cooperative deformation of mineral and collagen in bone at the nanoscale. *Proceedings of the National Academy of Sciences*, 103(47):17741–17746, 2006.

R. Hao, D. Li, and W. Liu. A novel three-dimensional structure model of biomimetic staggered composites. *Composite Structures*, 239:112042, 2020.

R. Häsä and S. Pinho. Failure mechanisms of biological crossed-lamellar microstructures applied to synthetic high-performance fibre-reinforced composites. *Journal of the Mechanics and Physics of Solids*, 125:53–73, 2019.

J. Henry and S. Pimenta. Bio-inspired non-self-similar hierarchical microstructures for damage tolerance. *Composites Science and Technology*, 201:108374, 2021.

J. J. Henry. *Designing and modelling bio-inspired discontinuous composites*. PhD thesis, Imperial College London, 2018.

W. Huang, D. Restrepo, J.-Y. Jung, F. Y. Su, Z. Liu, R. O. Ritchie, J. McKittrick, P. Zavattieri, and D. Kisailus. Multiscale toughening mechanisms in biological materials and bioinspired designs. *Advanced Materials*, 31(43):1901561, 2019.

A. Ingrole, T. G. Aguirre, L. Fuller, and S. W. Donahue. Bioinspired energy absorbing material designs using additive manufacturing. *Journal of the Mechanical Behavior of Biomedical Materials*, 119:104518, 2021.

B. Ji. A study of the interface strength between protein and mineral in biological materials. *Journal of biomechanics*, 41(2):259–266, 2008.

B. Ji and H. Gao. Mechanical properties of nanostructure of biological materials. *Journal of the Mechanics and Physics of Solids*, 52(9):1963–1990, 2004a.

B. Ji and H. Gao. A study of fracture mechanisms in biological nano-composites via the virtual internal bond model. *Materials Science and Engineering: A*, 366(1):96–103, 2004b.

S. Khaderi, P. Murali, and R. Ahluwalia. Failure and toughness of bio-inspired composites: Insights from phase field modelling. *Computational materials science*, 95:1–7, 2014.

Y. Kim, Y. Kim, T.-I. Lee, T.-S. Kim, and S. Ryu. An extended analytic model for the elastic properties of platelet-staggered composites and its application to 3d printed structures. *Composite Structures*, 2018.

Y. Kim, H. Jeong, G. X. Gu, and S. Ryu. A three-dimensional fracture pattern diagram of staggered platelet structures. *Composite Structures*, 220:769–775, 2019.

A. Kitchener. An analysis of the forces of fighting of the blackbuck (antilope cervicapra) and the bighorn sheep (ovis canadensis) and the mechanical design of the horn of bovids. *Journal of Zoology*, 214(1):1–20, 1988.

S. Kotha, S. Kotha, and N. Guzelsu. A shear-lag model to account for interaction effects between inclusions in composites reinforced with rectangular platelets. *Composites Science and Technology*, 60(11):2147–2158, 2000.

W. J. Landis. Mineral characterization in calcifying tissues: atomic, molecular and macromolecular perspectives. *Connective tissue research*, 34(4):239–246, 1996.

W. J. Landis, K. J. Hodgens, J. Arena, M. J. Song, and B. F. McEwen. Structural relations between collagen and mineral in bone as determined by high voltage electron microscopic tomography. *Microscopy research and technique*, 33(2):192–202, 1996.

H. Lei, B. Liu, C. Wang, and D. Fang. Study on biomimetic staggered composite for better thermal shock resistance. *Mechanics of Materials*, 49:30–41, 2012a.

H. Lei, Z. Zhang, and B. Liu. Effect of fiber arrangement on mechanical properties of short fiber reinforced composites. *Composites Science and Technology*, 72(4):506–514, 2012b.

H. Lei, Z. Zhang, F. Han, B. Liu, Y.-W. Zhang, and H. Gao. Elastic bounds of bioinspired nanocomposites. *Journal of Applied Mechanics*, 80(6), 2013.

D. Li and B. Ji. Fracture toughness of biological composites with multilevel structural hierarchy. *Journal of Applied Mechanics*, 87:071004–1, 2020.

Y.-Q. Li, T. Yu, T.-Y. Yang, L.-X. Zheng, and K. Liao. Bio-inspired nacre-like composite films based on graphene with superior mechanical, electrical, and biocompatible properties. *Advanced Materials*, 24(25):3426–3431, 2012.

F. Libonati and M. J. Buehler. Advanced structural materials by bioinspiration. *Advanced Engineering Materials*, 19(5):1600787, 2017.

F. Libonati, V. Cipriano, L. Vergani, and M. J. Buehler. Computational framework to predict failure and performance of bone-inspired materials. *ACS Biomaterials Science & Engineering*, 3(12):3236–3243, 2017.

G. Liu, B. Ji, K.-C. Hwang, and B. C. Khoo. Analytical solutions of the displacement and stress fields of the nanocomposite structure of biological materials. *Composites Science and Technology*, 71(9):1190–1195, 2011.

H. Lu, P. Zhu, and R. Li. A computational study of adhesive properties of bio-inspired surfaces. *Materials Today Communications*, 34:105113, 2023.

S. Luke and P. Vukusic. An introduction to biomimetic photonic design. *Europhysics News*, 42(3):20–23, 2011.

H. Ma, Y. Wei, J. Song, and L. Liang. Mechanical behavior and size effect of the staggered bio-structure materials. *Mechanics of Materials*, 126:47–56, 2018.

S. Ma, I. Scheider, and S. Bargmann. Continuum damage modeling and simulation of hierarchical dental enamel. *Modelling and Simulation in Materials Science and Engineering*, 24(4):045014, 2016.

M. Maghsoudi-Ganjeh, L. Lin, X. Yang, and X. Zeng. Computational modeling and simulation of bioinspired nacre-like composites. *Journal of Materials Research*, 36(13): 2651–2661, 2021.

I. A. Malik and F. Barthelat. Toughening of thin ceramic plates using bioinspired surface patterns. *International Journal of Solids and Structures*, 97:389–399, 2016.

R. Manno, W. Gao, and I. Benedetti. Engineering the crack path in lattice cellular materials through bio-inspired micro-structural alterations. *Extreme Mechanics Letters*, 26:8–17, 2019.

L.-B. Mao, H.-L. Gao, H.-B. Yao, L. Liu, H. Cölfen, G. Liu, S.-M. Chen, S.-K. Li, Y.-X. Yan, Y.-Y. Liu, et al. Synthetic nacre by predesigned matrix-directed mineralization. *Science*, 354(6308):107–110, 2016.

F. J. Martínez-Vázquez, E. Sánchez-González, O. Borrero-López, P. Miranda, A. Pajares, and F. Guiberteau. Novel bioinspired composites fabricated by robocasting for dental applications. *Ceramics International*, 2021.

S. Mathiazhagan and S. Anup. Influence of platelet aspect ratio on the mechanical behaviour of bio-inspired nanocomposites using molecular dynamics. *Journal of the mechanical behavior of biomedical materials*, 59:21–40, 2016a.

S. Mathiazhagan and S. Anup. Investigation of deformation mechanisms of staggered nanocomposites using molecular dynamics. *Physics Letters A*, 380(36):2849–2853, 2016b.

S. Mathiazhagan and S. Anup. Effect of interface strength on the mechanical behaviour of bio-inspired composites: A molecular dynamics study. *Mechanics of Materials*, 132: 93–100, 2019.

M. Mazzotti, A. Foehr, O. R. Bilal, A. Bergamini, F. Bosia, C. Daraio, N. M. Pugno, and M. Miniaci. Bio-inspired non self-similar hierarchical elastic metamaterials. *International Journal of Mechanical Sciences*, 241:107915, 2023.

A. Melaibari, A. Wagih, M. Basha, A. Kabeel, G. Lubineau, and M. Eltaher. Bio-inspired composite laminate design with improved out-of-plane strength and ductility. *Composites Part A: Applied Science and Manufacturing*, 144:106362, 2021.

M. A. Meyers, P.-Y. Chen, A. Y.-M. Lin, and Y. Seki. Biological materials: structure and mechanical properties. *Progress in Materials Science*, 53(1):1–206, 2008.

M. A. Meyers, J. McKittrick, and P.-Y. Chen. Structural biological materials: critical mechanics-materials connections. *science*, 339(6121):773–779, 2013.

C. Miehe, M. Hofacker, and F. Welschinger. A phase field model for rate-independent crack propagation: Robust algorithmic implementation based on operator splits. *Computer Methods in Applied Mechanics and Engineering*, 199(45-48):2765–2778, 2010.

M. Mirkhalaf, J. Tanguay, and F. Barthelat. Carving 3D architectures within glass: Exploring new strategies to transform the mechanics and performance of materials. *Extreme Mechanics Letters*, 7:104–113, 2016.

R. Mirzaeifar, L. S. Dimas, Z. Qin, and M. J. Buehler. Defect-tolerant bioinspired hierarchical composites: simulation and experiment. *ACS Biomaterials Science & Engineering*, 1(5):295–304, 2015.

E. Munch, M. E. Launey, D. H. Alsem, E. Saiz, A. P. Tomsia, and R. O. Ritchie. Tough, bio-inspired hybrid materials. *Science*, 322(5907):1516–1520, 2008.

P. Murali, T. K. Bhandakkar, W. L. Cheah, M. H. Jhon, H. Gao, and R. Ahluwalia. Role of modulus mismatch on crack propagation and toughness enhancement in bioinspired composites. *Physical Review E*, 84(1):015102, 2011.

P. K. Nukala and S. Simunovic. A continuous damage random thresholds model for simulating the fracture behavior of nacre. *Biomaterials*, 26(30):6087–6098, 2005.

K. Okumura and P.-G. De Gennes. Why is nacre strong? elastic theory and fracture mechanics for biocomposites with stratified structures. *The European Physical Journal E*, 4(1):121–127, 2001.

P. Patpatiya, K. Chaudhary, A. Shastri, and S. Sharma. A review on polyjet 3D printing of polymers and multi-material structures. *Proceedings of the Institution of Mechanical Engineers, Part C: Journal of Mechanical Engineering Science*, page 09544062221079506, 2022.

X. Peng, B. Zhang, Z. Wang, W. Su, S. Niu, Z. Han, and L. Ren. Bioinspired strategies for excellent mechanical properties of composites. *Journal of Bionic Engineering*, 19(5): 1203–1228, 2022.

S. Pimenta and P. Robinson. An analytical shear-lag model for composites with 'brick-and-mortar'architecture considering non-linear matrix response and failure. *Composites Science and Technology*, 104:111–124, 2014.

M. M. Porter and J. McKittrick. It's tough to be strong: Advances. *Am. Ceram. Soc. Bull*, 93:18–24, 2014.

M. Qwamizadeh, P. Liu, Z. Zhang, K. Zhou, and Y. Wei Zhang. Hierarchical structure enhances and tunes the damping behavior of load-bearing biological materials. *Journal of Applied Mechanics*, 83(5), 2016.

R. Rabiei, S. Bekah, and F. Barthelat. Failure mode transition in nacre and bone-like materials. *Acta biomaterialia*, 6(10):4081–4089, 2010.

K. Raj and P. Murali. Mixed mode crack propagation in staggered biocomposites using phase field modelling. *Journal of the mechanical behavior of biomedical materials*, 101: 103421, 2020.

J.-Y. Rho, L. Kuhn-Spearing, and P. Zioupos. Mechanical properties and the hierarchical structure of bone. *Medical engineering & physics*, 20(2):92–102, 1998.

N. San Ha and G. Lu. A review of recent research on bio-inspired structures and materials for energy absorption applications. *Composites Part B: Engineering*, 181:107496, 2020.

A. Saroj, K. J. Rose, C. Arun, and S. Anup. Design of a bio-inspired composite using probabilistic fracture mechanics. *Journal of the mechanical behavior of biomedical materials*, 95:96–102, 2019.

D. Sen and M. J. Buehler. Structural hierarchies define toughness and defect-tolerance despite simple and mechanically inferior brittle building blocks. *Scientific reports*, 1:35, 2011.

Y. Shao, H.-P. Zhao, X.-Q. Feng, and H. Gao. Discontinuous crack-bridging model for fracture toughness analysis of nacre. *Journal of the Mechanics and Physics of Solids*, 60 (8):1400–1419, 2012.

R. Shu, X. Jiang, H. Sun, Z. Shao, T. Song, and Z. Luo. Recent researches of the bio-inspired nano-carbon reinforced metal matrix composites. *Composites Part A: Applied Science and Manufacturing*, 131:105816, 2020.

SIMULIA. *ABAQUS/Standard User's Manual, Version 2022*. Providence, RI, 2022.

A. Singh, T. S. Sandhu, and S. Pal. Interplay of various fracture mechanisms in bio-inspired staggered structure. *Mechanics of Materials*, 139:103215, 2019.

V. Slesarenko, N. Kazarinov, and S. Rudykh. Distinct failure modes in bio-inspired 3d-printed staggered composites under non-aligned loadings. *Smart Materials and Structures*, 26(3):035053, 2017.

K. Song, D. Li, C. Zhang, T. Liu, Y. Tang, Y. M. Xie, and W. Liao. Bio-inspired hierarchical honeycomb metastructures with superior mechanical properties. *Composite Structures*, 304:116452, 2023.

I. Spears. A three-dimensional finite element model of prismatic enamel: a re-appraisal of the data on the young's modulus of enamel. *Journal of Dental Research*, 76(10): 1690–1697, 1997.

A. R. Studart. Towards high-performance bioinspired composites. *Advanced Materials*, 24 (37):5024–5044, 2012.

C. Sun and R. Vaidya. Prediction of composite properties from a representative volume element. *Composites Science and Technology*, 56(2):171–179, 1996.

I. The Mathworks. *MATLAB version 9.9 (R2020b)*. Natick, Massachusetts, 2020.

P. Tran, T. D. Ngo, A. Ghazlan, and D. Hui. Bimaterial 3d printing and numerical analysis of bio-inspired composite structures under in-plane and transverse loadings. *Composites Part B: Engineering*, 108:210–223, 2017.

P. Tseng, B. Napier, S. Zhao, A. N. Mitropoulos, M. B. Applegate, B. Marelli, D. L. Kaplan, and F. G. Omenetto. Directed assembly of bio-inspired hierarchical materials with controlled nanofibrillar architectures. *Nature nanotechnology*, 12(5):474–480, 2017.

S. M. M. Valashani and F. Barthelat. The effect of dilution in natural and bio-inspired staggered composites. In *Mechanics of Biological Systems and Materials, Volume 4: Proceedings of the 2013 Annual Conference on Experimental and Applied Mechanics*, pages 83–91. Springer, 2014.

A. E. Vellwock, L. Vergani, and F. Libonati. A multiscale xfem approach to investigate the fracture behavior of bio-inspired composite materials. *Composites Part B: Engineering*, 141:258–264, 2018.

H. D. Wagner and S. Weiner. On the relationship between the microstructure of bone and its mechanical stiffness. *Journal of Biomechanics*, 25(11):1311–1320, 1992.

A. Wang, S. Wang, H. Yin, R. Bai, J. Liu, Z. Zhang, and P. Zhou. Structural effects in 'brick-and-mortar'architecture: Bio-inspired ceramic matrix composites developed through a new method. *Ceramics International*, 49(3):5042–5048, 2023.

U. G. Wegst and M. Ashby. The mechanical efficiency of natural materials. *Philosophical Magazine*, 84(21):2167–2186, 2004.

U. G. Wegst, H. Bai, E. Saiz, A. P. Tomsia, and R. O. Ritchie. Bioinspired structural materials. *Nature materials*, 14(1):23, 2015.

S. Weiner and H. D. Wagner. The material bone: structure-mechanical function relations. *Annual review of materials science*, 28(1):271–298, 1998.

J. Wiener, F. Arbeiter, A. Tiwari, O. Kolednik, and G. Pinter. Bioinspired toughness improvement through soft interlayers in mineral reinforced polypropylene. *Mechanics of Materials*, 140:103243, 2020.

R. P. Wilkerson, B. Gludovatz, J. Watts, A. P. Tomsia, G. E. Hilmas, and R. O. Ritchie. A study of size effects in bioinspired,"nacre-like", metal-compliant-phase (nickel-alumina) coextruded ceramics. *Acta Materialia*, 148:147–155, 2018.

J. Wilmers and S. Bargmann. Nature's design solutions in dental enamel: Uniting high strength and extreme damage resistance. *Acta Biomaterialia*, 2020.

G. Wu, X. Wang, Y. Wang, C. Ji, and C. Zhao. Bioinspired nacre-like steel-polyurea composite plate subjected to projectile impact. *Materials & Design*, 224:111371, 2022.

K. Wu, Z. Zheng, S. Zhang, L. He, H. Yao, X. Gong, and Y. Ni. Interfacial strength-controlled energy dissipation mechanism and optimization in impact-resistant nacreous structure. *Materials & Design*, 163:107532, 2019.

W. Wu, J. Owino, A. Al-Ostaz, and L. Cai. Applying periodic boundary conditions in finite element analysis. In *SIMULIA Community Conference, Providence*, pages 707–719, 2014.

G. X Gu, I. Su, S. Sharma, J. L. Voros, Z. Qin, and M. J. Buehler. Three-dimensional-printing of bio-inspired composites. *Journal of biomechanical engineering*, 138(2), 2016.

Y. Xu, P. Zhang, H. Lu, and W. Zhang. Hierarchically modeling the elastic properties of 2d needled carbon/carbon composites. *Composite Structures*, 133:148–156, 2015.

W. Yang, B. Gludovatz, E. A. Zimmermann, H. A. Bale, R. O. Ritchie, and M. A. Meyers. Structure and fracture resistance of alligator gar (atractosteus spatula) armored fish scales. *Acta biomaterialia*, 9(4):5876–5889, 2013.

W. Yang, X. Zhang, Y. Chen, B. Fei, and X. Yi. Strength analysis of bio-inspired composites reinforced by regularly and randomly staggered platelets. *Composite Structures*, 2019.

Y. Yang, X. Song, X. Li, Z. Chen, C. Zhou, Q. Zhou, and Y. Chen. Recent progress in biomimetic additive manufacturing technology: from materials to functional structures. *Advanced Materials*, 30(36):1706539, 2018.

H. Yao and H. Gao. Reprint of "multi-scale cohesive laws in hierarchical materials"[in. j. solids struct. 44 (2007) 8177–8193]. *International Journal of Solids and Structures*, 45 (13):3627–3643, 2008.

H.-B. Yao, H.-Y. Fang, X.-H. Wang, and S.-H. Yu. Hierarchical assembly of micro-/nano-building blocks: bio-inspired rigid structural functional materials. *Chemical Society Reviews*, 40(7):3764–3785, 2011.

S. Yin, W. Guo, H. Wang, Y. Huang, R. Yang, Z. Hu, D. Chen, J. Xu, and R. O. Ritchie. Strong and tough bioinspired additive-manufactured dual-phase mechanical metamaterial composites. *Journal of the Mechanics and Physics of Solids*, 149:104341, 2021.

H. Yulong, J. Tao, L. Xin, Q. Ji, and S. Xuefeng. Crashworthiness design of hexagonal tubes using self-similar inspired structures. *Materials Today Communications*, 33: 104934, 2022.

Y. Zhang, M. Lu, C. H. Wang, G. Sun, and G. Li. Out-of-plane crashworthiness of bio-inspired self-similar regular hierarchical honeycombs. *Composite Structures*, 144:1–13, 2016.

Z. Zhang, B. Liu, Y. Huang, K. Hwang, and H. Gao. Mechanical properties of unidirectional nanocomposites with non-uniformly or randomly staggered platelet distribution. *Journal of the Mechanics and Physics of Solids*, 58(10):1646–1660, 2010.

Z. Zhang, Y.-W. Zhang, and H. Gao. On optimal hierarchy of load-bearing biological materials. *Proceedings of the Royal Society of London B: Biological Sciences*, 278(1705): 519–525, 2011.

L. Zhou, Y. Zhu, Z. He, X. Jin, and H. Wu. Multi-parameter structural optimization to reconcile mechanical conflicts in nacre-like composites. *Composite Structures*, 259: 113225, 2021.

LIST OF PUBLICATIONS BASED ON THE RESEARCH WORK

Publications in Peer-Reviewed International Journals

1. Abhirami A J and Anup S (2021), *"Mechanical Properties of Unidirectional Bio-inspired Composites with Two Non-self-similar Hierarchical Structures"*, **Mechanics of Materials** , Vol-163, p.104082. (DOI: 10.1016/j.mechmat.2021.104082)

2. Abhirami A J, Devendra Prakash Ghate, and Anup (2023). *"Generalization and optimization of two hierarchical non-self-similar bio-inspired composites "*, **Forces in Mechanics**, Vol-10, p.10017. (DOI: 10.1016/j.finmec.2023.100172)

3. Abhirami A J and Anup S, *"Studies on Effect of Failure Modes on Mechanical Properties of Staggered Composites "*, **Bioinspiration and Biomimetics** (Under Review)

4. Abhirami A J, Bijjam Chandra Sekhar Reddy, and Anup S, *"Numerical Analysis of Failure in Bio-inspired Two Hierarchical Staggered Composites"*, **Extreme Mechanics Letters**, (Under preparation)

Presentations in Conferences

1. A.J Abhirami and S. Anup, *"Influence of Scaling on Fracture Toughness of Bio-inspired Nanocomposites"*, **International Conference on Composite Materials and Structures (ICCMS 2017)**, organized by IIT Hyderabad, India, Dec 17 – 21, 2017.

2. A.J Abhirami and S. Anup , *"Development of Bio-inspired Composites"*, **International Conference on Recent Trends in Materials Science and Technology 2018 (ICMST 2018)** organized by IIST & MRSI Thiruvananthapuram Chapter, India, October 10-13, 2018.

3. A.J Abhirami and S. Anup, *"Elastic Properties of Non-self-similar Two Hierarchical Bio-inspired Unidirectional Composites"*, **Second International Conference on Structural Integrity (ICONS 2018)**, IIT Madras, India, Dec 14 - 17, 2018.

4. Abhirami A J, Ujjval Sai V and Anup S, *"Finite Element Validation of Uniform Shear along Platelet-Matrix Interface in a Unidirectional Bio-inspired Composite "*, **ISAMPE National Conference on Composites (INCCOM 16)**, organized by Indian Society for Advancement of Materials and Process Engineering - Thiruvananthapuram Chapter, Kerala, India, Sep 20 - 21, 2019.

5. A.J Abhirami and S. Anup, *"Analysis of Failure Modes in Unidirectional Bio-inspired Regular Staggered Composite"*, **The 64th Congress of Indian Society of Theoretical and Applied Mechanics (ISTAM-2019)**, IIT Bhubaneswar, India, Dec 9 - 12, 2019.

6. A.J Abhirami and S. Anup, *"Finite element analysis of stiffness of bio-inspired two-hierarchical (2H) stairwise staggered composite with regular staggered composite (SR) as platelets"*, **8th International Conference on Product Lifecycle Modeling, Simulation Synthesis (PLMSS 2021)**, online conference hosted by IIST & VSSC, India, Dec 17 -18, 2021.

7. A.J Abhirami and S. Anup, *"Stress Transfer in Two-hierarchical Non-self-similar Bio-inspired Composites"*, **4th Structural Integrity Conference and Exhibition (SICE 2022)**, the Department of Mechanical and Aerospace Engineering, Indian Institute of Technology Hyderabad under the aegis of InSIS, India, Dec 14 -16, 2022

8. A.J Abhirami and S. Anup, *"A Case Study on Effect of Failure Modes on the Mechanical Properties of Bio-inspired Staggered Composites"*, **2024 SEM Annual Conference & Exposition on Experimental & Applied Mechanics**, Washington, USA, June 3-6, 2024. (Abstract Accepted)

Appendix A

Equations for normal and shear stresses in a regular staggered composite

In this section, the derivation of equations for stress along a platelet in a regular staggered composite done by Kim et al. (2018), using modified shear lag model is included as follows: Consider the Figure A.1 in which the schematic of a regular staggered model with half platelet thickness b and matrix thickness h is shown. The overlapped and non overlapped lengths are denoted by L_a and $2L_b$, respectively.

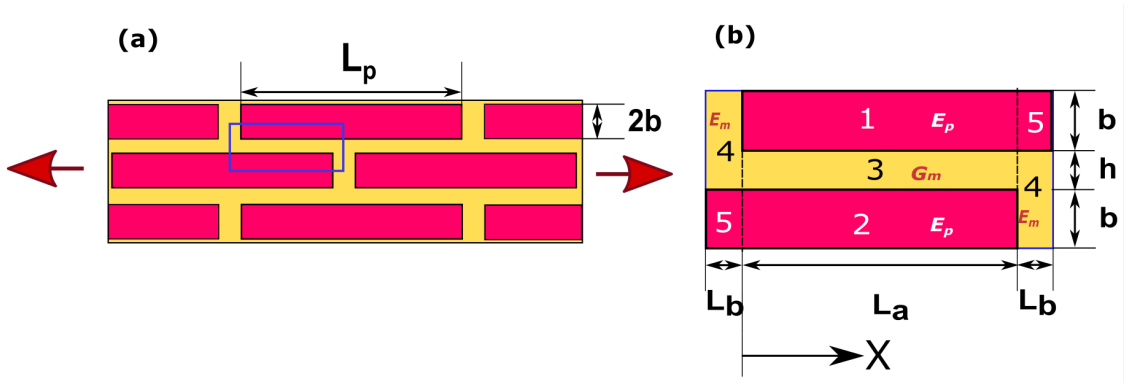

Figure A.1: (a) Schematic diagram of a regularly staggered composite with length and width of platelet L_p and h respectively (b) Representative Volume Element (RVE) for a regularly staggered composite, proposed by Kim et al. (2018); E_p and E_m are Young's moduli of platelet and matrix respectively, and G_m is the Shear modulus of the matrix.

A total number of five non-dimensionalized material & geometric parameters are defined for the ease in the description of the theoretical model. They are:

1. Geometric parameters:

   (a) platelet to overall thickness ratio, $\phi = \frac{2b}{2b+h}$

(b) overlapped length to platelet thickness ratio, $\rho = \frac{L_a}{b}$

(c) half non-overlapped length to overlapped length ratio, $\xi = \frac{L_b}{L_a}$

2. Material parameters:

(a) matrix shear modulus to platelet tensile modulus ratio, $\alpha = \frac{G_m}{E_p}$

(b) matrix tensile modulus to platelet tensile modulus ratio, $\beta = \frac{E_m}{E_p}$

$$\begin{aligned} \frac{\mathrm{d}^2\sigma_1(x)}{\mathrm{d}x^2} &= \frac{G_m}{E_p hb}\left(\sigma_1(x) - \sigma_2(x)\right) \\ \frac{\mathrm{d}^2\sigma_2(x)}{\mathrm{d}x^2} &= \frac{G_m}{E_p hb}\left(\sigma_2(x) - \sigma_1(x)\right) \end{aligned} \tag{A.1}$$

Where the subscripts denote the number of the partition. Equation A.1 is valid for both the case of stress-controlled as well as strain-controlled.

Since the governing differential equations as obtained in Equation A.1 is a set of two second-order differential equations composed of two variables, the model requires a total of four boundary conditions. It is assumed that partitions 4 and 5 experienced uniform tensile stress due to the significantly smaller non-overlapped length, resulting in relatively less stress variation compared to partitions 1, 2, and 3 with longer overlapped lengths. This assumption gives two boundary conditions as follows:

$$\sigma_1\left(L_a\right) = \sigma_5 = \sigma_2(0) \tag{A.2}$$

where σ_5 represents the uniform stress in partition 5. The condition of stress continuity across parts 5 and 1, or between parts 5 and 2 is ensured by Equation A.2. The remaining equations to define the stress distributions inside the unit cell are derived based on Equation A.2, in terms of σ_5.

It is to be noted that partitions 1 & 4, or 2 &4 are not of the same size of sections, where the stress continuity does not hold well. Therefore, the next boundary condition is formulated by taking into account the force equilibrium at the interface region between parts 4 and 1.

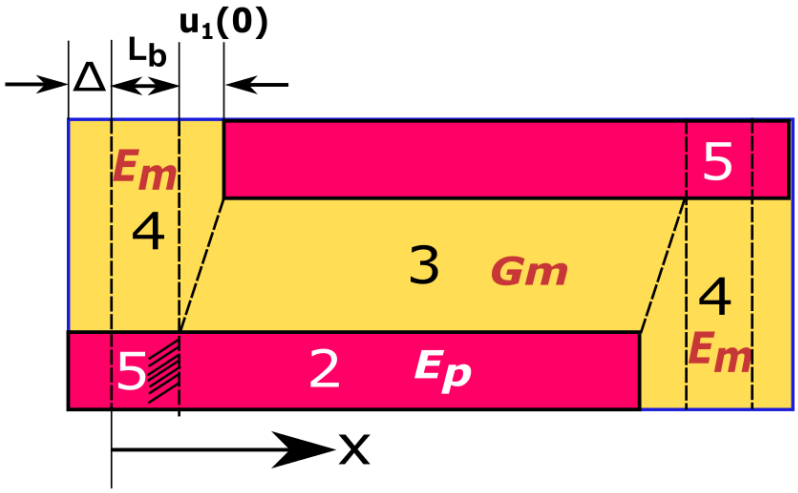

Figure A.2: Schematic diagram of the deformed unit cell of regular staggered composite. L_b represents the undeformed lengths of parts 4 and 5. $\Delta, u_1(0)$ represent partial deformed lengths due to the uniform deformation, and displacement of the upper platelet at x = 0, respectively.

Consider Figure A.1 in which the parameters $u_1(0)$, and Δ are shown. $u_1(0)$ is the upper platelet's displacement at $x = 0$ and Δ is the uniform deformation. It is assumed that part 4 is deformed into a trapezoidal shape as shown in Figure A.1 due to the following forces: (i) force applied by σ_5, (ii) force from part 1's left end displacement.

When the force equilibrium on the interface between parts 4 and 1 is considered, the following equation is obtained.

$$b\sigma_1(0) = \left(b + \frac{h}{2}\right) E_m \frac{u_1(0)}{L_b} + (b+h)\frac{\sigma_5}{E_p} E_m \tag{A.3}$$

where, the left hand side represents the force on the side of part 1 while the right hand side represents the force on the other side. The shear lag model's governing equation given below can be used to determine the term $u_1(0)$.

$$G_m \frac{u_1(x) - u_2(x)}{h} = b\frac{d\sigma_1(x)}{dx} \tag{A.4}$$

where the terms $u_1(x)$ and $u_2(x)$ represent the displacements of the partitions 1 and 2, respectively. Since a fixed boundary is assumed at $x = 0$, $u_2(0)$ is zero.

Now, substituting $u_1(0)$ from Equation A.4 into Equation A.3 results as,

$$\sigma_1(0) = \frac{E_m h(2b+h)}{2G_m L_b}\frac{\mathrm{d}\sigma_1(0)}{\mathrm{dx}} + \sigma_5\frac{E_m}{E_p}\frac{(\mathrm{b}+\mathrm{h})}{\mathrm{b}} = \sigma_2\left(L_a\right) \tag{A.5}$$

Here, the first term pertains to the trapezoidal deformation due to $u_1(0)$, which is the upper platelet's displacement at $x = 0$. The second term is associated with the uniform deformation represented by Δ.

By solving the Equation A.1 with the boundary conditions as in Equations A.3 & A.4 the stress distribution function can be obtained as,

$$\begin{aligned}
\sigma_1(x) &= \sigma_5\left(\frac{\left(1-\beta+\frac{2\beta}{\phi}\right)A\sinh(A)+B\cosh(A)+\left(1+\beta-\frac{2\beta}{\phi}\right)A\sinh\left(A\left(\frac{2x-L_a}{L_a}\right)\right)}{2A\sinh(A)+B\cosh(A)}\right)\\
\sigma_2(x) &= \sigma_5\left(\frac{\left(1-\beta+\frac{2\beta}{\phi}\right)A\sinh(A)+B\cosh(A)+\left(1+\beta-\frac{2\beta}{\phi}\right)A\sinh\left(A\left(\frac{L_a-2x}{L_a}\right)\right)}{2A\sinh(A)+B\cosh(A)}\right)\\
\tau_3(x) &= \sigma_5\alpha\frac{L_a}{h}\left(\frac{\left(1+\beta-\frac{2\beta}{\phi}\right)\cosh\left(A\left(\frac{L_a-2x}{L_a}\right)\right)}{2A\sinh(A)+B\cosh(A)}\right)
\end{aligned} \tag{A.6}$$

Here, A & B are non-dimensional parameters that signify the influence of overlapped partitions 1, 2, 3, and non-overlapped partitions 4, 5, respectively.

$$\mathrm{A} = \frac{\rho}{2}\sqrt{\alpha}\sqrt{\frac{\phi}{1-\phi}}, \quad \mathrm{B} = \frac{\beta}{\phi\xi} \tag{A.7}$$

In the present study, the normal stress along a full platelet, $\sigma^p_{reg}(x)$ in a regularly staggered composite is obtained as a function of the maximum normal stress in the platelet ($\sigma^p_{reg,max}$) (which is equal to the uniform normal stress in region 5 in Figure 2.1 (b)) by extending the equations for the unit cell by Kim et al. (2018) as follows:

$$\sigma^p_{\mathrm{reg}}(x) = \begin{cases}
\sigma^p_{\mathrm{reg\ ,\ max}}\left(\frac{\left(1-\beta+\frac{2\beta}{\phi}\right)A\sinh(A)+B\cosh(A)+\left(1+\beta-\frac{2\beta}{\phi}\right)A\sinh\left(A\left(\frac{2x-L_a}{L_a}\right)\right)}{2A\sinh(A)+B\cosh(A)}\right), & 0 \le x < L_a\\
\sigma^p_{reg,\max}, & L_a \le x < L_a + 2L_b\\
\sigma^p_{reg,\max}\left(\frac{\left(1-\beta+\frac{2\beta}{\phi}\right)A\sinh(A)+B\cosh(A)+\left(1+\beta-\frac{2\beta}{\phi}\right)A\sinh\left(A\left(\frac{(-2(x-L_a-2L_b))+L_a}{L_a}\right)\right)}{2A\sinh(A)+B\cosh(A)}\right), & L_a + 2L_b \le x < L_p
\end{cases} \tag{A.8}$$

The maximum value of normal stress in the platelet in a regular staggered composite $\left(\sigma^{p}_{reg,max}\right)$ will be equal to the platelet strength $(\sigma^{p}_{critical})$ and occurs at $x = L_a + 2L_b$ (Kim et al., 2018). The shear stress along a platelet matrix interface at the top and bottom of a platelet in a regular staggered composite is given by, (Kim et al., 2018)

$$\tau^{m}_{\text{reg,top}}(x) = \begin{cases} \sigma^{p}_{\text{reg,max}}\,\alpha\frac{L_a}{h}\left(\frac{\left(1+\beta-\frac{2\beta}{\phi}\right)\cosh\left(A\left(\frac{2x-L_a}{L_a}\right)\right)}{2A\sinh(A)+B\cosh(A)}\right), & 0 \le x \le L_a \\ \sigma^{p}_{\text{reg,max}}\,\alpha\frac{L_a}{h}\left(\frac{\left(1+\beta-\frac{2\beta}{\phi}\right)\cosh(A)}{2A\sinh(A)+B\cosh(A)}\right), & L_a < x \le L_a + 2L_b \\ \sigma^{p}_{\text{reg,max}}\,\alpha\frac{L_a}{h}\left(\frac{\left(1+\beta-\frac{2\beta}{\phi}\right)\cosh\left(A\left(\frac{3L_a-4L_b-2x}{L_a}\right)\right)}{2A\sinh(A)+B\cosh(A)}\right), & L_a + 2L_b < x \le L_p \end{cases} \tag{A.9}$$

$$\tau^{m}_{\text{reg,bottom}}(x) = \begin{cases} \sigma^{p}_{\text{reg ,max}}\alpha\frac{L_a}{h}\left(\frac{\left(1+\beta-\frac{2\beta}{\phi}\right)\cosh\left(A\left(\frac{L_a-2x}{L_a}\right)\right)}{2A\sinh(A)+B\cosh(A)}\right), & 0 \le x \le L_a \\ \sigma^{p}_{\text{reg,max}}\,\alpha\frac{L_a}{h}\left(\frac{\left(1+\beta-\frac{2\beta}{\phi}\right)\cosh(-A)}{2A\sinh(A)+B\cosh(A)}\right), & L_a < x \le L_a + 2L_b \\ \sigma^{p}_{\text{reg ,max}}\,\alpha\frac{L_a}{h}\left(\frac{\left(1+\beta-\frac{2\beta}{\phi}\right)\cosh\left(A\left(\frac{2x-3L_a-4L_b}{L_a}\right)\right)}{2A\sinh(A)+B\cosh(A)}\right), & L_a + 2L_b < x \le L_p \end{cases} \tag{A.10}$$

The peak value of shear stress in the platelet matrix interface occurs at $x = L_a + 2L_b$ and is given by,

$$\tau^{m}_{max,reg} = \sigma^{p}_{max,reg}\alpha\frac{L_a}{h}\left(\frac{\left(1+\beta-\frac{2\beta}{\phi}\right)\cosh(A)}{2A\sinh(A)+B\cosh(A)}\right) \tag{A.11}$$

The normal stress in the matrix at the vertical interface (σ^{m}_{max}) is assumed to be equal to the normal stress at the end of the platelet, which is given by,

$$\sigma^{m}_{max,reg} = \sigma^{p}_{max}\left(\frac{\left(1-\beta+\frac{2\beta}{\phi}\right)A\sinh(A)+B\cosh(A)+\left(1+\beta-\frac{2\beta}{\phi}\right)A\sinh(A)}{2A\sinh(A)+B\cosh(A)}\right) \tag{A.12}$$

Appendix B

Equations for normal and shear stresses in a stairwise staggered composite

$$\sigma_a(x) = \sigma_u^p \left(\frac{\gamma A_1 \sinh(A_1) + B_1 \cosh(A_1) + \lambda A_1 \sinh\left(A_1 \left[\frac{2n(x+L_b)-L}{L-2nL_b}\right]\right)}{2A_1 \sinh(A_1) + B_1 \cosh(A_1)} \right) \tag{B.1}$$

$$\sigma_b(x) = \sigma_u^p \left(\frac{\gamma A_2 \sinh(A_2) + B_2 \cosh(A_2) + \lambda A_2 \sinh\left(A_2 \left[\frac{L(n+1)-2n(x+L_b)}{(n-1)L-2nL_b}\right]\right)}{2A_2 \sinh(A_2) + B_2 \cosh(A_2)} \right) \tag{B.2}$$

$$\sigma_c(x) = \sigma_u^p \left(\frac{\gamma A_2 \sinh(A_2) + B_2 \cosh(A_2) + \lambda A_2 \sinh\left(A_2 \left[\frac{2n(x+L_b)-L(n-1)}{(n-1)L-2nL_b}\right]\right)}{2A_2 \sinh(A_2) + B_2 \cosh(A_2)} \right) \tag{B.3}$$

$$\sigma_d(x) = \sigma_u^p \left(\frac{\gamma A_1 \sinh(A_1) + B_1 \cosh(A_1) + \lambda A_1 \sinh\left(A_1 \left[\frac{L(2n-1)-2n(x+L_b)}{L-2nL_b}\right]\right)}{2A_1 \sinh(A_1) + B_1 \cosh(A_1)} \right) \tag{B.4}$$

Thus, the normal stress along a platelet in a stairwise staggered composite, $\sigma_{sw}^p(x)$ can be written as,

$$\sigma_{sw}^p(x) = \frac{\sigma_{sw}^{p,top}(x) + \sigma_{sw}^{p,bot}(x)}{2} \tag{B.5}$$

where,

$$\sigma_{sw}^{p,top}(x) = \begin{cases} \sigma_c & \text{if } 0 \leq x < L_{a2} \\ \sigma_u^p & \text{if } L_{a2} \leq x < L_{a2} + 2L_b \\ \sigma_d & \text{if } L_{a2} + 2L_b \leq x \leq L_p \end{cases} \tag{B.6}$$

$$\sigma_{sw}^{p,bot}(x) = \begin{cases} \sigma_a & \text{if } 0 \leq x < L_{a1} \\ \sigma_u^p & \text{if } L_{a1} \leq x < L_{a1} + 2L_b \\ \sigma_b & \text{if } L_{a1} + 2L_b \leq x \leq L_p \end{cases} \tag{B.7}$$

where,

$$\sigma_u^p = \frac{2\sigma_{crit}^p \left(2A_2 \sinh(A_2) + B_2 \cosh(A_2)\right)}{2\left[\gamma A_2 \sinh(A_2) + B_2 \cosh(A_2)\right] + A_2\lambda\left[\sinh\left(A_2\, C_1\right) + \sinh\left(A_2\, C_2\right)\right]} \tag{B.8}$$

where,

$$C_1 = \frac{L(n+1) - 2n(x + L_b)}{(n-1)L - 2nL_b} \tag{B.9}$$

$$C_2 = \frac{2n(x + L_b) - L(n-1)}{(n-1)L - 2nL_b} \tag{B.10}$$

Also, $\gamma = 1 - \beta + \frac{2\beta}{\phi}$, $\lambda = 1 + \beta - \frac{2\beta}{\phi}$, and $L = L_p + 2L_b$

$A_1 = \frac{\rho_1}{2}\sqrt{\alpha}\sqrt{\frac{\phi}{1-\phi}}$, $B_1 = \frac{\beta}{\phi\xi_1}$, $\rho_1 = \frac{L_{a1}}{b}$, and $\xi_1 = \frac{L_b}{L_{a1}}$

$A_2 = \frac{\rho_2}{2}\sqrt{\alpha}\sqrt{\frac{\phi}{1-\phi}}$, $B_2 = \frac{\beta}{\phi\xi_2}$, $\rho_2 = \frac{L_{a2}}{b}$, and $\xi_2 = \frac{L_b}{L_{a2}}$

Also, the variation of shear stress in the matrix along the top and bottom interfaces of the platelet with length L_p, can be found out in a similar manner as,

where,

$$\tau_{sw}^{m,top}(x) = \begin{cases} \tau_c & \text{if } 0 \leq x < L_{a2} \\ \tau^{ut} & \text{if } L_{a2} \leq x < L_{a2} + 2L_b \\ \tau_d & \text{if } L_{a2} + 2L_b \leq x \leq L_p \end{cases} \tag{B.11}$$

$$\tau_{sw}^{m,bot}(x) = \begin{cases} \tau_a & \text{if } 0 \leq x < L_{a1} \\ \tau_{ub} & \text{if } L_{a1} \leq x < L_{a1} + 2L_b \\ \tau_b & \text{if } L_{a1} + 2L_b \leq x \leq L_p \end{cases} \tag{B.12}$$

where,

$$\tau_a(x) = \sigma_{max}^p \alpha \frac{L_{a1}}{h} \left[\frac{\lambda \cosh(A_1 \frac{L_{a1}-2x}{L_{a1}})}{2A_1 \sinh(A_1) + B_1 \cosh(A_1)} \right] \tag{B.13}$$

$$\tau_{ub}(x) = \sigma_{max}^p \alpha \frac{L_{a1}}{h} \left[\frac{\lambda \cosh(-A_1)}{2A_1 \sinh(A_1) + B_1 \cosh(A_1)} \right] \tag{B.14}$$

$$\tau_b(x) = \sigma_{max}^p \alpha \frac{L_{a2}}{h} \left[\frac{\lambda \cosh(A_2 \left[\frac{L(n+1)-2n(L_b+x)}{L(n-1)-2nL_b} \right]}{2A_2 \sinh(A_2) + B_2 \cosh(A_2)} \right] \tag{B.15}$$

$$\tau_c(x) = \sigma_{max}^p \alpha \frac{L_{a2}}{h} \left[\frac{\lambda \cosh\left(A_2 \left[\frac{L_{a2}-2x}{L_{a2}} \right] \right)}{2A_2 \sinh(A_2) + B_2 \cosh(A_2)} \right] \tag{B.16}$$

$$\tau_{ut}(x) = \sigma_{max}^p \alpha \frac{L_{a1}}{h} \left[\frac{\lambda \cosh(-A_2)}{2A_1 \sinh(A_1) + B_1 \cosh(A_1)} \right] \tag{B.17}$$

$$\tau_d(x) = \sigma_{max}^p \alpha \frac{L_{a1}}{h} \left[\frac{\lambda \left(A_1 \left[\frac{(n+1)L-2n(L_b+x)}{(n-1)L-2nL_b} \right] \right)}{2A_1 \sinh(A_1) + B_1 \cosh(A_1)} \right] \tag{B.18}$$

Appendix C

Limiting value of stiffness

C.1 Regular Staggered Model

Equation C.1 is analysed for maximum stiffness ratio as $E_p/E_m \to \infty$ by expressing α in terms of β and limiting $\beta \to 0$.

$$\left(\frac{E}{E_{B=0}}\right)_{reg} = \frac{(A\sinh(A) + B\cosh(A))(\cosh(A) + A\sinh(A))}{(\cosh(A) + A\sinh(A) + B\cosh(A))A\sinh(A)} \tag{C.1}$$

$$\begin{aligned}\left(\frac{E}{E_{B=0}}\right)_{\text{reg},\frac{E_P}{E_m}\to\infty} &= \Lambda(\rho, \nu_m, v_f, b, \xi) \\ &= \frac{-b^2\left(2\nu_m + 2\right)\left[\frac{\Gamma_2(\xi+1)}{\xi v_f \Gamma_1} - \frac{v_f\Gamma_1\Gamma_2^2}{b^3\rho\left[\frac{v_f\Gamma_1}{b\rho}-1\right]2(\nu_m+2)4}\right]4}{\Gamma_1^2\frac{v_f\Gamma_1}{b\rho\left[\frac{v_f\Gamma_1}{b\rho}-1\right]}}\end{aligned} \tag{C.2}$$

where,

$$\begin{aligned}\Gamma_1 &= \rho b + \frac{b\xi\rho}{\xi+1} \\ \Gamma_2 &= \rho b - \frac{b\xi\rho}{\xi-1}\end{aligned} \tag{C.3}$$

where ρ, ν_m, v_f, b, and ξ represent the platelet aspect ratio, poisson's ratio of matrix, platelet volume fraction, width of platelet, and overlap ratio, respectively.

Substituting the values for the above terms, we get the limiting value of stiffness ratio

for regular staggered composite as,

$$\Lambda(4, 0.38, 0.8, 10, 0.02) = 10.94 \tag{C.4}$$

C.2 Stairwise staggered composite

The limiting values of the stiffness ratio for a stairwise staggered composite can also be computed by applying a limit to the two parts of the regular staggered RVEs inside a stairwise staggered RVE. The limiting value is found to be 17.8 for the set of parameters: $(\rho, \nu_m, v_f, b, \xi, n) = (4, 0.38, 0.8, 10, 0.02, 5)$.

C.3 Limiting value of $\frac{\sigma^p_{crit}}{\tau^m_{crit}}$

To find the limiting value of $\frac{\sigma^p_{critical}}{\tau^m_{critical}}$, the ratios $\frac{\sigma^m_{critical}}{\sigma^m_{max}}$, $\frac{\tau^m_{critical}}{\tau^m_{max}}$, and $\frac{\sigma^p_{critical}}{\sigma^p_{max}}$, are checked for aspect ratios from 1 to 500 and varying $\frac{\sigma^p_{critical}}{\tau^m_{critical}}$. The sequences of failure are obtained for all the aspect ratios for each value of $\frac{\sigma^p_{crit}}{\tau^m_{crit}}$. Then, using a search algorithm in MATLAB (The Mathworks, 2020), the minimum value of $\frac{\sigma^p_{crit}}{\tau^m_{crit}}$ is extracted, for which platelet failure would never occur in the range of aspect ratios chosen.

Appendix D

Derivation of Mechanical Properties of Regular Staggered Composites using TSC model

D.1 Regular Staggered Model using TSC model

The foundational assumptions of the tension–shear chain model proposed by (Gao et al., 2003) and Ji and Gao (2004a) are as follows (Zhang et al., 2010):

- The elastic modulus of the matrix is 2 to 3 orders of magnitude smaller than that of the platelet, thus the matrix cannot transfer any normal stress between neighboring platelets. In the longitudinal direction (z), the load can only be transferred through shear in the matrix.

- The platelet thickness (h) is 1 to 2 orders of magnitude smaller than its length (L), rendering the mineral essentially one-dimensional (depending only on z, as shown in Figure).

- The platelet distribution exhibits repetition after two rows of platelets.

- The neighbouring platelets have an overlapping of half of their length along the longitudinal direction.

Additionally, the longitudinal gap (z) between the platelets is significantly smaller than the length of the platelet (L). Consider Figure D.1 in which the undeformed (b) and deformed representative volume elements (RVE) of a regular staggered composite with an overlap of

ξ is shown. We have the equation of equilibrium along the horizontal direction as,

$$(1-\xi)\tau^R - \xi\tau^L = 0 \tag{D.1}$$

where, τ^L and τ^R are the shear stresses acting on the left and right parts of the matrix as shown in Figure D.1 (c).

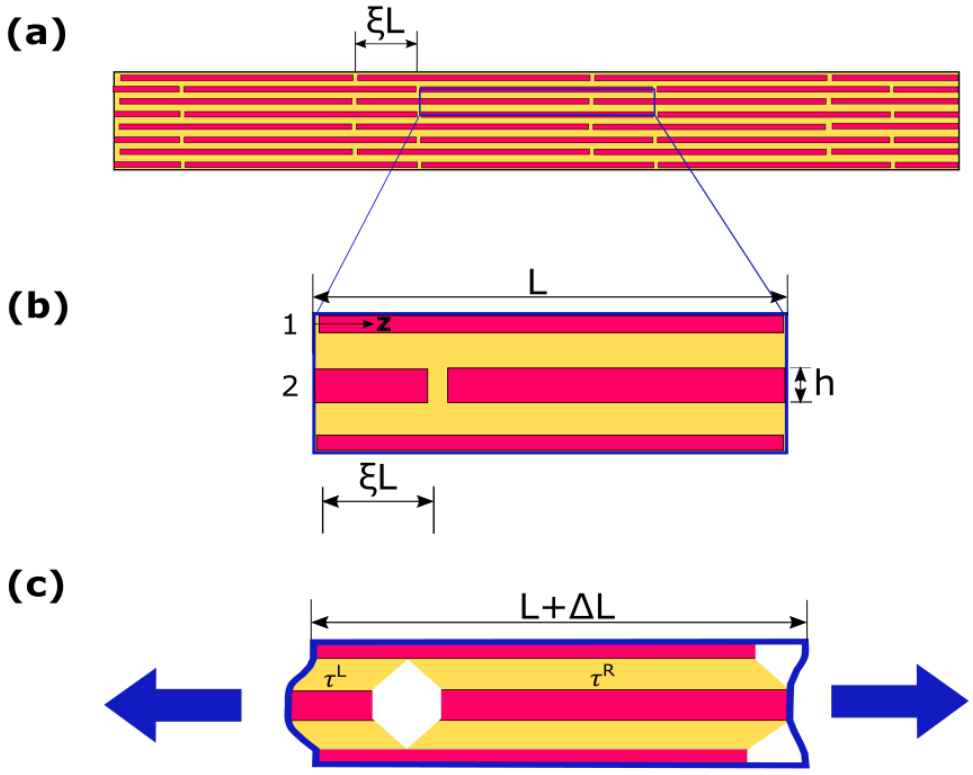

Figure D.1: Regular staggered composite with an offset ξL. (a) Overall structure of the composite, (b) Representative volume element (RVE), (c) deformed RVE after the application of longitudinal displacement Δ. The platelet dimension is $L \times h$, and τ^L, τ^R represent the shear stresses in the left and right parts of the matrix, respectively.

The normal stress in the (first) platelet is obtained from the force equilibrium as

$$\sigma_p = \begin{cases} \frac{2}{h}\tau^L z, & 0 \le z \le \xi L, \\ \frac{2}{h}\tau^R (L-z), & \xi L < z \le L \end{cases} \tag{D.2}$$

The strain energy in the platelets in the unit cell is $2h\int_0^L \left(\sigma_p^2/\left(2E_p\right)\right) dz$, where E_p is

Young's modulus of the platelets. e strain energy in the matrix is

$$2\frac{(1-\phi)h}{\phi}\left[\xi L\frac{\left(\tau^L\right)^2}{2G_m}+(1-\xi)L\frac{\left(\tau^R\right)^2}{2G_m}\right] \tag{D.3}$$

G_m is the shear modulus of the matrix and ϕ is the platelet volume fraction. Let σ^p and E^p be the normal strength and Young's modulus of the platelets, respectively. The complementary energy of the unit cell is,

$$\begin{aligned}\mathbf{\Pi}_C &= 2h\int_0^L \frac{\sigma_p^2}{2E_p}dz + 2\frac{(1-\phi)h}{\phi}\left[\xi L\frac{\left(\tau^L\right)^2}{2G_m}+(1-\xi)L\frac{\left(\tau^R\right)^2}{2G_m}\right] - F\Delta \\ &= \left[\frac{4\xi^2L^3}{3hE_p}+\frac{(1-\phi)\xi hL}{\phi(1-\xi)G_m}\right]\left(\tau^L\right)^2 - 2\xi L\tau^L\Delta,\end{aligned} \tag{D.4}$$

where F represents the axial force on the platelet which is given by,

$$F = 2\tau^L\xi L \tag{D.5}$$

By the minimization of complementary energy obtained by Equation D.4 we get,

$$d\Pi_C/d\tau^L = 0 \Rightarrow \tag{D.6}$$

$$\tau^L = \frac{\Delta}{\frac{4\xi L^2}{3hE_p}+\frac{(1-\phi)h}{\phi(1-\xi)G_m}}. \tag{D.7}$$

We have the average stress in the composite as,

$$\sigma = \frac{F}{2h+2(1-\phi)h/\phi} = \frac{\phi F}{2h} \tag{D.8}$$

Equation D.8 can be rewritten by substituting F in terms of τ_L from Equations D.5 and D.6 as,

$$\sigma = \frac{1}{\frac{4}{3\phi E_p}+\frac{1-\phi}{\phi^2\xi(1-\xi)\rho^2G_m}}\frac{\Delta}{L} \tag{D.9}$$

Thus, the modulus of elasticity of the regular staggered composite can be found out by

taking the ratio of the average stress (σ) to the average strain $\left(\frac{\Delta}{L}\right)$ from Equation D.9 as,

$$E = \frac{1}{\frac{4}{3\phi E_p} + \frac{1-\phi}{\phi^2 \xi(1-\xi)\rho^2 G_m}} = \phi E_p \frac{1}{\frac{4}{3} + \frac{1}{3\xi(1-\xi)\alpha}} \tag{D.10}$$

A similar approach can be applied to obtain the equations of stiffness, strength and strain in stairwise staggered composites, by considering a model with overlap of L/n where n is the number of platelets in a period.

Appendix E

Python code for implementing PBC

E.1 Code snippet to impose PBC

```
  mdb.models['Model-1'].StaticStep(name='Step-1', previous='Initial')
#Lrve: Length of the model
#Wrve: Width of the model

###Create top, right, left, and bottom edge groups
  finalInstance=mdb.models['Model-1'].rootAssembly.instances['Composite-
                                    1']
  a = mdb.models['Model-1'].rootAssembly
  a.Set(edges=finalInstance.edges.findAt(((Lrve/2., Wrve, 0.0),), ),
                                    name="top")
  a.Set(edges=finalInstance.edges.getByBoundingBox(xMin=Lrve-0.), name="
                                    right")
  a.Set(edges=finalInstance.edges.getByBoundingBox(xMax=hg/5.), name="
                                    left")
  a.Set(edges=finalInstance.edges.getByBoundingBox(yMax=vg), name="
                                    bottom")

#Connecting nodesets from top & bottom, left & right, by periodic
                                    boundary conditions

  nodesets = {}
  for set,i in zip(["top","bottom","right","left"],[1,1,2,2]):
  nodesets[set]=[]
  for node in a.sets[set].nodes:
  nodesets[set].append((node.label,node.coordinates[0],node.coordinates[
                                    1]))
  nodesets[set].sort(key=lambda value: value[i])
```

```
  mdb.models['Model-1'].keywordBlock.synchVersions(True)
  keywordblock = mdb.models['Model-1'].keywordBlock
  for i,kw in enumerate(keywordblock.sieBlocks):
  if kw.startswith("*End Part"):
  endpart = i
  elif kw.startswith("*End Instance"):
  endinstance = i
  elif kw.startswith("*Elset"):
  endassembly = i
  elif kw.startswith("*Static"):
  static = i
  elif kw.startswith("*Output, history"):
  history = i
  break

# Creating dummy node to assign displacement
  partstring="*Part, name=dummy-LR\n"
  partstring+="*End Part\n"
  partstring+="**\n"
  partstring+="*Part, name=dummy-TB\n"
  partstring+="*End Part\n"
  partstring+="**\n"
  keywordblock.insert(position=endpart+1,text=partstring)
  endinstancestring="*Instance, name=dummy-LR-1, part=dummy-LR\n"
  endinstancestring+="*Node\n"
  endinstancestring+="100000, -10., 10., 0.\n"
  endinstancestring+="**This dummy node can be arbitrary\n"
  endinstancestring+="*Nset, nset=dummy-LR-1-RefPt_, internal\n"
  endinstancestring+="100000,\n"
  endinstancestring+="*End Instance\n"
  endinstancestring+="*Instance, name=dummy-TB-1, part=dummy-TB\n"
  endinstancestring+="*Node\n"
  endinstancestring+="200000, 10., 0., 0.\n"
  endinstancestring+="**This dummy node can be arbitrary\n"
  endinstancestring+="*Nset, nset=dummy-TB-1-RefPt_, internal\n"
  endinstancestring+="200000,\n"
  endinstancestring+="*End Instance\n"
  endinstancestring+="** Define nset Set-dummy-LR and Set-dummy-TB for
                                  the two dummy nodes\n"
  endinstancestring+="**\n"
  endinstancestring+="*Nset, nset=Set-dummy-LR, instance=dummy-LR-1\n"
  endinstancestring+="100000,\n"
```

```
  endinstancestring+="*Nset, nset=Set-dummy-TB, instance=dummy-TB-1\n"
  endinstancestring+="200000,\n"
  keywordblock.insert(position=endinstance+1,text=endinstancestring)
# Defining equations
  equationstring = "*Equation\n"
  for ntop,nbot in zip(nodesets["top"],nodesets["bottom"]):
  equationstring += "3\n"
  equationstring += "Composite-1.%d, 1, 1.0, Composite-1.%d, 1, -1.0, %s
                                    , 1, -1.0\n" % (ntop[0],nbot[0],'Set
                                    -dummy-TB')
  equationstring += "3\n"
  equationstring += "Composite-1.%d, 2, 1.0, Composite-1.%d, 2, -1.0, %s
                                    , 2, -1.0\n" % (ntop[0],nbot[0],'Set
                                    -dummy-TB')
  for nright,nleft in zip(nodesets["right"],nodesets["left"]):
  equationstring += "3\n"
  equationstring += "Composite-1.%d, 1, 1.0, Composite-1.%d, 1, -1.0, %s
                                    , 1, -1.0\n" % (nright[0],nleft[0],'
                                    Set-dummy-LR')
  equationstring += "3\n"
  equationstring += "Composite-1.%d, 2, 1.0, Composite-1.%d, 2, -1.0, %s
                                    , 2, -1.0\n" % (nright[0],nleft[0],'
                                    Set-dummy-LR')
  keywordblock.insert(position=endassembly,text=equationstring)
  bcstring = "**\n*Boundary\n"
  bcstring += "Set-dummy-TB,1,1, 0.0\n"
  bcstring += "**\n*Boundary\n"
  bcstring += "Set-dummy-LR,1,1, 0.01\n"
  bcstring += "**\n*Boundary\n"
  bcstring += "Set-dummy-LR,2,2, 0.0\n"
  bcstring += "**\n*Boundary\n"
  bcstring += "Set-dummy-TB,2,2, 0.0\n"
  keywordblock.insert(position=static+3,text=bcstring)
```

Appendix F

Mesh dependency study

F.1 Regular Staggered Model

A mesh sensitivity analysis for a regular staggered composite has been conducted by varying the mesh-size. For this, we choose a regular staggered composite with volume fraction 80% and platelet aspect ratio of 12 with $E_p/G_m = 1000$, as shown in Figure F.1. Periodic boundary conditions with a displacement of 0.01 at the right end as described in section3.4 is applied for the model since a regular staggered model is a stairwise staggered model with $n = 2$.

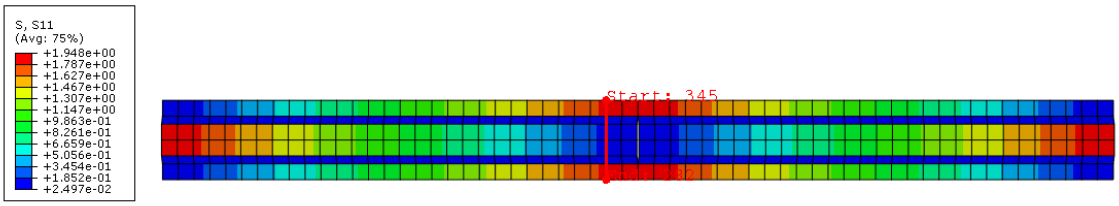

Figure F.1: Path chosen in a regular staggered model of 80% platelet volume fraction and platelet aspect ratio 12, to check mesh dependency

The mesh size of the model is by default kept as half of the vertical interface thickness (L_a) in the present study. For the regular staggered model shown in Figure F.1, the mesh size is $2L_a$ which is 0.5. The models with mesh size 0.25, 0.125, and 0.0625 are also analysed to conduct the mesh dependency study. The normal stress (σ_{11}) along the path shown in Figure F.1 is plotted as shown in Figure F.2, for different mesh sizes 0.5, 0.25, 0.125, and 0.0625. It can be seen that the maximum variation of stress at a point for the coarsest and the finest mesh size is within 0.01, which ensure the mesh independence of the obtained results.

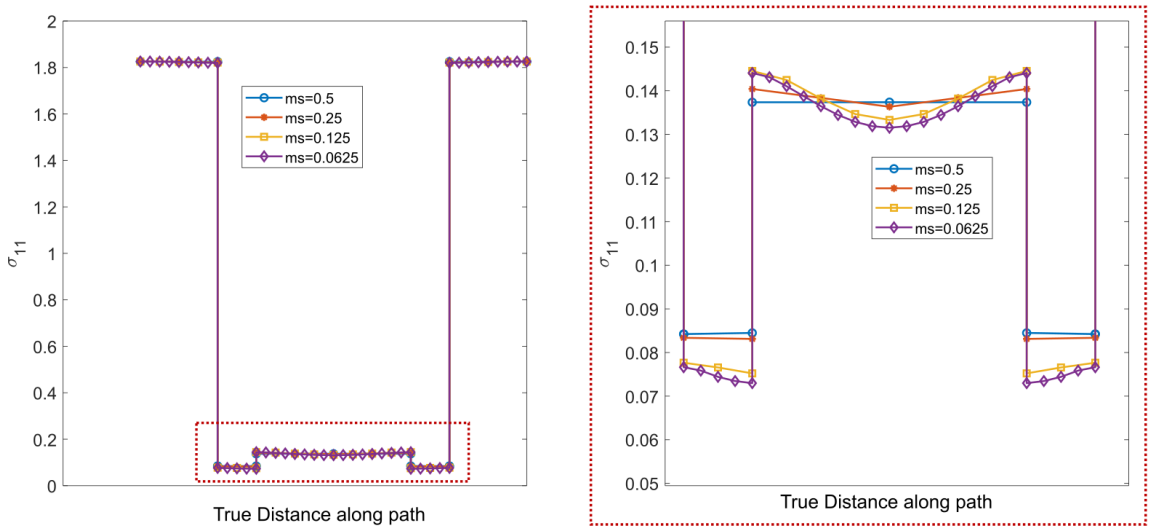

Figure F.2: Comparison of stress along the path for different mesh sizes (a) normal stress (σ_{11}) along the path shown in Figure F.1 (b) zoomed view of the plot highlighted in (a)